NOVEL CONTROL STRATEGIES FOR SINGLE-PHASE INVERTER BASED MICROGRIDS CONSIDERING GRID INTEGRATED AND ISLANDED CONDITIONS

by

Robin Pratap Singh Bisht

A dissertation submitted to the faculty of
The University of North Carolina at Charlotte
in partial fulfillment of the requirements
for the degree of Doctor of Philosophy in
Electrical Engineering

Charlotte

2021

Approved by:

_____

Dr. Sukumar Kamalasadan

_____

Dr. Valentina Cecchi

_____

Dr. Abasifreke Ebong

_____

Dr. Brett Tempest

ABSTRACT

ROBIN PRATAP SINGH BISHT. Novel Control Strategies for Single-Phase
Inverter based Microgrids Considering Grid Integrated and Islanded Conditions.
(Under the direction of DR. SUKUMAR KAMALASADAN)

This dissertation focuses on designing and developing single-phase inverter (SPIs) control typologies for different microgrid (MG) frameworks. SPIs are considered a major part of the distributed energy resources (DERs), especially at the power distribution level laterals. Thus, effective and collective management of SPIs at normal grid operating conditions and under disturbances is a critical factor for reliable and efficient operation of grid integrated DERs with SPIs. The major contribution of this dissertation is that, first, a local control architecture is designed that works for Stand-Alone (SA) and Grid-Connected (GC) modes of operation of SPI and does not require switching between control modes. The architecture also provides a seamless transfer of the SPIs from GC to SA without compromising the grid quality and confirming to interconnect on standards. Second, a control architecture for multiple inverters connected to the same phase that can share the loads is designed. This is extended to multiple inverters connected to each phase in one lateral during normal operation and under unbalance conditions. Third, an architecture that can be used for grid support function with SPIs connected at different parts of the power distribution network is designed. For this, an adaptive droop-based architecture is explored that identifies the system's impedance matrix and can be applied for varying network topology. The approach is based on the alternate direction method of multipliers (ADMM) for identifying the grid impedance as a multiple input-multiple output (MIMO) trans. Finally, a coordinated framework is proposed for using SPIs along with legacy grid controllers to support the power distribution system.

DEDICATION

Dedicated to my parents, Rashmi Bisht and Pratap Singh Bisht, and my grandparents, late S.R. Chauhan and Kamla Chauhan, who have been a constant source of support and inspiration throughout my life. I also dedicate this work to my schools, Ryan International School, Visvesvaraya National Institute of Technology, and University of North Carolina at Charlotte, and my teachers who helped me every step of the way to achieve this milestone.

ACKNOWLEDGEMENTS

TABLE OF CONTENTS

LIST OF TABLES

LIST OF FIGURES

LIST OF ABBREVIATIONS

ADMM Alternating Direction Method of Multipliers

CARMA Controlled Auto RegressiveMoving Average

DER Distributed Energy Resource

DN   Distribution Network

DQ   Direct-Quadrature Axis

ECE An acronym for Electrical and Computer Engineering.

EPS Electric Power System

GC   Grid Connected

HDI High Density Index

HV   High Voltage

IGBT Insulated Gate Bipolar Transistor

LQR Linear Quadratic Regulator

LV   Low Voltage

MG   Microgrid

MIMO Multiple Input Multiple Output

P   Generally used in this dissertation as Active Power

PCC Point of Common Coupling

PI   Proportional and Integral

POI Point of Interconnection

POIn Point of Interconnection

PR   Proportional and Resonant

PV   Photovoltaic

Q   Generally used in this dissertation as reactive Power

SA   Stand Alone

SAIDI System Average Interruption Duration Index

SAIFI System Average Interruption Frequency Index

SMIB/OMIB Single/One Machine Infinite Bus System

SPI   Single Phase Inverter

VVO Volt-VAR Optimization

CHAPTER 1: Introduction

Increasing interest and demand for research towards the decentralization of power generation in all forms of power system networks have been observed in the last couple of decades. The last decade has seen a rise in solar energy installations and applications; up to 98 GW of PV capacity was installed on- and off-grid markets in 2017 across the globe [1]. In 2019, the U.S. solar market was responsible for installing 13.3 GW_{dc} of PV, a 13% increase from 2018. This has brought grid-forming inverters and the concept of micro-grids to the main stage, primarily because the inverter is the primary equipment or device used to interface renewable sources like PVs to the grid. Over the years, manufacturers of inverters have become intensely competitive on efficiency, weight, and economical design. The use of SiC switches has seen an increase in switching frequency, which can decrease inductor sizes. The next few decades will see a tremendous increase in PV penetration, not only because of high power medium and low voltage (MVLV) DGs but rooftop PVs where smaller communities will have the capability of islanding and forming micro-grids. Therefore, there is an obligation to investigate different control topologies for three-phase inverters but single-phase inverters.

For this dissertation, a single-phase full-bridge inverter topology will be utilized for interfacing PV-battery systems with the grid. For inverter-based micro-grid applications, the control functionalities that will be discussed in this dissertation will adhere to the regulations and definitions provided by the U.S. Department of Energy (DOE) and IEEE standards for interconnecting Distributed Energy Resources (DERs) with Electric Power Systems (EPS) i.e. IEEE1547. According to the DOE, a micro-grid is a local energy resource or a grid with its control architecture that

can connect and disconnect from the traditional grid and operate autonomously [2]. Therefore, the initial chapters will focus on the off-grid or Stand Alone (SA) mode and the grid-connected mode of operation of the Single-Phase Inverters (SPIs). At least one inverter interfaced DER is responsible for forming the grid or stiff bus voltage for the island or the micro-grid in the SA mode. The formulation of the control loops for SPIs to achieve stiff bus voltage and constant frequency at the PCC for single machine-based micro-grids forms the basis of single DER-based micro-grids and ensures smooth transitioning between grid-connected mode to SA and vice-versa.

Control of multiple DERs is always going to be complex; therefore a multiple micro-grid control strategy is needed that will enable individual micro-grids to manage their DERs to achieve one overall objective. Multiple micro-grids management has been studied under economics, and optimal power flow, but coordinated control of micro-grids with legacy devices has seldom been investigated. Reverse power flow and misoperation of legacy devices in the current architecture of distribution systems is an issue on the rise with the increasing penetration of PV-inverter systems. Parallel connection and control of multiple inverters is an essential area of research in micro-grid systems [3]. Even though there are various advantages of renewable energy integration, several significant issues need to be addressed with the growing integration of renewable sources in distribution networks. One major issue is the voltage imbalances in the power distribution network with higher penetration of Single-Phase and Three-Phase inverter-based energy resources.

If the consumer end actively contributes towards regulating the system (via injecting active and reactive power), much of the voltage and power balance issues can be mitigated [4]. Management of grid and control of power inverters is the key to voltage improvement. Control of Single-Phase inverters (SPIs) for these modes have been explored [5, 6, 7, 8, 9], but it still proves to be a difficult task due to the varying grid requirements. Three-Phase power distribution systems, especially with high pen-

etration of DERs (Three-Phase and Single-Phase), suffer from unbalanced loading, voltage sags, and power quality issues.

Earlier research work has been performed for solving these problems by placing compensating devices such as capacitor banks[10] (also aided by power electronic elements), series compensation devices[11], and voltage support using the power output of the converters[12]. However, the use of power electronic equipment and penetration has been increasing in such a drastic way that these methods prove costly. There is a notion that with the already existing inverters in the system or consumer-end inverters, local problems can be quenched locally [13, 14]. Reactive power generation by inverters is a valuable commodity for the grid, and dynamically controlling the inverter output powers (active and reactive power) can be a great way to manage local voltage or frequency changes [15].

Having multiple DERs in a micro-grid needs more complex control architectures discussed in the past with traditional droop topologies on SA mode. Active and reactive power control topologies for grid-connected operation mode are some examples of more passive control methodologies. With the ever-changing network (also due to the addition of DERs and non-linear loads), there is a need for local controllers to be adaptive. Hence, the requirement for a hierarchical-based control topology can provide power management strategies to multiple DER-based micro-grids.

Much of the research is now focused on the localized grid support functionalities of the DERs. With the updated IEEE 1547-2108 standard, mandating voltage support features to be provided to the distributed inverters via reactive power control, it is necessary to evaluate the Volt-Var relation's intricacies in medium and low voltage networks with proper control strategies in place [16]. The issue addressed in this chapter is the coordination of inverters based on reactive powers for voltage regulation. The reactive power sourcing and sinking capability of distributed energy sources via inverters allow supervisory controllers to allocate set-points based on a coordinated

approach to individual inverters.

The dissertation focuses on Single-Phase inverter-based micro-grids and their primary-, secondary- and tertiary level control. The chapter organization is as follows: chapter 2 indulges in the overview of existing local and higher-level controllers existing in current literature, which helped formulate the SA and grid-connected inverter control for this dissertation. Chapter 3 investigates the SA and grid-connected control architecture for single DER-based micro-grids and the transition between the mentioned modes of operation during abnormal grid operation. This chapter also provides a novel unified controller architecture on the outer loop and a novel adaptive control technique for the same architecture. Chapter 4. introduces multiple DER management methodologies in a single micro-grid system and how the local control loops can be modified to perform power management for the stand-alone mode of operation. Chapter 5 moves on to multiple micro-grid concepts and the different techniques for DER power management and control and how the flexibility of multiple Single-Phase based micro-grids can be utilized to tackle different issues relating to power unbalance and voltage regulation. Chapter 6 explores the benefits of DER penetration in an LV distribution system with legacy voltage regulating devices.

CHAPTER 2: Literature Review

As we move towards sustainable power generation, implementing Distributed Energy Resources (DER) at the consumer end, there is a solid need to effectively manage power and energy from these sources, including Distributed Generator (DG) based architecture. High proliferation of DERs can impact low and medium voltage systems even though DERs can provide distributed power and thus can be used to serve local loads. For example, widely varying DERs with energy resources can cause problems in voltage regulation in distribution networks. To take care of such issues that exist in our DN, micro-grid systems are developed.

Micro-grids can be defined as a collection of DER over a small area, capable of operating independently from the grid. These smaller power networks eliminate problems in their areas, reducing the impact of having multiple DER over the larger power grid. Perturbations and micro-grids changes still exist, such as load changes, varying power generation, and weather-related issues. It is important that any micro-grid can withstand these changes and adapt accordingly. A robust controller on the devices in the micro-grid is a must to solve such problems. Today's DGs typically include solar and wind generation systems. Such renewable energy sources (RESs) are connected to the distribution network in distributed generations (DGs). The nature of power generated from RES RESs is mainly DC-based, so power electronic converters (PECs) are required to interconnect these devices to the grid. PECs are mainly voltage source inverters (VSIs) that regulate voltage, frequency, and power output to the network while fulfilling the grid requirements. Inverter's operation and control strategies can vary depending on the types of loads and micro-grids modes of operation. Different types of controller architectures are reported in the literature, which helps the DG

comply with the new codes and interconnection standards. It can be seen that an inverter (whether Single-Phase or Three-Phase) is a critical component for DG interconnection and a fast and robust controller is necessary to regulate the output power and voltage of the inverter in all operating conditions of the grid.

2.1   Control Strategies for Grid-Connected Inverters

Inverters are made of insulated-gate bipolar transistors (IGBTs) and anti-parallel diodes allow bi-directional power flow. IGBTs are preferred over metal-oxide-semiconductor field-effect transistors (MOSFETs) because IGBTs offer more significant lower power losses, higher power gain, higher voltage operation. The DC voltage at the DC-link of the inverter is converted to sinusoidal AC using these elements. An LC filter is used to attenuate the higher frequency harmonics. The AC waveform is generated by switching these IGBTs between ON and OFF states and changes in the dc power flow direction. These sequences are generated by a pulse width modulation (PWM) adjusted by the current/voltage controller taking feedback output current and voltage from the LC filter. Two principal operations of inverter in a micro-grid operation are grid-following and grid-forming. The grid-following operating mode, also known as grid feeding and PQ control mode, is achieved by controlling the output current of the inverters or CSIs. In the grid-forming operation, voltage source inverters (VSIs) are usually used for the voltage and frequency control of the Point of Common Coupling (PCC). Both the grid-forming and grid-following units utilize VSIs. They employ different control topologies or algorithms to perform in these modes of operation. The primary control that we see in most inverters is controlling the grid current, as the voltage at the PCC is held constant by the grid.

2.1.1   Methods of Inverter Current Control

Control of current is an essential task in grid-connected inverters; as mentioned before, the voltage is held constant by the grid. The main idea for the controller

is to track the reference current applied with minimum error. The output voltage should have a good transient performance and dynamic response. The methods for the current control of single-phase inverters are reviewed in the following sections.

2.1.1.1   Linear Regulator

In this approach, the inverter output current is controlled with carrier-based PWM. There have been modifications to reduce the THD of the inverter output current. Among them are: the SPWM methods, centroid-based switching, hybrid PWM, and random hybrid PWM. Proportional plus Integral control (PI) has poor performance when tracking a sinusoidal reference due to the steady-state error at frequencies other than DC. Elimination of noise in the current signal is also less due to the integral term reacting to past errors. It does not respond to the state of the instantaneous current efficiently. Therefore, the system is slow to reach the set-points and reacting to perturbations. The advantage of the carrier-based control with linear regulators is the constant switching frequency operation. The PI controller's modification is the PR control, where a sinusoidal transfer function is combined with the PI transfer function. This controller is very sensitive to perturbations in the fundamental frequency, which can cause stability problems in the system. Compared to other direct current control methods, the carrier-based method's general drawback is the inadequate dynamic response of linear compensators, which causes a poor overall transient response.

2.1.1.2   Hysteresis Control Method

This method is a direct current control method, in which the current is controlled using a hysteresis loop. In this method, the inverter output current is forced to follow the current reference. The upper and lower band limits the deviation between reference and output current in a hysteresis loop; this guarantees a peak current limiting capability. On reaching the upper limit of the hysteresis band, the inverter leg is switched off, allowing the current to reach the lower band of the hysteresis loop where

the inverter leg is once again switched on the current increases. The sinusoidal wave shape of the reference signal causes variation of the inverter switching frequency. It yields a current ripple magnitude that varies during one entire output period despite the hysteresis band's constant width. Hence, the current control with a fixed hysteresis band has the disadvantage that the PWM switching frequency varies because peak-to-peak current ripple must be controlled at all points of the fundamental frequency wave. This simple controller has a variable switching frequency and, therefore, a relatively high THD.

2.1.1.3   Peak Current Control Method

Peak current-mode control operates by comparing the actual inductor current to the current reference level. The peak inductor current control functions by comparing the up-slope of the inductor current to a current level set by the reference value. At a fixed interval in time, the power switching device is turned on, but when the instantaneous current reaches the set reference value, it turns off. Although this method gives constant switching frequency, it can produce instability under certain circumstances. A compensating saw tooth signal is added to or subtracted from the reference current signal. The slope of the sawtooth signal is maintained constant for stable operation and to eliminate the sub-harmonic oscillation. The peak current mode control method is inherently unstable at duty ratios exceeding 0.5. In inverter applications, the inductor slopes change over a wide range. The inductor current is tracking the fundamental, and average current control methods suffer from the difficulty of implementation when applied to inverters.

2.1.1.4   Proportional Resonant Control Method

PI controllers are standard in DC-to-DC converters, but it gives a relatively poor performance in inverter applications. This is because the PI controller serves well in DC applications and performs horribly for sinusoidal tracking applications. The

reason is the time-variant steady-state error produced when tracking the sinusoidal reference. Hence, introduced the Proportional-Resonant (PR) current controller. In this approach, the classical PI is transformed into an equivalent AC-compensator having the same frequency response characteristics in the bandwidth of concern. Ref. [17] presents a single-phase grid-connected inverter system with the quasi-PR control scheme, addressing some of the reasons that make PR controllers challenging to implement in reality. Firstly, the infinite gain introduced by a PR controller leads to an infinite quality factor that cannot be achieved in either an analog or a digital system. Secondly, the PR controller's gain is much reduced at other frequencies, and, in itself, it is not adequate to eliminate harmonic influence caused by the presence of grid voltage harmonics. However, in the case of digital implementation on a low-cost fixed-point DSP, the limited computational power and the limited numerical representation precision can restrict this method's utilization.

2.1.2 Stationary Reference frame Control Method in Three-Phase System

Using the previously mentioned current controller, the three-phase inverter controller uses three channels to provide the required three-phase PWM sources (individual single-phase sources). Using the Clarke transform, the three-phase system signals decomposes to two orthogonal signals in stationary reference frame components. These two components are the key for SVPWM. From the transformation matrix, we derive that the phase angle is not needed for the transformation. These components derived from the transformation are time-varying. Therefore, using a simple PI control will not remove the steady-state error. Some approaches employ a proportional resonant controller (P-R), which has gained attention in the stationary reference frame control methodology. The proportional resonant controller transfer

function is defined as:

$$G_{P-R}^{\alpha-\beta} = \begin{bmatrix} K_p + K_i\frac{s}{s^2+\omega^2} & 0 \\ 0 & K_p + K_i\frac{s}{s^2+\omega^2} \end{bmatrix} \tag{2.1}$$

where ω is the controller's resonant frequency, Kp is the proportional gain, and Ki is the controller's integral gain. The PR controller is compatible with the sinusoidal signals as it can eliminate the steady-state error. This controller also compensates low-order harmonics by using a harmonic compensator function

2.1.3 Rotating Reference frame Control Method in Three-Phase System

The other method used for structuring the control loop architecture is the rotating reference frame. The rotating reference frame method is also called the dq- control. This type is widely used in Three-Phase systems by implementing a PI-based control approach. This controller works efficiently for grid-tied inverters due to the advantage of presenting infinite control gain at the steady-state operating point, leading to zero steady-state error. These rotating reference-frame or synchronous-frame regulators have become industry standard for high-performance current-control [18, 19, 20]. The three-phase quantities (such as voltages and currents) are expressed in terms of space vectors. The model generated using this technique adequately describes the performance of the system [21]. Vector control performed in the dq- domain makes the controller side efficient for a wide range of applications. The Three-Phase components are first transformed using Clarke transform to their α-β components, which are time-varying. These time-varying quantities are then subjected to Park transformation, where they form their dq- components. For current control on the inverter, the dq- components of the current are compared to their referred value. The error is fed to a compensator that generates the desired voltages in the synchronous reference frame. The active and reactive power (or voltage) consists of a combination of feedforward signals and decoupling of the inductive cross-coupling. The cross-coupling is

due to the interaction between the inverter, filter, and PWM modulation. The decoupling causes the current interaction between the two components to be eliminated, giving control over the active and reactive power independently. In SPWM, the dq-components must be transformed back to their α-β components. By inverse transformation from rotating synchronous frames to the stationary frame, the modulator can generate the switching device gate signals.

2.1.4 Overview of the relevant published work for single-phase inverters employing the synchronous rotating frame controller

The Clarke Transformation in single-phase inverter controller has been attempted and is discussed in [22, 23, 24, 25, 26, 27, 28]. The idea is that a single-phase quantity can be complemented by a virtual phase that is orthogonal to the actual system. This virtual quantity is obtained either by the derivative of the fundamental signal or through time delaying the original signal by 1/4th of its time. Observations made from literature:

- The synchronous-reference frame controller is popular in Three-Phase inverters as it can achieve zero steady-state tracking error. This occurs because the fundamental frequency components are converted to DC. However, it has limitations in Single-Phase, requiring additional significant computational burden to make use of it at all.

- The theoretical concepts of synchronous-frame converters are presented and discussed in [29]. The author observed that "The only complication with this equivalent single-phase conversion is that the chosen frequency component not only appears as a DC quantity in the synchronous frame, it also contributes to harmonic terms at a frequency of 2ω this is unlike three-phase synchronous dq-conversion where the chosen frequency component contributes only towards the DC term)".

- The harmonics associated with the dq- current components increase with the inductive load. This is due to the increasing phase difference between the current and voltage, which causes feedback current and voltage signal to have the same phase problems. As a result, the reactive loads contribute to an increase in the harmonic terms at a frequency of $2\,\omega$.

- In a Three-Phase system, an unbalanced load can cause the quantities in the rotating reference frame to be no longer be completely time-invariant and they contain a double line frequency component.

- The 2ω harmonics issue can be resolved with various efficient dq- conversion as seen in [30, 31, 32, 33]. The new transformation strategies are no longer computational burdensome. As a result, the system can be implemented with a low-cost fixed-point DSP. The feedback signals are transformed from stationary to rotating reference frames without using trigonometric function computation (in the DSP application the trigonometric function calculation can be time-consuming).

- The idea for stationary reference frame control is credible and efficient but introduces different additional dynamics to the entire loop systems. The capability to achieve infinite gain at the line frequency of the synchronous frame controller, therefore, seems superior.

2.2 Building Blocks for Single-Phase Inverter Controller

In this section, we will be talking about the blocks that revolve around the controller supporting it by modifying and generating certain signals which generally are inputs to our main controller. Grid signals must be modified into their respective α-β and dq- depending on the type of inverter controller we are working with.

2.2.1   Orthogonal Phase Generation in Single-Phase systems

There is a limitation in Single-Phase systems for the implementation of the synchronous-frame controller. As discussed previously, it is the orthogonal component of the real axis or phase. To create the additional phase from the information of the single-phase inverter system, there are few methods in literature to solve the issue:

- Differentiating the inverter output voltage and inductor current. Although the process seems simple enough, this method is susceptible to noise. The presence of harmonics in the real phase to the fundamental component might pose a problem as differentiation does not yield a purely orthogonal component. This will affect the feedback signals, and hence the control actions will not be adequate. Differentiation also requires a higher processing time for micro-controllers.

- In literature, people have proposed observer to construct the orthogonal component. This approach is viable in terms of the result, but it is complex to implement and requires high processing time and high software implementation.

- Earlier work in Hilbert transform to correctly realize the phase shift of the fundamental and harmonics. The Hilbert transform could be found that signal can retain its amplitude and change its frequency after Hilbert transform. The positive frequency is making -90° phase shift and the negative frequency is making 90° phase shift.

- Some of the methods involve eliminating the phase-shifting block from the system. In one approach [34], the filter capacitor voltage and current are inherently 90° phase shifted. However, this is not a good strategy, as the capacitor currents have high switching harmonics.

- There is another approach where the inductor current's orthogonal component

is generated by emulating the inverter output filter in the controller. This method is a model-based approach and the system parameters are likely to undergo changes which will cause a problem in the performance of the signal generation.

- [35] presents a more instantaneous formulation of the orthogonal signal. It is based on the estimation of the fundamental component to creating the orthogonal component. This method is independent of system parameters. It has excellent dynamic performance and can be used for inverters used for power regulation effectively.

2.2.2 Phase Locked Loop

Single-Phase grid-connected power electronic converters have become quite popular in today's systems. These systems thrive on the grid components' knowledge and information (voltage, current, and phase angle). The control performance is dependent on how efficiently and accurately these signals are realized or measured[36, 37]. Voltage phase angles and magnitude have been used to generate references for the inverters. The phase angle information is also used to realize the dq- components of the inverter system [38]. Not only this, island detection and reconnecting back to the grid from islanded-mode is highly dependent on the accuracy of the information that PLL provides.

2.2.2.1 Stationary Frame PLL

These types of PLL are used in single-phase systems due to the lack of multiple signals to synchronize. Another bonus is the higher synchronization speeds over other methods. Usually, systems employ a sinusoidal phase detector (PD) that creates the voltage error, Verror, for the loop filter (LF), which generates ω. The issue with this type of PD is that the 2ω ripple term is inherently created, which causes pollution as it passes through the Loop-filter[39, 40]. To solve this issue, a low pass filter

has been implemented on these PLLs to attenuate this 2ω term [41]. This causes the loop filter's bandwidth to decrease, causing a slower transient response time to perturbation. This also affects synchronization speeds to deteriorate.

$$V_{err} = A\sin(\omega_i t)\cos(\omega_e t) = \frac{A}{2}[\sin{(\omega_i + \omega_e)t)} + \sin{)(\omega_i - \omega_e)t)]} \tag{2.2}$$

In steady-state the 2ω term appears, as seen from (2.2) when ω_e tracks the frequency provided at the input, ω_i. This is because the grid side voltage consistently keeps varying around the nominal value within a small band, this will be the same at the input to the PLL. The mismatch as seen in ((2.3)), causes the angle mismatch between the actual and the PLL estimation value; as such, no matter the state of the PLL, there will always be a 2ω ripple present in the error voltage.

$$V_{err} = \frac{1}{2}A(\sin{(2\theta_i + \psi)}) + \frac{1}{2}(\sin\psi)) \tag{2.3}$$

A common way to reduce the 2ω term is to use LPFs before the LF to attenuate the ripple. The results of adding a 1st order or second-order LPF to the loop. Depending upon the type and order of the filter, this method is seen to reduce the ripple effect but at the cost of re-synchronization speed of the PLL. It is seen that under nominal conditions, the Original PD (O-PD) has a steady-state ripple of approximately 1.2 Hz [41], while the Modified PD (M-PD) has no ripple; under amplitude mismatch, the O-PD can be seen to have about the same ripple, while the M-PD now produces a small 2ω term.

2.2.2.2   Synchronous Frame PLL

Synchronous Frame PLL's are also a common type of PLL found in Single-Phase implementations. The transformation of the grid components to dq- components acts as the PD for the PLL, while the LF and the voltage oscillator remain the same as the generic PLL. The issue here remains the same, which is the accurate generation of the orthogonal component. This affects the PLL frequency and angle estimation

and also the voltage and current signals the inverter controller uses to regulate the output. It is important to keep the information of the grid components in the purest form possible.

- In one of the methods for DQ-based PLL or SRF-PLL, the orthogonal component generation is through a dynamic APF (active power filter). This has an added benefit compared that to the other filters, it preserves the signal quality during the transformation and hence does not affect the synchronization process.

- As mentioned before in the quadrature component generation section, one method is the use of the Hilbert transformer. By using the Hilbert transformer, it is possible to generate a signal, which is orthogonal with the input signal. A Park transformation is then applied to generate the d and q-axis voltages, used in the control loop, in a way similar to the previous algorithm. For low order filters, the gain at the fundamental frequency is low, compared with the gains at harmonic frequencies, suggesting a PLL output highly affected by distortions in the input signal; For higher-order filters, the added time delay makes the utilization of this algorithm not viable for on-line applications.

- The transport delay block is an easier implementation using a FIFO buffer, with size set to $1/4_t h$ the number of samples contained in one cycle of the fundamental frequency.

In [41] the three PLL algorithms presented were implemented in a digital signal processor (DSP), suited for motion control and power electronics applications (TMS320LF2407, Texas Instruments). The table shows the processing time for each PLL, with the Hilbert transformer-based algorithm used as a reference. As it is seen, the transport delay-based PLL exhibits the lowest processing time, followed by the inverse Park algorithm.

Table 2.1: Processing Time for each PLL algorithm

Algorithm	Processing Time
Inverse Park	86.4%
Hilbert Transformer	100%
Transport Delay	74.4%

2.3   Modes of Operation for Grid-Interactive Inverters

The concept of Distributed generation has come in recently. It provides us with many benefits, such as peak shaving to reduce the overall cost of power by generating power during peak load hours and standby generators to provide power during system outages until service can be restored. Grid-interactive inverters play an important part in the distributed generation [42, 43, 44, 45, 46, 47, 48, 49, 50]. The grid-interactive inverter should be able to perform well in both the modes of operation (Grid-connected and islanded-mode), this is to accomplish all the benefits stated above. Sensitive and critical loads can have the benefit of having constant electricity even when there is an outage. Moreover, there should be a seamless transition between the modes to diminish any sudden voltage change across the emergency load or any sudden current change to the grid.

We have advanced significantly in DSPs technology; hence the implementation of complicated algorithms to control the utility-interactive system is now easier, which is beneficial for local loads as they are unaffected by the transition of the grid-interactive inverters. The control methodology used in the two modes follow the ideology,

- The PWM inverter is operated in current-controlled mode when it is connected to the utility and regulates the current injected into the point of common coupling. This also helps us regulate and aid the voltage and frequency at the PCC, but generally, the utility is assumed to be relatively stiff and maintains the voltage across the load. In the stand-alone mode, the PWM inverter is operated in the voltage-controlled mode, which means the controller action changes from

regulating the output power to regulating the output voltage. Thus, the PWM inverter has to be capable of shifting between current-controlled and voltage-controlled modes, to maintain the voltage across the load in the presence of faults on the grid.

- The algorithm must include a technicality required for a smooth transition; that is, when the transfer between the control modes takes place, the circuit breaker must be turned off before the switching of controllers. This is because both the controllers might have a different voltage reference for the output load voltage and could cause high inrush currents.

- For the transfer between the voltage-controlled mode and the current controlled mode, the inverter voltage should match the grid voltage both in magnitude and phase before the transfer switch can be turned on.

2.3.1 Grid Forming Inverters

During the off-grid mode of operation of the inverter, the inverter must feed the local loads with active and reactive power keeping the voltage constant across the loads. Inverter control works in Voltage Control Mode (VCM) which follows the V-f control strategy, keeping the voltage and frequency constant and the loads dictate the current flow. Many strategies have been implemented in literature, allowing PV to be implemented in P-Q control mode (CCM) during on-grid and off-grid, whereas the battery to be operated in V-f (VCM) during the islanded-mode of operation. But this includes a lot of control topologies to be implemented on one single PV-Battery system itself. The type of control used for Grid Forming Inverters and the accuracy of phase-detection by the PLL play an important role in the switching between on-grid and off-grid mode of inverter operations. Recent research has used droop-based control for the grid forming inverters, as they provide power-sharing capability between the inverters and provide the necessary V-f control.

2.3.2   Grid Following Inverters

Converters are termed grid following if their controls are designed for a stiff grid, and they deliver power to the AC grid. Usually, the inverter can be operated by both VCM and CCM as the voltage and frequency are held constant by the grid. The choice is dependent upon the necessity of the user. However, CCM is famous for this operation mode due to the control over the active and reactive power at the inverter output. Droop control methods have made their way in grid-connected modes. They provide the necessary V-f regulation with the control on active and reactive power, similar to Grid-supporting inverters, as discussed in the next section.

2.3.3   Grid Supporting Inverters

In inverter-dominated grids, grid-forming or grid-feeding is not an option since they have to share the active and reactive power amongst them. Also, they are responsible for forming the grid voltage and frequency. These Inverters can operate in grid-connected modes as well; these are called the Grid-support Grid-forming (Gs-Gfm) and Grid-support Grid-feeding (Gs-Gfd) inverters. The GsGfd inverter needs at least one other inverter to be online for regulating voltage and frequency level in the network; otherwise, this type of inverter control is required to switch over to grid-forming or GsGfm control while MG transits to islanding mode.

2.3.4   Grid-Interactive Mode to Stand-Alone Mode

In [50], the inverter remains in current control mode with the grid maintaining the voltage at the PCC constant. On the instant of fault, the grid voltage collapses, which will cause the voltage at the PCC to drop (depending upon the type and distance of the fault). The breaker should trigger instantly (if voltage falls below a preset value), causing the inverter to operate in stand-alone mode. However, the grid current controller and the output voltage controller must be switched between the two modes, so the outputs of both controllers may not be equal during the transferred

instant, which will cause the current or voltage spikes during the switching process [51]. To solve the aforementioned problem, [51] proposes the output voltage controller to compensate the filter capacitor current, and the grid current controller is used to control the grid current. In stand-alone mode, the output voltage controller is used to regulate the output voltage, and the output of the grid current controller is zero. Therefore, the transfer between the two controllers does not exist in this method. The seamless transfer can be achieved with the proposed control method between both modes, even in polluted grid voltage.

2.3.5   Stand-Alone Mode to Grid-Interactive Mode

We are under the assumption that there was a problem on the grid side, causing the inverter to be in islanded-mode. Therefore, right now, the inverter is operating in the voltage-controlled mode with the breaker open. When the fault is cleared, the inverter must reconnect with the grid. During this re-connection, the inverter output voltage and the phase might not be matching with that of the grid. This matching of the inverter and grid side voltages (amplitude and phase) is studied in the literature, and many have proposed several solutions [52, 53, 54, 55]. The process of matching the phase and amplitude of the inverter output voltage depends on the outer loop of the controller and the type of PLL used in the system. Voltage references to the outer voltage control loop are altered to match the magnitude and phase in most cases.

- To avoid the energy intrusion caused by the voltage phase error between the inverter and the grid and maintain the dc side voltage of the inverter steady, the PLL will advance the phase to match it with the grid side every time step. The inverter voltage phase φ_s is detected by PLL, the advanced-phase is defined as δ, and the phase of the reference voltage is $\varphi = \varphi_s + \delta$, where δ is calculated as

following

$$\delta = \delta + \Delta\delta \tag{2.4}$$

- For systems with droop implemented, ω and Voltages are altered by the droop equations either by provided weights or phase advance methods on the equations [56].

- Certain seamless transfer algorithm implementation has been done by the use of SRF-PLL. During the transition, the inverter operates under PLL (Phase-locked loop) mode to synchronize the restored grid voltage; in this mode, the PLL will take the grid as the reference to generate the phase angle (under the circumstance that the fault has been cleared). Therefore, the mode conversion takes place sequentially in the grid-connected mode, the islanded-mode, the PLL mode, and the grid-reconnected [57]. This method applies phase advance strategies on the PLL.

- Estimation techniques or algorithms have been applied to evaluate the grid angle to make the control or corrective action faster [58].

2.4   Power and Energy Management of Inverter Based Devices in Power Grid

The inverter is one of the central devices in various systems requiring energy conversion and interconnection to the AC main utility. The inverter converts DC to AC for the interconnection to take place, in addition to acting as the interface between the energy conversion systems, the local loads, and the grid. It manages the variations in electric power that it receives due to varying generation levels by renewable energy sources (RESs), varying loads, and varying grid voltages. Control topologies or methodologies influence the PCC grid frequency and voltage. Due to the abilities as mentioned above, it is the primary building block of smart-grids in low and

medium voltage levels [59]. Hybrid interconnections of various units are the essential components of the modern micro-grid, such as:

- AC and DC energy sources

- storage (Batteries, Ultra-capacitors)

- AC and DC loads

- different types of converters (AC/DC, DC/DC or DC/AC)

- Active power filters

Storage devices are connected to the utility by PECs as the nature of their generation differs from that of the grid. Usually, an inverter (DC/AC) is used for their interconnection. Batteries are also used in conjunction with other energy sources such as wind and solar for different purposes.

- DC-DC converters are used for connecting DC-based storage elements with RESs which also produces in DC. Storage elements give an extra advantage of storing extra power not required by the loads (usually in off-grid mode of operation). In grid-connected modes, control on batteries can be used for power smoothing purposes, DC-link voltage control, and Active and Reactive power flow control depending on the necessity of the situation.

- DC-AC converters can be used to connect these storage elements to the grid. The type of controller on these converters can modulate the power coming out of the storage elements and help in voltage control, active power filtering, and smoothing [60, 61, 62].

A DSTATCOM is a power electronic converter-based device connected in shunt with the distribution system. However, the use of DSTATCOM like devices increases the cost of the entire system. Inverters nowadays are designed to act both as an inverter, and a FACTs device [63].

- Individual control on active and reactive power on inverters has provided a benefit of controlling voltage and frequency at the point of common coupling locally [64].

- Several identification algorithms and MPC controllers have used inverters to serve as an active power filtering device in power systems [65, 66]. Passive Power Filters earlier were widely used to suppress current harmonics and compensate reactive power in distribution networks due to their low cost, simplicity, and high-efficiency characteristics. Unfortunately, they have many disadvantages such as low dynamic performance, filtering characteristics easily be affected by small variations of the system parameters, resonance problems.

2.4.1   Decentralized Power Management Concept

In General, decentralized power means the generation of power distributed over smaller generators in multiple places rather than having one big generator in one place. This allows more power to travel with less impedance to reach the customers. This concept shows us that smaller areas will benefit from electricity even with an upstream supply outage. Research has shown increasing micro-sources with interdependent strategies will cause the network to become complex. However, this will allow the decentralized power not to require extensive communication with the central power plants.

On the other hand, the concern is that the increasing deployment of individual energy sources uses static inverters. They have different properties when compared to conventional power plants based on rotating electromagnetic generators. For the integration of these decentralized generators, there is a need to develop decentralized control techniques and strategies at different levels to deploy these resources.

When a distributed generator is grid-tied, the voltage and frequency are dictated by the grid. This means that the distributed generator has control over the current

flowing out of the inverter. Synchronization is also an issue that has to be taken care of by the inverter control system to remain grid-tied or switch from islanded to grid-tied mode. Researchers have recently started to use droop methodology for active and reactive power control for the grid-tied mode. [67]

2.4.2 Collective Control of Single-Phase Inverter Devices

Energy management schemes determine output power and voltages of each distributed generation; these signals or information are fed to the interfacing device controller (inverter). Real-time adjustments are feasible in such systems through frequent alterations of the generation output to mitigate problems and meet other targets [68]. Strategies can be made to coordinate such functions. A micro-grid or Single-Phase inverter with an energy source can be operated either in grid-connected mode or in stand-alone mode. The system-level dynamics are dictated by the main grid due to the relatively small renewable energy sources when the inverters are operating in grid-connected mode. In the case of stand-alone mode, its dynamics are dependent upon the connected sources, and the power regulation ability of the inverter [69]. The droop-controlled inverter offers the autonomous operation, and analysis has shown that the parameters determining power-sharing significantly affect stability in stand-alone operation.

- Droop equations suggest the link between voltage and frequency to reactive and active power of the inverter respectively. In transmission systems, this is true due to the high X/R ratio, But in distribution networks, this ratio is smaller and hence the effect of active and reactive power on the voltage and frequency are coupled [70, 71]. This is resolved by modifying the droop equations given in [72, 73]. These equations are given by (2.5),(2.6) and (2.7).

$$f = f_o - K_p \frac{X}{Z} P - P_o + K_p \frac{R}{Z} Q - Q_o \qquad (2.5)$$

$$V = V_o - K_q \frac{R}{Z} P - P_o - K_q \frac{X}{Z} Q - Q_o \tag{2.6}$$

$$\begin{bmatrix} P' \\ Q' \end{bmatrix} = \begin{bmatrix} \frac{X}{Z} & \frac{-R}{Z} \\ \frac{R}{Z} & \frac{X}{Z} \end{bmatrix} \times \begin{bmatrix} P \\ Q \end{bmatrix} \tag{2.7}$$

- The micro-grid is structured to operate in isolated mode from the main utility grid. The system has to make sure that the generation can meet the load energy demands. This is why in designing a micro-grid, sizing is a crucial component for minimizing the cost of operation. Sometimes, the power management systems might fail to serve the load; this can happen when the demand is more than the generation. We can deploy backup systems and generators or apply demand-side management (DSM) during these scenarios, which reduces the mismatch. One of the DSM's critical objectives is to minimize the mismatch during peaks by altering the system load curve. We have several schemes for optimally ensuring the quality and reliability of the supply [74]. Altering the system load curve can be done on the utility side or the consumer side. Demand response (DR)-management program allows the consumers to participate directly. DR is a load shaping tool where plug-in loads can be deployed on the consumer end or plug-in storage systems (batteries) to alter the distribution network's loading.

Centralized control systems are superior in achieving high power quality. However, the main concern is that it has a high cost of implementation and is not reliable as it has a single point of failure. Hierarchical and distributed control systems are reliable and flexible, but their performance is dependent on the communication network. These power management techniques may not be suited for microgrids, especially when the generation is widely dispersed. The autonomous operation of the microgrid is more reliable and easily imple-

mented locally. This can be done by using the droop control methodology, which supports plug-and-play. However, traditional droop fails to achieve economic operation. Hence, several new non-linear droop schemes have been proposed [75, 76]

2.5   Dissertation Direction

This section delves into the direction that this dissertation will provide for power and energy management of inverter-based DERs. We spoke about the control topologies for inverter and various energy management systems employed in current literature. Using this information, we can predict the formulate the skeleton of this research.

2.5.1   Grid and Islanded-mode of Operation of Single-Phase inverters

As discussed, we need to employ the control architecture for both the modes of operation of inverters. We have seen that inverters must regulate the voltage in the off-grid mode and when grid-connected, we can plug and play with our active and reactive powers. This can be done with the concept of *dq*- control [26]. Operating individually is simpler compared to transitioning between the two modes of operation for the inverter. Keeping in mind the switching dynamics between the control modes and the circuit breaker, a novel way for seamless switching is presented in [26]. The switching works on the basic idea of checking the grid's normalcy by using an SRF-PLL, and when the grid is in the acceptable range of operation, the SRF-PLL decides the type of controller to be called upon for the inverter. This can be incorporated in a micro-grid with multiple DGs, as the switching operation's condition is irrespective of the load demand and the power generation.

2.5.2   Unified Inverter Control

The transition between grid-forming and grid-following modes should be seamless, as mentioned in the previous sections. We have seen that in grid-forming mode,

droop control methodology has been implemented for V-f regulation and specific other VCM techniques. Simulation results have shown that for a distribution network, the changes in active and reactive power can affect voltage and the frequency at the PCC significantly, both in off-grid and grid-connected mode. Theoretically, V-control in the off-grid and P-Q control in the on-grid can then be achieved by one controller architecture. The controller's outer loop will have to be a combination of PQ-V control, where the inner current loop reference will be generated by the deviation in the voltage and the Active and Reactive power set-points. The same controller architecture for both grid-forming and grid-following modes can help solve controller complexity and the unnecessary transitioning/switching between various other controller topologies. The additional benefit of the unified controller is, due to its inherent nature of V-f regulation as the priority, the seamless transition between the modes is more straightforward and faster. When talking about seamless transition, this is mentioned when the voltage on the load could be different for CCM and VCM control modes. This could cause high inrush currents, so additional care should be taken for the same.

2.5.3   Strategy for Power Management for Inverters in AC Micro-Grids

There are many ways of controlling individual inverters, as mentioned in the previous sections. As we talk about a Single-Phase grid-interactive inverter, we have discussed that it can regulate active and reactive power during the grid-connected operation mode. Batteries connected to the DC-link allow the bidirectional flow and power smoothing at the output of the inverter. However, the main idea is to keep them operating in islanded-mode as well as grid-connected mode. On-grid, the grid holds the voltage, and the inverter can choose to operate in UPF operation or generate the powers at the set points provided by the utility or operate by the set-points given by the droop control via the unified control architecture. There are several control strategies proposed in the open literature for DG inverters for droop-based control.

These can be classified into Droop-based and Virtual Synchronous Generator-based control strategies [77]. VSG technique utilizes virtual inertia and has damping properties that emulate the dynamic characteristics of a synchronous generator. The droop method does not possess both, and it only emulates the steady-state characteristics of a synchronous generator. Generator Emulation Control (GEC) is a type of VSG-based control that can perform load sharing with droop characteristics. In grid-connected mode, the load power is shared between the grid and GEC inverters, whereas in the islanded-mode, the GEC inverters use the P-ω and Q-V droop control to perform the load sharing. The characteristics of the generator are embedded into the inverter by using impedance and emf emulation techniques [78].

- Cost based: Certain studies have shown advancement in droop topologies by incorporating operating costs. According to these studies, power-sharing for microgrids should not be based on ratings alone [76, 75]. Other factors, such as costs, pricing schedules, should be included in the evaluation and power dispatch, just like most centralized systems.

- Need based: Including the droop topology that just focuses on load sharing based on the ratings, generation-demand inconsistencies can be realized in the algorithm and these inverters can help curb the issue. A different generation or backup system (battery, ultracapacitors) can be deployed to ensure the supply's quality and reliability.

- Balanced Power Flow: Load imperfections can cause unbalance in current and voltage waveforms. This can propagate from the distribution system to the higher power system and vice versa. The recent inverters' ability to control active and reactive power, also regulation V-f locally, can help in curing or dealing with these unbalances. Single-Phase inverters can be deployed in each phase; looking into the grid side for abnormalities and taking corrective action

can be a solution.

- D-STATCOM: Power electronic-based FACTs devices have been developing recently to provide more knowledge and control on power systems. Initially, capacitors banks were used for reactive power compensation. However, as we mentioned the inverter's active and reactive power control capability, we can use this power electronic device for the same. Combining the two concepts, we can develop a so-called D-STATCOM inverter.

CHAPTER 3: Single DER Based Microgrids

This chapter focuses on Single-Phase inverter modeling and control for Grid-Connected (GC) and Stand Alone (SA) mode of operation in dq-domain. A schematic of this can be seen in Fig. 3.1 that utilizes the voltage and current measurement on the output of the inverter and after the Static Transfer Switch, (STS) (or breaker) as feedback signals for GC and SA controls. For the SA mode of operation, a grid-forming methodology is explained where the Single-Phase Inverter (SPI) provides the critical load with a stiff grid, i.e., constant voltage and frequency. For GC mode of operation, a decoupled active and reactive power control is implemented, which provides flexibility for either grid-following or supporting operation. While transferring from GC- to SA-mode of operation, the transition needs to be seamless, i.e., no current and voltage spikes due to phase mismatch or voltage level mismatch with the grid. Hence, a seamless transfer algorithm is proposed in this chapter that enables the SPI to work in SA-/GC-mode and has a manual and auto override option when transitioning between the two modes. Different building blocks for the transition to happen seamlessly, explained in this chapter, are the Synchronous Reference Frame Phase Locked Loop (SRF-PLL), Synchronization check blocks, inner current control, and outer voltage or active and reactive power loop.

3.1   Introduction

Distributed energy resources (DER), connected at the consumer point, are rapidly increasing in the power distribution network (DN). Such a proliferation of DER has altered the power flow pattern and has created voltage regulation issues in the DN [79]. The interconnection of renewable energy resources with the DN is a widely studied

application and is achieved through inverters. These DERs operate in tandem with the grid, having the capability of working in grid-connected mode or islanded/Stand Alone (SA) mode, which forms the basis of what we know as micro-grids. Fig.3.1 is an example of such an inverter connected to the grid via a static switch or breaker. The control loops with the seamless transition allow the inverter to operate in SA or GC mode depending on the grid's normal functioning. One of the major issues with connecting multiple DER to form a micro-grid is the issue of power-sharing and stability of the interconnected system [80]. It is always desirable that such a micro-grid system operates robustly under varying load conditions and generation changes. A robust controller that would act to dampen the effects of disturbances in the system is a requirement for the micro-grid's stable operation.

Considering the rapid implementation of inverter-based DERs in DNs, studies of single-phase inverters' performance, topology, and application for residential systems and low-voltage DERs should be performed. Hence, this chapter will focus on the design and control of single-phase inverter-based micro-grids in grid-connected and stand-alone/islanded-modes.

In terms of energy security, multiple small generators are more efficient than one large generator [81]. Having multiple DG makes the chance of an all-out failure less likely, as there is a backup generator capable of acting quickly and efficiently. Having a component such as a master controller creates a single point of failure, which is not ideal when the end-user demands high reliability of power. [82].

In a DG system, an inverter is usually used to interface a renewable energy source to the grid. This grid-tied inverter should need to operate in grid-connected and off-grid or islanded-mode, depending on the scenario. In the grid-tied mode of operation, the inverter provides the active and reactive power to the loads and the grid if there is a surplus. This is done by controlling the current on the output of the inverter. There have been many strategies proposed; however, in this chapter, a conventional
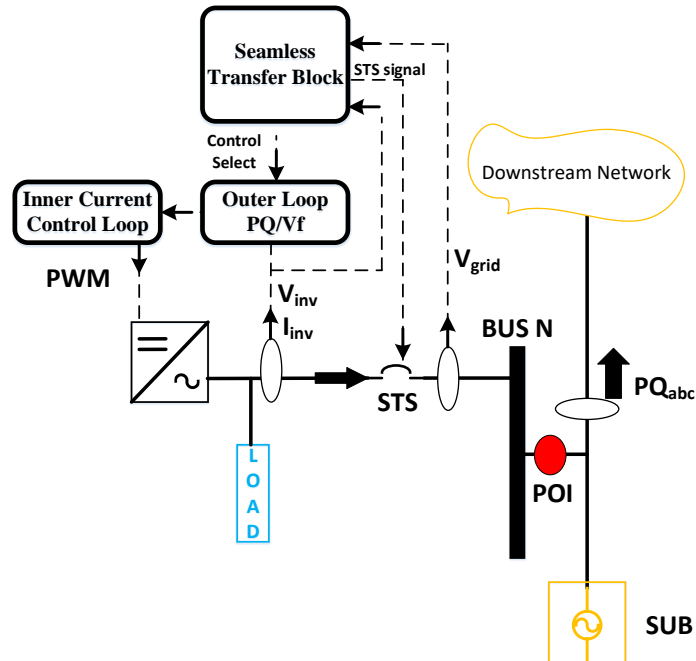
Figure 3.1: Single-Phase Inverter and local controllers for seamless transfer usecase

PI controller is used to regulate the inverter output current in the dq- reference frame. During the off-grid mode of operation, the inverter cannot regulate the current as the active and reactive power is determined by the local loads. It is necessary to control the output voltage in case synchronization needs to be performed. This is to match the synchronization criteria put forth by IEEE.

If a fault occurs on the grid, such as voltage sag or swell, the inverter has to disconnect from the grid and operate in islanded or off-grid mode. In this case, traditionally, the inverter is operated in voltage control mode, as mentioned in the previous paragraph. As the grid recovers from the voltage sag or swell, the inverter system has to reconnect to the grid and operate for the active and reactive power control [83]. The transfer between these two operating modes causes many voltages and current spikes, which causes chattering of the breaker. To avoid such spikes, a seamless transfer has to take place [84].

It mainly focuses on a) Modifications on the outer loop for grid supporting, grid feeding, and grid forming applications based on a unified control topology of the SPI,

b) Accurate and dynamic response of the modified SF-PLL, and c) voltage regulation and unbalance mitigation. This work's contribution is to provide a strategy for customer end inverters to detect grid conditions (anomalies) and decide the inverter's apt mode of operation.

3.2   Main Contributions

The major contributions of this chapter are as follows:

- Formulated a cascaded control topology in dq-frame for single-phase inverters that work in the grid-forming mode for Stand Alone (SA) applications and grid-supporting and following mode for Grid-Connected (GC) applications.

- Seamless transfer algorithm developed for a single inverter-based MG with manual and auto override depending on the application requirement that reduces current and voltage spikes and reduces STS chattering. This is accomplished due to zero current transfer operation, and PLL-assisted seamless transfer.

- Modified dq-control topology is presented in this chapter that eliminates the switching between control modes (Voltage and frequency control mode in SA and Current control mode in GC) when transitioning between islanded and grid-connected modes of operation of MG and vice-versa.

- Utilized a minimum variance-based control methodology to improve current controller response to measurement noise, power tracking, and steady-state error. This also enables scaling the inverter with the same controller architecture and utilizing it in a large LV distribution network.

- Demonstrating the flexible nature of SPIs and the control framework by utilizing it in a three-phase distribution network for mitigating unbalances present in power and locally quenching voltage deviations.

3.3   Simulation Model Description

The modeling was performed on MATLAB Simulink. The simulation model contains the DC module (PV+Batt), the AC module (Synchronous Generator or an infinite voltage source) with an H-Bridge inverter acting as an interface between them. The DC module contains the PV array with the charge controller and boost converter. It contains the DC bus and the battery charging module. The Maximum PowerPoint Tracking (MPPT) algorithm maintains the power output at a constant level for a particular operating point. The MPPT algorithm also provides the duty for the boost converter so that the DC bus voltage is stabilized at 400V. The DC bus is connected to the battery system through a bi-directional buck-boost converter. This is the energy storage element connected in the circuit to provide voltage support and reactive power support to the AC load and the grid.
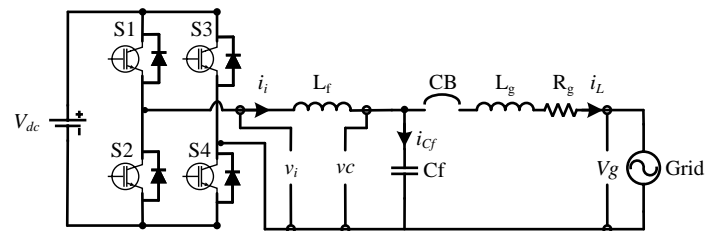
Figure 3.2: Schematic Diagram of the proposed control framework for the Single-Phase inverter.

3.3.1   H-Bridge Inverter

Fig.3.2 shows a schematic of the H-bridge inverter connected to the grid. This inverter is a fundamental topology in power electronics due to its ability to support bidirectional power flow and ease in implementation. This topology enables the battery charging when there is adequate power being pushed into the load by the PV system and the grid and enables the battery's power supply when the grid and PV are not running at their total capacity. Active power is the actual power being delivered to the load to do useful work. This active power is supplied by the PV and the

Table 3.1: Power Transfer corresponding to switching cycle

S.No	Path	Grid Voltage	Grid current	Power Transferred
1	S_1, D_3	$V_g > 0$	$I_g > 0$	Q
2	S_3, D_1	$V_g < 0$	$I_g < 0$	Q
3	S_1, S_4	$V_g > 0$	$I_g > 0$	P
4	S_3, S_2	$V_g < 0$	$I_g < 0$	P
5	S_4, D_2	$V_g > 0$	$I_g > 0$	Q
6	S_2, D_4	$V_g < 0$	$I_g < 0$	Q

battery system on the DC side. Reactive power is that power that keeps circulating in a system between the source and the load; hence it does not contribute to the work done by the load. This power is mainly responsible for charging the magnetizing elements like inductors in the power system. It is essential to understand that the DC side does not deliver the reactive power. It is satisfied by the switch and the freewheeling diode [7].

Table I indicates the various switching intervals and the corresponding relationship between the grid voltage V_g and the grid current I_g. The switching states ('S' to denote the switch as 'closed' and 'D' for the corresponding diode to be 'forward-biased) shown in the table also indicate which type of power is being transferred corresponding to that switching state. 'P' denotes active power, while 'Q' denotes reactive power [85].

3.3.2   AC Module

The AC module contains the AC load and a synchronous generator that acts as the grid. The use of a synchronous generator in the system enables us to analyze the inverter module's performance much better than the use of a rigid ac voltage source. The generator module has the default parameters set, and MATLAB load flow provided the generator's necessary initial parameters. A Single-Phase load is connected to phase A, used to perturb the system. The main focus is to simulate the effect of a PV inverter system working on a grid and the power-sharing it can provide.

3.3.3   Filter Design

An LC low-pass filter is placed in between the inverter and the AC load. Equation (10) shows the relation between the filter cutoff frequency (f_c) and the inductance (L) and capacitance (C) values of the LC Filter.

$$f_c = \frac{1}{2\pi\sqrt{LC}} \tag{3.1}$$

f_c is chosen such that it eliminates the harmonics caused due to the switching frequency, without affecting the fundamental grid frequency. It is imperative that resonant frequency is not too close to the operating frequency, to prevent a region of instability. For the calculations presented in this chapter, the frequency is set as $f_c = 1960Hz$. As there are two unknowns in the equation, one of the values is selected to find the other. Here, $L = 3mHH$ is selected to get a capacitance value of $C = 2.2uF$.

$$tf(s) = \frac{1}{6.6 \times 10^{-9}s^2 + 1} \tag{3.2}$$

Using these values, the transfer function $tf(s)$ of the LC filter is determined as shown in (3.2).

3.4   Grid Connection and Operation

With the current state of the grid changing every year with more renewable-based DERs being integrated at the LV and MV networks, the requirements for power inverters are upgrading and becoming more interactive with the power grid. Grid Connection and disconnection of any grid-tied inverter is based on interconnection and interoperability requirements stated in IEEE 1547. To keep DERs involved or operating during remote faults and various other short-lived voltage and frequency excursions, some settings are adjustable, which needs to be confirmed with the area EPS operator and built into the local DER controller. Hence the DERs are separated

into three abnormal operating performance categories:

- Category I: DERs that meet the minimum Bulk EPS requirement and need to achievable by all DER technologies.

- Category II: Full coordination with the bulk EPS requirements, this category DERs are coordinated with existing reliability standards to avoid tripping for a wider range of disturbances (than Category I).

- Category III:Designed for all bulk system needs and distribution system reliability/power quality needs. Coordinated with existing requirements for very high DER levels.

For this dissertation, category III inverters will be the focus as eventually higher penetration of DER levels will be investigated. Unscheduled intentional islanding will also be the prime focus of this dissertation, these are formed autonomously from local detection of abnormal conditions at the interconnection(s) with the Area EPS, and then automatic relay action that triggers switching action to isolate the intentional island rapidly from the Area EPS.

Table 3.2: Synchronization Limits defined by IEEE 1547 2018

DER unit rating (KVA)	Frequency difference ($\Delta f, Hz$)	Voltage difference ($\Delta V, \%$)	Phase difference ($\Delta \Phi,°$)
0-500	0.3	10	20
500-1500	0.2	5	15
>1500	0.1	3	10

3.4.1   Synchronization and STS operation

Synchronization of the power converters to the grid or the area EPS or bulk EPS is dependent on the parameters described in Table 3.2. Disconnection from the grid depends on the agreement between the area EPS operator and the local controller on certain ride-through functionalities. However, the connection does not have any

time limitations as such for the DERs and power converters. The for connecting back to the grid or area EPS or bulk EPS, three major parameters should be checked for synchronization, namely:

- Voltage check: Considering the grid is back to normalcy, voltages on either side of the STS or switch are compared with each other and the check is passed based on parameters set in Table 3.2. Voltage RMS is the most suitable way to determine the comparison-based result in real-time, therefore RMS values are utilized for this check.

- Frequency check: PLL is utilized to determine the operating frequency of the voltages on either side of the STS. The steady-state difference should be within the band defined in Table 3.2.

- Phase angle check: Similarly, utilizing the same PLL the phase mismatch can be determined and an appropriate check response can be generated when the inverter voltage output is in phase with the grid side voltage angle.
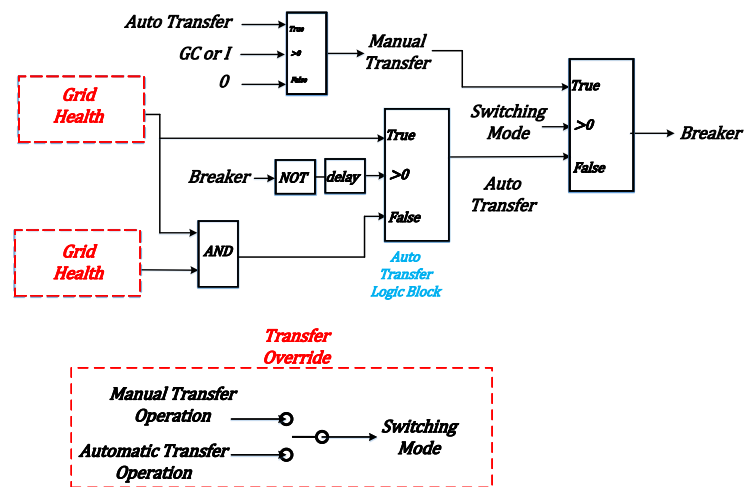
Figure 3.3: high level transfer logic block

Several parts of the local controller are responsible for the entire synchronization process to commence and finally be accomplished. If the microgrid or the local EPS is

islanded from the area EPS or the local grid, the first level of checks would be on the grid side, i.e., grid health. Based on the grid health, a decision (which includes some control setpoint changes) to reconnect to a healthy grid can be made. Therefore, firstly grid health and decision-making blocks surrounding grid health need to be defined. Fig. 3.4b unwraps the transfer logic block at a high level; the sub-set blocks can be explained as follows:

- Grid health block is made up of voltage and frequency-based checks on the grid side. The voltage RMS and its measured frequency are per unitized and compared with 1. This block does not include the phase angle check as this block is to update the local controller on the grid health only so that the follow-up decisions to match the voltage, frequency, and angle can be initiated.

- Synch Check block: This is the block that compares the two voltages on either side of the STS at the PCC. This block includes the frequency, voltage, and phase angle check, and it is only called upon once the grid health has been confirmed as normal operating conditions. Otherwise, the synch check can throw a positive result even when the grid is contaminated or abnormal. Synch check output is based on Table 3.2, only when these parameters are satisfied the synch check block generates a high output for the breaker operation.

- Transfer mode: Transfer mode selectors lets the area EPS operator decide whether to operate the microgrid in islanded or grid-connected mode. The manual transfer mode is equipped with an auto-override where if the grid goes into anomalous operation, the auto override disconnects the microgrid from the area EPS or the grid.

3.4.1.1 Transition from Grid-connected mode to islanded or stand alone mode

Contamination on the grid such as grid voltage sag/swell and faults will cause the signal check block to trip the STS and protect the critical load and the inverter. To

Table 3.3: DER response to abnormal grid operation for performance catergory III

Voltage (p.u.)	Min clearing time (s)	Max clearing time (s)
V>1.2	0.16	fixed at 0.16 (s)
1.1≤V≤1.2	13	0.083
0.88≤V≤1.1	infinite	NA
0.70≤V≤0.88	20	NA
0.55≤V≤0.70	10	NA
V<0.55	1	0.083

Table 3.4: Frequency ride through requirements for abnormal grid operation: catergory III

Voltage (p.u.)	Min clearing time (s)	Max clearing time (s)
V>62	No ride through	instantaneous trip
61.2≤f≤61.8	NA	299
58.8≤V≤61.2	infinite	NA
57≤V≤58.8	NA	299
V<57	0	0.16

avoid the potential escalation of anomalous operation of the inverter; based on Table 3.3 and 3.4 the PLL switches to a stand-alone mode of operation when the grid health check blocks trigger a grid anomaly status. Where the PLL takes a 0 reference for the q-axis voltage rather than the grid side voltage reference. The detailed sequence of events can be illustrated as:

- Signal check block acquires the grid side voltage signal and checks for the frequency and voltage RMS value for normal operating conditions. It evaluates the RMS value and the 60Hz frequency operation every $50\mu s$.

- Signal check block trips the STS based on the ride-through specifications in Table 3.3 and 3.4.

- Immediately upon receiving the trip signal, the PLL provides a constant phase angle refers to the inverter controller by running the inverter PWM are $\omega_o t$.

- PLL reference is switched from v_{qg} to zero, which neutralizes the phase angle's sudden jump and sets the values just before the disconnection. This will ease

(a) synchronism check block   (b) Grid Health Block
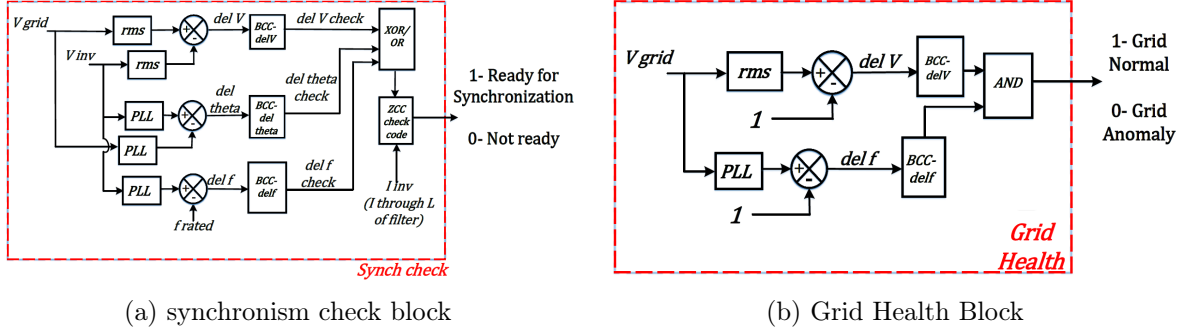
Figure 3.4: STS Transfer Logic block's grid health and synchronization checks

the transition when the frequency returns to nominal operating values.

- The control mode changes from power regulation (or current regulation) to voltage control mode.

3.4.1.2   Transition from Off-Grid to Grid Connected Mode

The removal of the fault will cause the voltage deviation to go away. However, connection to the grid without proper synchronization is not advisable. For synchronization to occur, inverter voltage and grid voltage magnitude must match, and then the phase error between the two voltages should be minimal. The switch on the PLL is dependent on the STS status; as soon as the breaker is switched off, the PLL functions with the q-axis component as zero (off-grid or islanded condition) as shown in Fig. Equation determines whether the frequency synchronism can take place or not. If $\Delta\omega t$ is within a tolerance level, we can use the STS signal to trigger our PLL to take the grid side voltages as the input reference to generate frequency and ωt. When the breaker closes and the Single-Phase inverter is in the grid-connected mode, the control architecture changes from the voltage control mode to the current control mode.

$$\Delta(\omega t) = (\omega t)_{\text{grid}} - (\omega t)_{\text{PCC}} \tag{3.3}$$

The sequence of events for the transition from stand alone mode to grid-connected mode can be explained as:

- Grid health block constantly monitors the grid side voltage and frequency to check for grid normalcy.

- If the parameters are within the range provided by Table 3.2, the PLL of the inverter changes the PWM operation from ω_ot to ω_gt. Where ω_gt is the grid side phase.

- This is when the synch check blocks come in and the three major checks are done,i.e, Voltage, frequency, and phase angle check between the grid and the inverter based on the measurements provided on either side of the STS.

- The control mode changes from voltage control mode to power regulation (or current regulation) mode as soon as the breaker signal is provided with a high value.

3.4.2   Synchronous Frame PLL

SF-PLL is commonly used in three-phase systems [86]. Here, the instantaneous phase angle θ is detected by synchronizing the PLL's rotating reference frame to the grid voltage vector. The PI controller sets the d or q axis reference voltage V_d or V_q to zero. This results in the reference being locked to the grid voltage vector and the phase angle. The grid frequency f and voltage amplitude V_m can be obtained as well. During the stable operation of the grid, PLL includes high bandwidth and accurate detection of amplitude and phase of the grid voltage vector. However, it does not mean that the PLL will not operate when there are harmonics present in the grid [87]. The bandwidth can be reduced to accommodate the distortion caused by high order harmonics, the trade-off being the reduction in the speed of response [88][89].
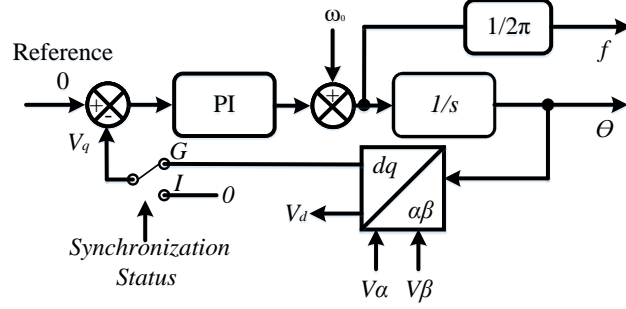
Figure 3.5: SF-PLL for grid-connected and off-grid mode of operation

Fig. 3.5 depicts the logic implementation of the PLL. The idea is to detect and synchronize with the grid while acting quickly to lock the inverter output with the output of the grid. Depending on the synchronization status, the PLL will work either on the grid-connected mode (G) or the islanded-mode (I), as shown in Fig. 3.5. Synchronization status is simply a voltage limit check; it is high when the grid voltage is within limits and low when the grid voltage is beyond the limits (fault condition). In the islanded-mode, we use a constant q axis voltage of 0, while at the grid-connected mode, we use the q axis voltage, which is synchronized to the grid.

$$\frac{di_{Lfd}}{dt} = \frac{-R_f}{L_f} i_{Lfd} + \omega_o i_{Lfq} + \frac{1}{L_f}(D_d * vdc) \tag{3.4}$$

$$\frac{di_{Lfq}}{qt} = \frac{-R_f}{L_f} i_{Lfq} - \omega_o i_{Lfd} + \frac{1}{L_f}(D_d * vdc) \tag{3.5}$$

$$\frac{dv_{Cfd}}{dt} = \omega_o v_{Cfq} + \frac{1}{C_f}(i_{Lfd}) - \frac{1}{C_f}(v_{Cfd}) \tag{3.6}$$

$$\frac{dv_{Cfq}}{dt} = -\omega_o v_{Cfd} + \frac{1}{C_f}(i_{Lfq}) - \frac{1}{C_f}(v_{Cfq}) \tag{3.7}$$

Here v_{Cfd}, v_{Cfq}, i_{Lfd} and i_{Lfq} are the inverter's d- and q-axis output voltages and currents; v_{cd}, v_{cq}, i_{Ld} and i_{Lq} represent the filter's d- and q-axis output voltages and currents; v_{Ld}, v_{Lq} are the d- and q-axis grid voltages. R_f, L_f, and C_f are LC filter variables; and R_g and L_g are the resistance and inductance of the coupling inductor,
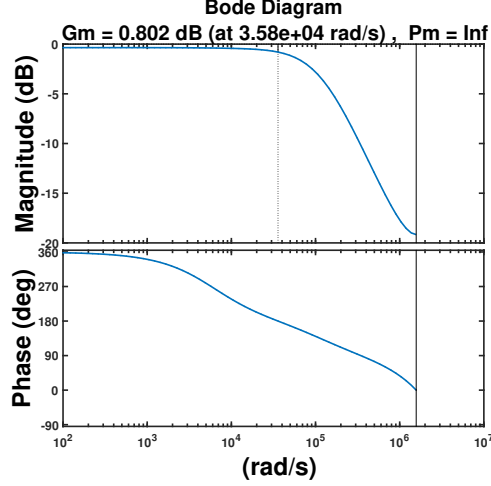
Figure 3.6: Bode plot of the closed loop system.

$$\mathbf{A} = \begin{bmatrix} -\frac{R_f}{L_f} & \omega_o & -\frac{1}{L_f} & 0 \\ 0 & 0 & & \\ \omega_o & -\frac{R_f}{L_f} & 0 & -\frac{1}{L_f} \\ 0 & 0 & & \\ \frac{1}{C_f} & 0 & 0 & \omega_o \\ -\frac{1}{C_f} & 0 & & \\ 0 & \frac{1}{C_f} & -\omega_o & 0 \\ 0 & -\frac{1}{C_f} & & \end{bmatrix} , \mathbf{B} = \begin{bmatrix} \frac{1}{L_f} & 0 & 0 & 0 \\ 0 & 0 & & \\ 0 & \frac{1}{L_f} & 0 & 0 \\ 0 & 0 & & \end{bmatrix}^T , \tag{3.12}$$

$$\mathbf{C} = \begin{bmatrix} 0 & 0 & 0 & 0 & v_{Cfd} & 0 \\ 0 & 0 & 0 & 0 & 0 & v_{Cfd} \end{bmatrix} \tag{3.13}$$

respectively. From this, active and reactive power output of the inverter, P_{inv} and Q_{inv}, is given as,

$$P_{inv} = v_{Cfd}i_{Lfd} + v_{Cfq}i_{Lfq}$$
$$Q_{inv} = v_{Cfd}i_{Lfq} + v_{Cfq}i_{Lfd} \tag{3.8}$$

With the rotating reference frame aligned with output voltage measured after the LC filter, the d-component is $v_{Ld} = V$ and the q-component $v_{Lq} = 0$, where V is the

magnitude of output voltage vector. Hence, the active and reactive power output can be approximated by,

$$P_{inv} = v_{Cfd} i_{Lfd}$$

$$Q_{inv} = v_{Cfd} i_{Lfq}$$

(3.10)

Generalizing (3.4)-(3.7), we get the following state-space form

$$\Delta \dot{x} = \mathbf{A} \Delta x + \mathbf{B} \Delta u$$

$$\Delta y = \mathbf{C} \Delta x$$

(3.11)

where

$$\Delta x = \begin{bmatrix} \Delta i_{Lfd} & \Delta i_{Lfq} & \Delta v_{Cfd} & \Delta v_{Cfq} \end{bmatrix}^T$$

$$\Delta u = \begin{bmatrix} \Delta v_d & \Delta v_q \end{bmatrix}^T$$

$$\Delta y = \begin{bmatrix} \Delta P_{inv} & \Delta Q_{inv} \end{bmatrix}^T$$

A, **B** and **C** are the system state, input and output matrices respectively as given in (3.12).

3.5   Control Strategy in dq- Reference Frame

The control logic begins with the per-unit reference power being provided to the outer-loop current control block this block generates and stabilizes a current reference.

Table 3.5: Base values for the DER inverter

Parameter	Base	Base peak
S_{base}	50000	NA
V_{base}	230	325
I_{base}	217.4	307.4

Table 3.6: Per-unitizing inverter signals before sending it to the local dq-controller

Signal to be per-unitized	p.u. formulae	p.u. value
Active Power or P	$\frac{P_{measured}}{Sbase}$	$\frac{P_{measured}}{50000}$
Reactive power or Q	$\frac{Q_{measured}}{Sbase}$	$\frac{Q_{measured}}{50000}$
Current for DQ-transformation	$\frac{I_{measured}}{I_{basepeak}}$	$\frac{I_{measured}}{307.4}$
Voltage for DQ-transformation	$\frac{V_{measured}}{V_{basepeak}}$	$\frac{V_{measured}}{325}$

$$v_d(t) = L_f \frac{di_{Lfd}(t)}{dt} - \omega_o L i_{Lfq}(t) + v_{Cfd}(t) \tag{3.12}$$

$$v_q(t) = L_f \frac{di_{Lfq}(t)}{dt} + \omega_o L i_{Lfd}(t) + v_{Cfq}(t) \tag{3.13}$$

$$v_{d,k} = L_f \frac{i_{Lfd,k} - i_{Lfd,k-1}}{Ts} - \omega_o L \frac{i_{Lfq,k} + i_{Lfq,k-1}}{2} + v_{Cfd,k-1} \tag{3.14}$$

$$v_{q,k} = L_f \frac{i_{Lfq,k} - i_{Lfq,k-1}}{Ts} + \omega_o L \frac{i_{Lfd,k} + i_{Lfd,k-1}}{2} + v_{Cfq,k-1} \tag{3.15}$$

Assuming within one sampling interval, the current at the consecutive sample intervals are constant.

$$v_{d,k+1} = \frac{L_f}{Ts} \left[i^*_{Lfd,k} - i_{Lfd,k-1} \right] - \omega_o L \frac{i_{Lfq,k} + i_{Lfq,k-1}}{2} + v_{Cfd,k-1} \tag{3.16}$$

$$v_{q,k+1} = \frac{L_f}{Ts} \left[i^*_{Lfq,k} - i_{Lfq,k-1} \right] - \omega_o L \frac{i_{Lfd,k} + i_{Lfd,k-1}}{2} + v_{Cfq,k-1} \tag{3.17}$$

$$v_{d,k+1} = K_p \left[i^*_{Lfd,k} - i_{Lfd,k} + \sum_{m=1}^{k-1} \left[i^*_{Lfd,m} - i_{Lfd,m} \right] \right] - K_c \frac{i_{Lfq,k} + i_{Lfq,k-1}}{2} + v_{Cfd,k}$$

$$\tag{3.18}$$

$$v_{q,k+1} = K_p \left[i^*_{Lfq,k} - i_{Lfq,k} + \sum_{m=1}^{k-1} \left[i^*_{Lfq,m} - i_{Lfq,m} \right] \right] - K_c \frac{i_{Lfd,k} + i_{Lfd,k-1}}{2} + v_{Cfq,k}$$

$$\tag{3.19}$$

Utilizing 3.20, the inner current loop controller has been described in the previous sections. This allows the inverter to control the inverter current output without having to control the output voltage, hence this can be utilized for grid-tied applications [90]. Although, the outer loop can be defined or formulated such that this current-controlled inverter can be utilized for not only grid-tied applications but for Stand-Alone (SA) applications as well. The next few sections will describe this structure in detail.

3.5.1 PQ-based Control for Grid-tied Operation

A grid-connected inverter is a current source when viewed from the grid side, and it is the inverter output current that is regulated by the current control loop. For this mode of operation, the grid side voltage and phase sensing are important as the dq-axis transformation is dependent on this. The control strategy used in this paper involves an active and reactive power control loop as the second outer loop and current control as the primary inner loop as shown in Fig. 3.7. The active power is linked

with the d-axis component of the inverter output current and reactive power with the q-axis component as already seen in (3.20). The *dq*-axis components of the current are acquired from the Park's transformation block with the phase angle estimated from the SF-PLL.

$$
\begin{aligned}
i_{Lfd}(t) &= \frac{P_{inv}(t)}{v_{Cfd}(t)} \\
i_{Lfq}(t) &= \frac{Q_{inv}(t)}{v_{Cfq}(t)}
\end{aligned}
\tag{3.20}
$$
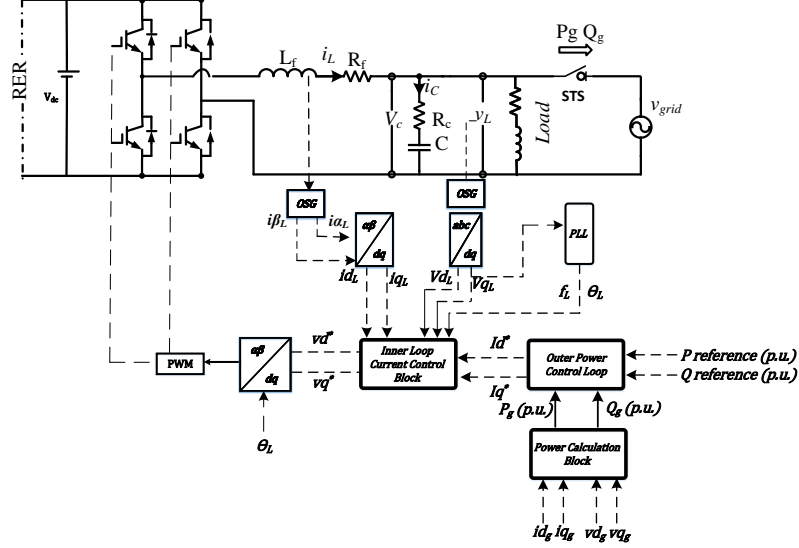
Figure 3.7: Grid connected inverter and controller architecture.

The active and reactive power calculation is performed using the equations, where the *dq*-axis signals of inverter output voltage and current are utilized to evaluate the output powers. This serves as the feedback signals to the outer power control loop, and the goal of this loop is to provide efficient active and reactive power tracking and zero steady-state error during normal grid conditions.

3.5.2 Vf-based Control for stand alone or islanded Operation

The inverter control topology is a dual loop controller; the outer loop regulates the voltage across the capacitor and the inner loop regulates the inductor current. PI controllers cannot achieve zero steady-state error for sinusoidal signals, hence converting the measured voltage and current signals are converted to their respective *dq*-axis components. Stand-alone or islanded-mode of operation requires the inverter to provide or form the grid, hence it is a necessity to maintain the output voltage and frequency constant. This can be achieved using the architecture shown in Fig. 3.8.
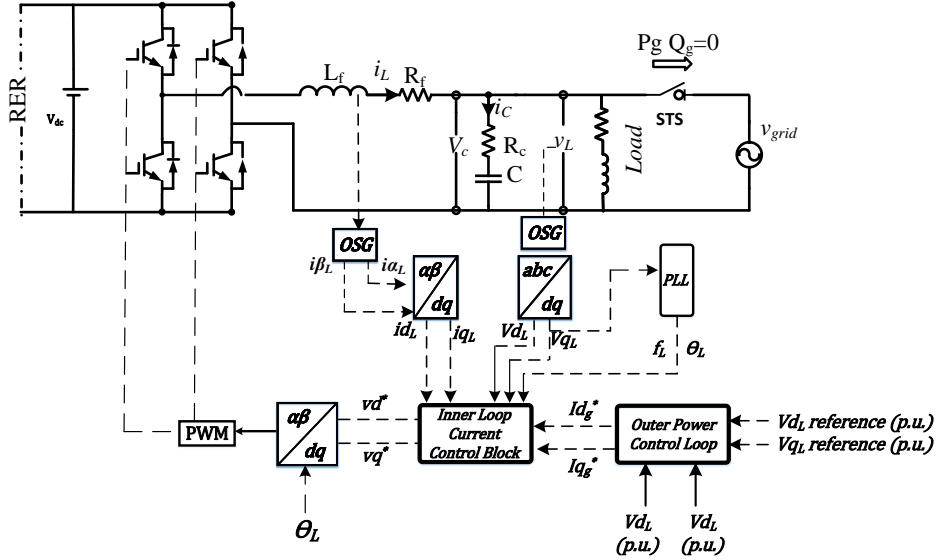
Figure 3.8: Stand Alone inverter and controller.

$$i_{Lfd,k} = -C_f \left[\frac{v_{Cfd,k} - v_{Cfd,k-1}}{Ts} \right] + \omega_o L \frac{v_{Lfq,k} + v_{Lfq,k-1}}{2} + v_{d,k-1} \qquad (3.21)$$

$$i_{Lfd,k+1} = -\frac{C_f}{Ts} \left[v_{Cfd,k}^* - v_{Cfd,k-1} \right] + \omega_o L \frac{v_{Cfq,k} + v_{Cfq,k-1}}{2} + v_{d,k-1} \qquad (3.22)$$

$$i_{Lfd,k+1} = K_p v \left[v^*_{Cfd,k} - v_{Cfd,k} + \sum_{m=1}^{k-1} \left[v^*_{Cfd,m} - v_{Cfd,m} \right] \right] + K_c \frac{v_{Cfq,k} + v_{Cfq,k-1}}{2} + v_{d,k}$$

$$(3.23)$$

3.6 Unified Inverter Control

This section discusses the unified inverter power control implemented on the SMIB MG system. The active and reactive power controller block is a constant in both islanded and grid-connected operations. The methodology is based out of droop where voltage deviation provides for the additional power references to the outer power control loop. Considering the islanded-mode of operation of the MG, the power controllers on the outer loop work on references set by the user which might cause the voltage to deviate from the nominal as power generated by the DER will not be the same as the power demanded by the MG. Hence, an additional ΔP or ΔQ is added to the power set-points to compensate for the voltage deviation. For low voltage distribution networks the voltage magnitude alteration is dependent on the active power and frequency is dependent on the reactive power (which is the opposite in traditional HV networks or transmission systems). Therefore, the outer loop is such that the d-axis voltage deviation provides for ΔP and q-axis voltage (which is utilized in PLL to modulate or track the frequency of the MG) is utilized to regulated or modulate reactive power set-point by providing ΔQ.

3.6.1 Inverter Control Design based on PI Control

The Grid-connected inverter has the grid side voltage maintained as shown in (4.46). From this, one can control the active and reactive power by controlling i_{Ld} and i_{Lq}, and further, the control action propagates to the modulating waveform by changing the output voltage v_{cd} and v_{cq}. v_{cd} and v_{cq} can be changed by changing the
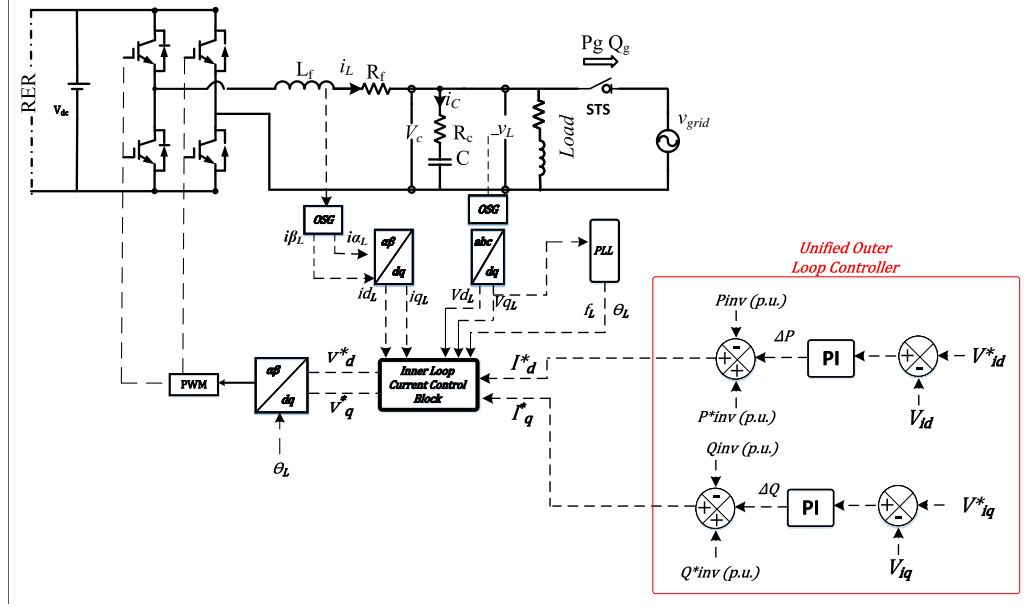
Figure 3.9: Proposed Unified Controller

inverter output voltage v_{invd} and v_{invq} respectively. For designing a conventional PI control, (3.11) and (3.12) are first converted into a transfer function form. The discrete model representation can then be written as (assuming a third-order approximation):

$$\frac{i_{invdq,k} - i_{invdq,k-1}}{Ts} = -\frac{R_f}{L_f}\left(\frac{i_{invdq,k} - i_{invdq,k-1}}{2}\right)$$
$$-\omega_o \frac{i_{invdq,k} - i_{invdq,k-1}}{2} + \frac{1}{L_f}\left(v_{invdq,k-1} - v_{dc,k-1}\right) \qquad (3.24)$$

Where Ts is the sampling of the simulation and, k is the current or kth sample of the respective parameter. Either using the discretized (3.11) or the Zero Order Hold (ZOH) representation, the controller can be tuned. A tuning method based on phase and gain margins [91] (see Fig. 3.6), is used for tuning the PI controller. Table 3.6 shows the PI control gains for simulation purposes. Plots in Fig. 3.6 show the designed gain and phase margins.

Table 3.7: PI control gains

Control Loop	Type	Kp	Ki
Outer Power Control	PI tuned based on SMIB	0.3	1
Inner Current	PI tuned based on SMIB	0.7	10
Outer Power Control	PI re-tuned for IEEE 123 bus system	0.8	3
Inner Current	PI re-tuned for IEEE 123 bus system	10	30

3.7   Simulation Results for Seamless Transfer Operation of Grid-tied Inverter

To verify the proper functioning of our proposed seamless transfer control, we set up a simulation in Simulink and the following cases were performed:

- Test PQ control mode only with the inverter in grid-tied mode.

- V-f control mode only with the DER and inverter in stand-alone mode.

- Transitioning between GC and SA mode during frequency swell

- Transitioning between GC and SA mode during voltage and frequency sag with manual override.

3.7.1   Active and Reactive Power Control in Grid-Connected Mode

Fig. 3.10 and Fig. 3.11 shows the simulation results of the grid-connected mode of our Single-Phase inverter. Active and reactive power control references were changed randomly and a similar change on the output of the inverter was observed as shown in Fig. 3.10. This type of control can be achieved by controlling the flow of current on the inverter output, this is done by the inner current loop in the control architecture and shown in Fig. 3.7. The frequency plot also validates the normal operation of SF-PLL during the random changes of active and reactive power flowing towards the grid.

3.7.2   Output Voltage Control in Off-Grid Mode

As stated in the previous section, in the off-grid mode of operation of our Single-Phase inverter the output voltage control mode is selected by the controller. This
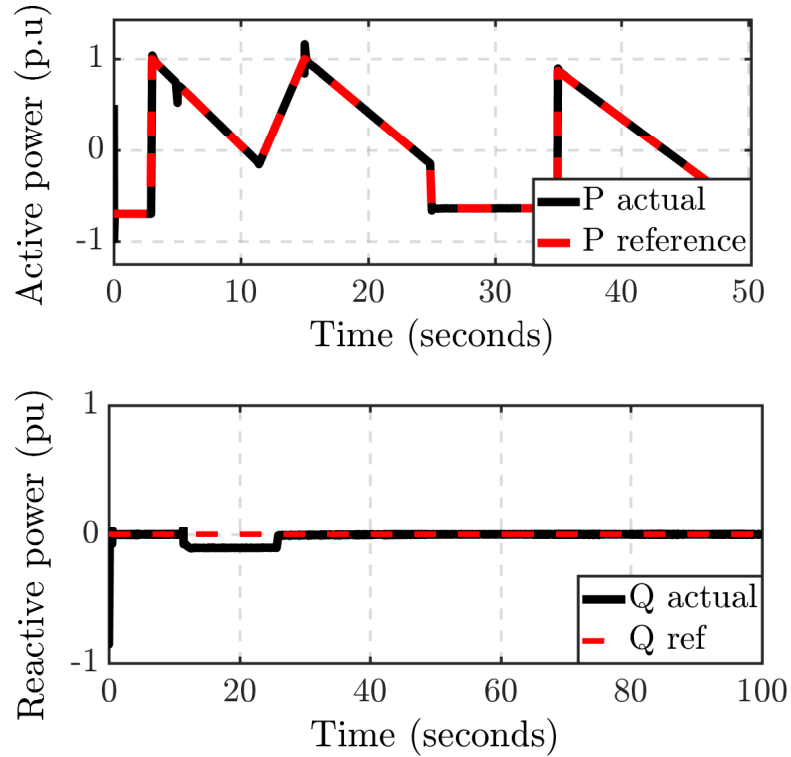
Figure 3.10: Active and Reactive power supplied by the inverter during grid connected mode according to their set references.

means that the primary function of the controller is not active and reactive power control, but to maintain the output voltage of the inverter constant at $230V_{rms}$.

Fig. 3.13 shows the *dq*- axis voltage and frequency of the inverter output. Small disturbance or transients are seen are due to the abrupt load changes, shown in Table 3.8, on the inverter output. Fig. 3.12 shows the active and reactive power changes due to the above-mentioned load changes and. This test was done to verify the proper functioning of the voltage control loop during the off-grid mode of operation of the

Table 3.8: Load Changes During Off-grid Mode Of Operation

Time (s)	Active Power (pu)	Reactive Power (pu)
0-13.5	0.28	0
13.5-24.5	0.44	0.06
24.5-42.5	0.85	0.15
42.5-81	0.43	0.06
81-100	0.3	0
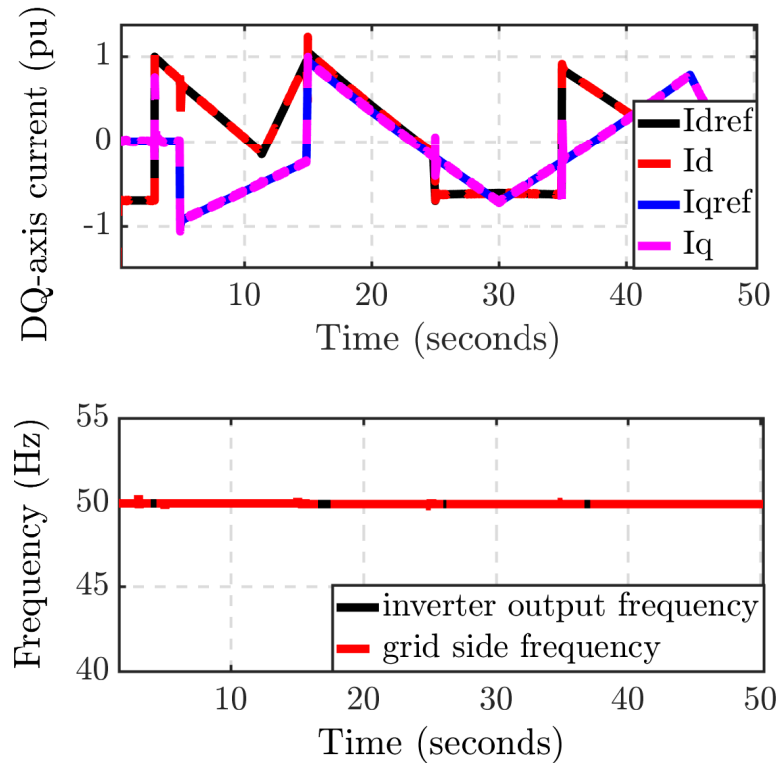
Figure 3.11: *dq*–axis reference and actual inverter output current, the grid and inverter output frequency during the grid-connected mode of operation

inverter.

3.7.3   Transfer Between On-grid and Off-grid Operation- Frequency Swell

We have discussed, in the previous sections, the transfer algorithm to be implemented on our Single-Phase grid-tied inverter. To validate the working of this algorithm, we connected the controller on our Single-Phase grid-tied inverter and tested it out for a voltage sag on the grid. To simulate the grid voltage sag, we lowered the field voltage of the synchronous generator (which acts as our grid). As the load connected to the system is voltage-dependent, lowering the voltage causes the generator to accelerate and consequently increasing the frequency of the grid as seen in Fig. 3.14. The voltage sag is seen in Fig. 3.16, we can observe that at around 10 seconds into the simulation the grid voltage starts dipping.

As soon as the voltage goes below 0.98 p.u. , the controller acknowledges it as an
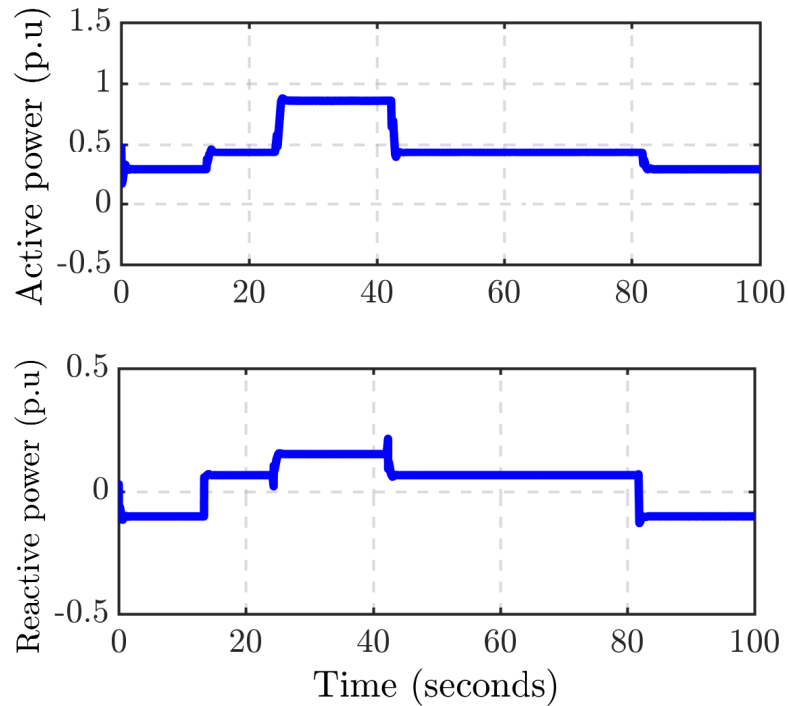
Figure 3.12: Active and Reactive power supplied by the inverter during off-grid mode of operation.

anomaly and trips the breaker as seen in Fig. 3.15. This breaker stays open even when the voltage is in the required limit as shown in the figure and shows the synch status or the synchronization status which is the voltage band test.

The synch status tells us whether the grid side voltage is within the limits or not, this is used to initiate the synchronization process. As soon as the grid frequency drops below 50.5 Hz the SFPLL switches back to the grid reference as seen in Fig. 3.14. The breaker is only closed when the phase difference or the $\Delta\omega t$ is within a small band limit, here we have it as 3 radians. In this case, we have considered unity power factor operation for the inverter.

3.7.4 Transfer Between On-grid and Off-grid Operation with Manual Override

This section discusses the addition of manual override to the seamless transfer block shown. The addition is shown in Fig. 3.4b, where the end-user has the benefit
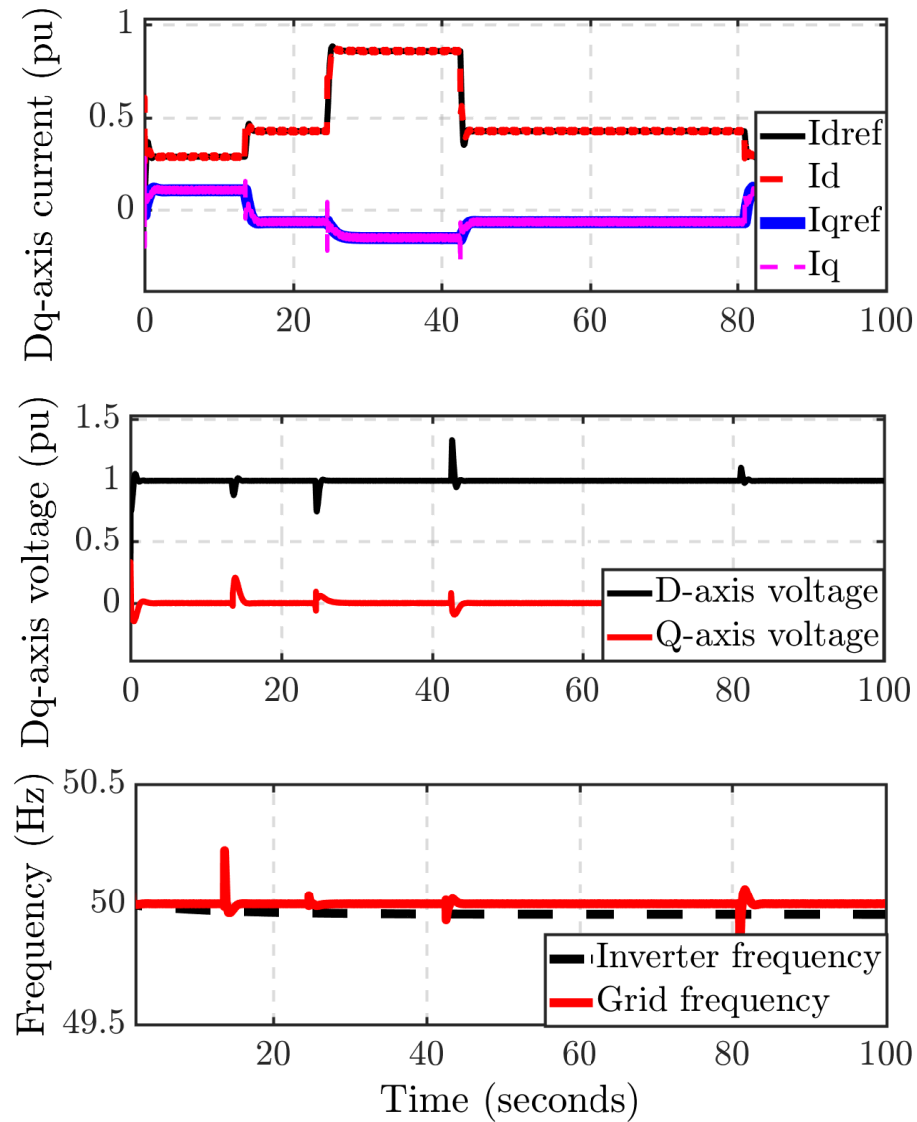
Figure 3.13: *dq*–axis reference and actual inverter output current, Dq-axis inverter output voltage and the grid and inverter output frequency during the off-grid mode of operation
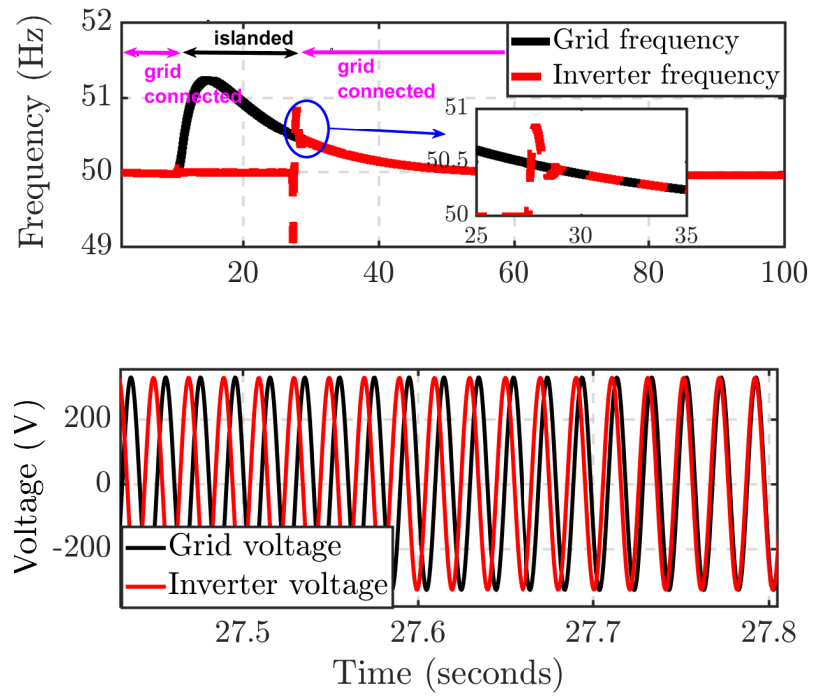
Figure 3.14: PLL performing seamless transfer from off-grid to grid connected mode as seen in the output frequency, inverter and grid voltage respectively.
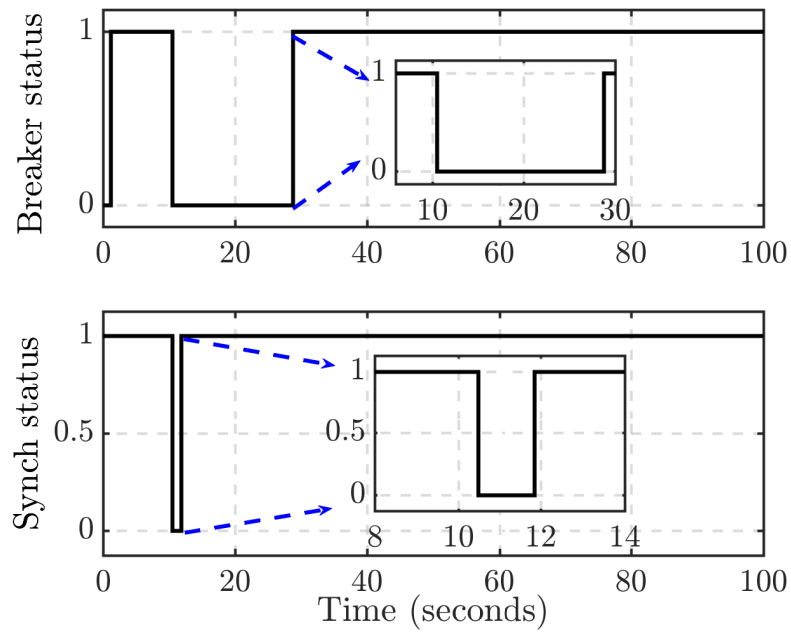
Figure 3.15: Breaker and synchronization statuses for initiating the seamless transfer for grid connection
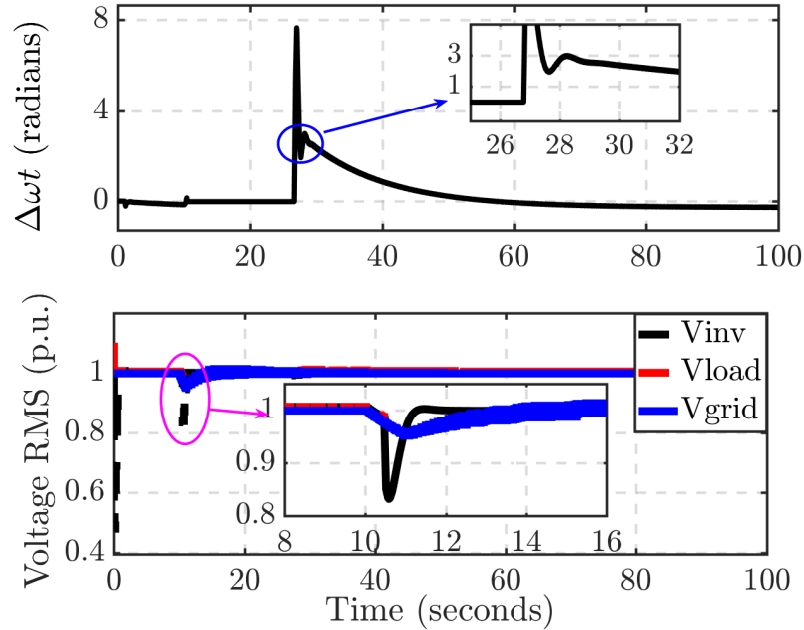
Figure 3.16: Phase angle difference (top) grid and inverter side voltages during the transition (bottom).

of manually disconnecting the DER from the local EPS. The two simulation cases are frequency and voltage sag on the grid side with manual transfer initiated at the 50-second simulation time mark.

case 1 harsh voltage sag with manual transfer: Fig. 3.17 shows the grid side and inverter output voltage during the voltage sag excursion. At 5 second mark, the grid-side voltage steps down to 0.64 p.u. The inverter rides through for 2 seconds and then disconnects from the grid to operate at the rated voltage of 1 p.u. with a 7% overshoot. This is in the allowable range of inverter operation.

case 2 frequency sag with manual transfer: Fig. 3.20 shows the grid side and inverter output frequency during the frequency sag excursion. The observation that can be made looking that the figure is that the inverter frequency is always within the allowable operating range of the inverter.

Fig. 3.22 shows the breaker operation during the frequency sag excursion, and it can be observed that the inverter was allowed to ride through for 0.16 seconds before
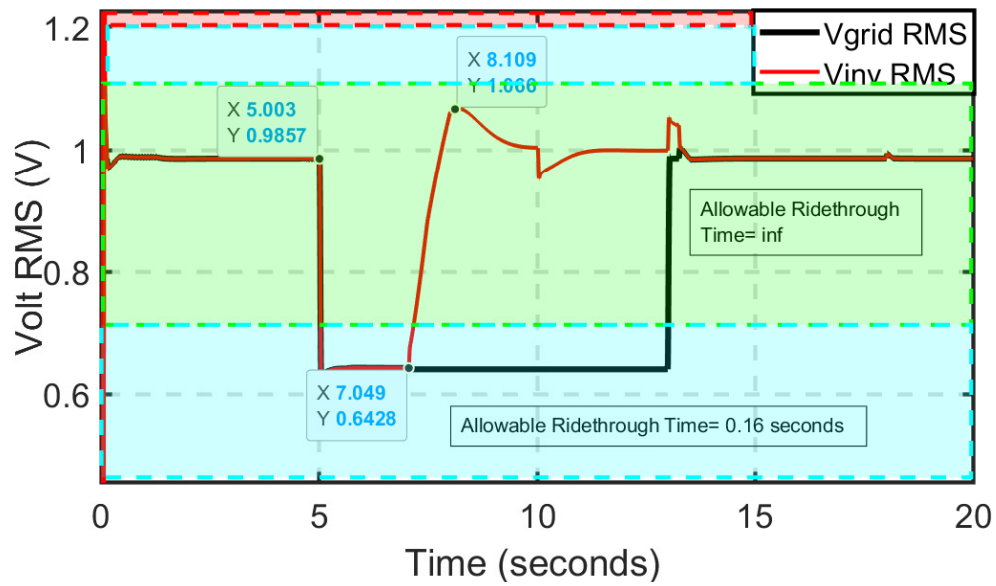
Figure 3.17: Transfer Logic Block with flexible manual override
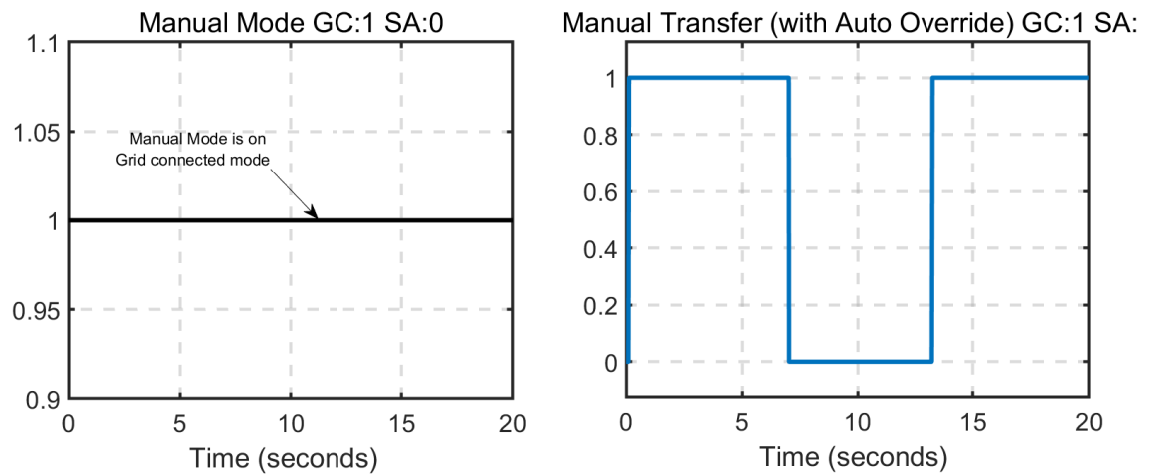
Figure 3.18: Transfer Logic Block with flexible manual override
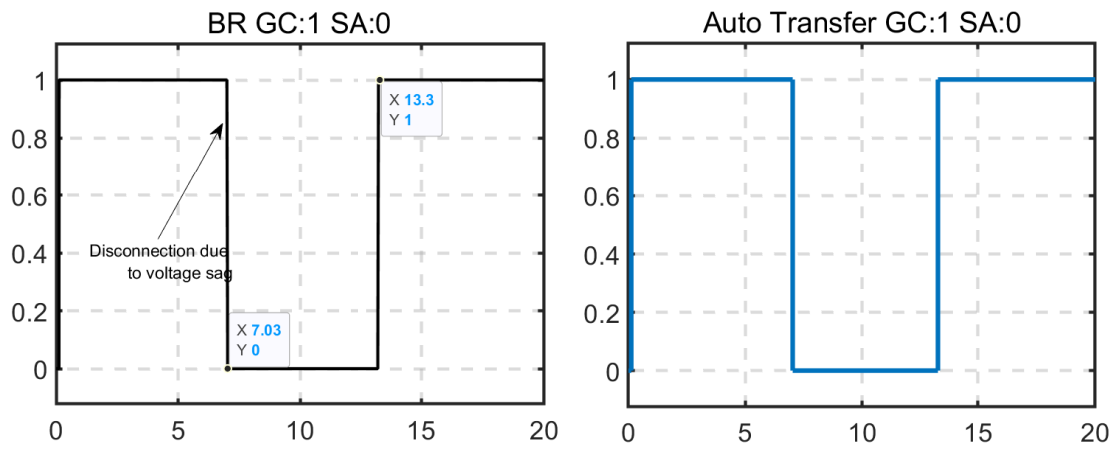
Figure 3.19: Transfer Logic Block with flexible manual override
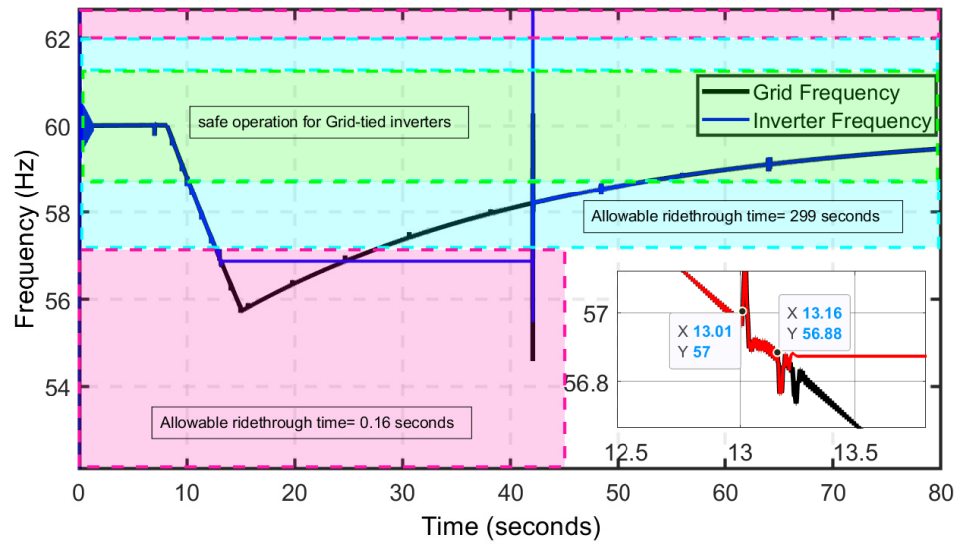
Figure 3.20: Frequency graph for frequency sag excursion

disconnecting from the grid.
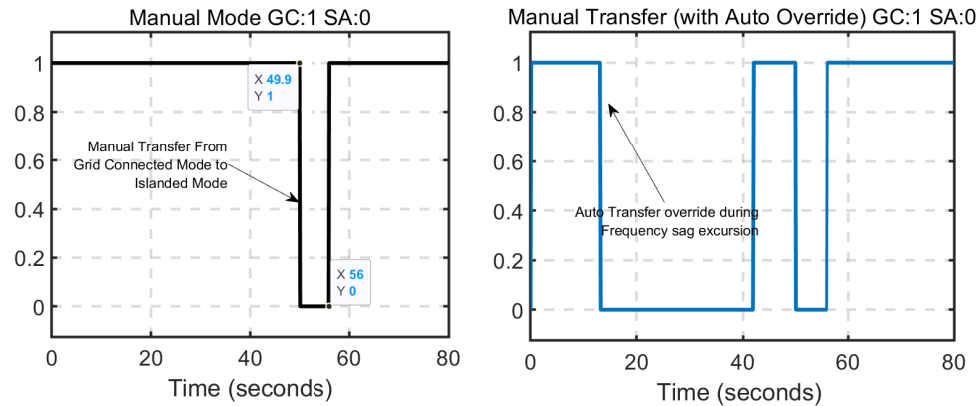
Figure 3.21: Manual Override graph for frequency sag excursion

During the manual transfer at the 50-second mark, as shown in Fig. 3.21, it can be observed that the inverter frequency tracks the grid side frequency. The reason for this is that the inner grid health and synch check blocks do not see an anomaly on the grid side and hence operate the inverter in tandem with the grid.
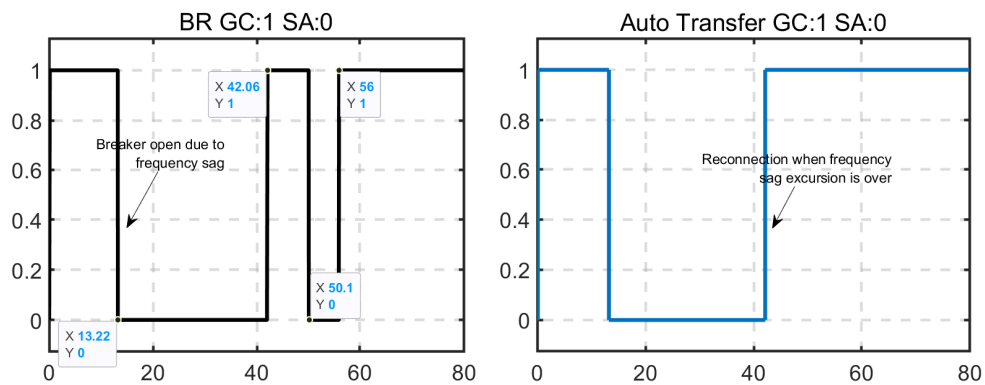
Figure 3.22: Breaker status for frequency sag excursion

3.8   Adaptive control of a Single-Phase Inverter

Fig. 3.23 presents the schematic of an adaptive control system implemented on a single-phase inverter. The adaptive controller comprises of three main components;

1. The plant to be controlled

2. System identifier

3. Controller-based on identified system parameters

Based on how the power variables are related to the inverter output voltage, presented in section 3.5, the system is represented by a third-order polynomial which is processed by the identifier. The design of the system identifier and the minimum variance adaptive control are presented below.

3.8.1 Recursive Least Squares Estimation

The z-domain transfer function parameters of the single-phase inverter system are identified every sample period $'k'$ using the input signal $'v_{invd}(k)'$ and output signal $'P_inv(k)'$ of the system. The system can be represented by a 3rd order z-domain transfer function of the following form for active power control loop:

$$\frac{P_{inv}(k)}{v_{invd}(k)} = \frac{b_0 z^{-1} + b_1 z^{-2} + b_1 z^{-3}}{1 + a_1 z^{-1} + a_2 z^{-2} + a_3 z^{-3}} = \frac{B(z^{-1})}{A(z^{-1})} \tag{3.13}$$

which in turn can be represented by a difference equation form for sample $'k'$ as,

$$P_{inv}(k) = -a_1 P_{inv}(k-1) - a_2 P_{inv}(k-2) - a_3 P_{inv}(k-3)$$
$$+ b_0 v_{invd}(k-1) + b_1 v_{invd}(k-2) + b_2 v_{invd}(k-3) \tag{3.14}$$

Similarly for sample $'k - N + 1'$

$$P_{inv}(k-N+1) = -a_1 P_{inv}(k-N) - a_2 P_{inv}(k-N-1) - ....$$
$$a_3 P_{inv}(k-N-2) + b_0 v_{id}(k-N) + ...$$
$$b_1 v_{id}(k-N-1) + b_2 v_{id}(k-N-2) \tag{3.15}$$

$'N'$ is the observation length and the group of difference equations (3.14) and (3.15) can be written in the following matrix form:

$$X = \begin{bmatrix} -P_{inv}(k-1) & . & -P_{inv}(k-3) & v_{invd}(k-1) & . & v_{invd}(k-3) \\ -P_{inv}(k-2) & . & -P_{inv}(k-4) & v_{invd}(k-2) & . & v_{invd}(k-4) \\ ... & . & ... & ... & . & ... \\ ... & . & ... & ... & . & ... \\ -P_{inv}(k-N) & . & -P_{inv}(k-N-2) & v_{invd}(k-N) & . & v_{invd}(k-N-2) \end{bmatrix}$$

(3.17)

$$\overbrace{\begin{bmatrix} P_{inv}(k) \\ P_{inv}(k-1) \\ \vdots \\ P_{inv}(k-N+1) \end{bmatrix}}^{N \times 1} = \overbrace{[X]}^{N \times 6} \overbrace{\begin{bmatrix} a_1 \\ \vdots \\ a_3 \\ b_0 \\ \vdots \\ b_2 \end{bmatrix}}^{6 \times 1}$$

(3.16)

$\underbrace{\qquad}_{\Phi_{\text{model}}} \qquad \underbrace{\qquad}_{\Theta}$

where X is given by (3.17).

The error between the actual system and the system model is given by $'\epsilon'$,

$$\epsilon = \Phi_{\text{system}} - \Phi_{\text{model}}$$

(3.18)

where Φ_{system} is the vector of measured system output variables.

From (3.16), $\Phi_{\text{model}} = X.\Theta$ can be substituted in (3.18) to get,

$$\epsilon = \Phi_{\text{system}} - X.\Theta$$

(3.19)

The basis of the least squares identification is to minimize the square of the error

$'\epsilon'$ for which a criterion $'J'$ is defined as,

$$J = \epsilon^t \epsilon = \sum_{i=k}^{k+N} \epsilon^2 \tag{3.20}$$

On minimizing the criterion $'J'$, the system parameters $'\Theta'$ representing the parameter vector is solved and the following form of the equation for $'\Theta'$ is obtained.

$$\Theta(k) = \Theta(k-1) + K(k) \left[\Phi(k) - X^t(k)\Theta(k-1) \right] \tag{3.21}$$

where

$$K(k) = \frac{P(k-1)X(k)}{\gamma + X^t(k)P(k-1)X(k)} \tag{3.22}$$

$$P(k) = \frac{[I - K(k)X^t(k)]\,P(k-1)}{\gamma} \tag{3.23}$$

where $K(k)$ is the Kalman filter gain, $P(k)$ is the co-variance matrix of the error during the estimation of parameter vector Θ which has the size of 6×6, I is the identity matrix of size 6×6 and, γ is the forgetting factor.

Once Θ is solved using (3.21), the parameters $a_1, a_2, \ldots, a_3, b_0, b_1, \ldots, b_2$ which define the 3rd order transfer function model of the system can be obtained. Once the parameters are obtained, the controller can be designed using the identified parameters.

3.8.2   Minimum Variance Control

In this section, the design methodology of the minimum variance controller is discussed. The minimum variance controller is a digital control technique utilizing the parameters of the transfer function representing the system along with the past inputs and outputs. The goal of the minimum variance controller is to closely regulate the

active and reactive power of the SPI by generating the proper voltage sequence to generate PWM pulses. The derivation of the minimum variance control law for the active power output of the inverter is shown below and a similar process is followed for the control law derivation of the reactive power. For the minimum variance control design, the system is assumed to be described by the Controlled Auto Regressive Moving Average (CARMA) model. i.e.

$$\epsilon_{P_o}(k) = \frac{B(z^{-1})}{A(z^{-1})} \times v'_{invd}(k) + \frac{C(z^{-1})}{A(q^{-1})} \times \varrho(k) \tag{3.24}$$

where $\epsilon_{P_o}(k) = P^*_{inv}(k) - P_{inv}(k)$, $P^*_{inv}(k)$ is the reference active power to be delivered to the grid, $P_{inv}(k)$ is the actual active power being delivered, v'_{invq} is the q-axis voltage sequence applied at k^{th} instant in time in the inverter, ϱ is the error in the model representation.

CARMA model is used in the proposed design, as this representation has some level of uncertainty and randomness built-in, which considers the future correlation of the inverter with past responses. The assumption is valid as the inverter operation in the power system has similar behavior. Moreover, the moving average part will filter or smooth out any short-term irregularity or inconsistencies in the data series, which helps in obtaining a smoother model of the system. White noise modeling for estimation error is included as it is assumed that the estimation error is independent of past errors and there is no auto-correlation of the estimation error with its past terms. This is also a valid assumption. Based on the system time delay information, the minimum variance controller minimizes the variance of the output at $k + d$ with respect to the expected value of output at $k + d$ using the information gathered at up to time instant k. i.e the controller goal is to minimize the following objective

function:

$$J(k) = E_x\{\epsilon_{P_o}(k+d)^2\}$$

where d is the assumed system delay and E_x represents the expected value of the output d steps into the future, which in this case is zero.

Based on the derivation of the relation between power variables and inverter output voltages in section 3.5, a third-order linear representation of the system is selected. This can be represented as

$$
\begin{aligned}
A(z^{-1})\epsilon_{P_o}(k) &= B(z^{-1})v'_{invd}(k) + C(z^{-1})\varrho(k) \\
A(z^{-1}) &= 1 + a_1 z^{-1} + a_2 z^{-2} + a_3 z^{-3} \\
B(z^{-1}) &= b_0 z^{-1} + b_1 z^{-2} + b_2 z^{-3} \\
C(z^{-1}) &= 1
\end{aligned}
\tag{3.25}
$$

From the system equation in (3.25), it can be observed that,

$$
\begin{aligned}
\epsilon_{P_o}(k) = &-a_1 z^{-1}\epsilon_{P_o}(k) - a_2 z^{-2}\epsilon_{P_o}(k) - a_3 z^{-3}\epsilon_{P_o}(k) + \\
&b_0 z^{-1}v'_{invd}(k) + b_1 z^{-2}v'_{invd}(k) + b_2 z^{-3}v'_{invd}(k) + \varrho(k)
\end{aligned}
\tag{3.26}
$$

Now, if the time index in prediction is shifted by one, (3.26) can be written as,

$$
\begin{aligned}
\epsilon_{P_o}(k+1) = &-a_1\epsilon_{P_o}(k) - a_2\epsilon_{P_o}(k-1) - a_3\epsilon_{P_o}(k-2) + \\
&b_0 v'_{invd}(k) + b_1 v'_{invd}(k-1) + b_2 v'_{invd}(k-2) + \varrho(k+1)
\end{aligned}
\tag{3.27}
$$

The left-hand side of equation (3.27) represents the output signal, and it is one-time step ahead. The right-hand side has the information about the present and past

output signal, present and past input signal, and future model estimation error. The control action $v'_{\text{invq}}(k)$ is computed to optimize the variance of the output one step ahead in the future as

$$\min_{v'_{\text{invd}}(k)} \{J(k)\} = Min E_x \{ \epsilon_{P_o}(k+1)^2 \} =$$

$$Min E_x \{ [(-a_1)\epsilon_{P_o}(k) + (-a_2)\epsilon_{P_o}(k-1) + (-a_3)\epsilon_{P_o}$$
$$(k-2) + (b_0)v'_{invd}(k) + (b_1)v'_{invd}(k-1) + (b_2)v'_{invd}$$
$$(k-2) + \varrho(k+1)]^2 \} \tag{3.28}$$

Equation (3.28) contains present and past inputs, present and past outputs and future model estimation error. The estimation error is assumed as white noise, and its future values cannot be correlated with past and/or present signals. Hence, one can achieve the minimum variance when the sum of the first six components is set to zero. i.e.

$$-a_1\epsilon_{P_o}(k) - a_2\epsilon_{P_o}(k-1) - a_3\epsilon_{P_o}(k-2)+$$
$$b_0 v'_{\text{invd}}(k) + b_1 v'_{\text{invd}}(k-1) + b_2 v'_{\text{invd}}(k-2) = 0 \tag{3.29}$$

The minimum variance control law for active power control is given by,

$$v'_{invd}(k) = (a_1\epsilon_{P_o}(k) + a_2\epsilon_{P_o}(k-1) + a_3\epsilon_{P_o}(k-2)$$
$$-b_1 v'_{invd}(k-1) - b_2 v'_{invd}(k-2))/b_0 \tag{3.30}$$
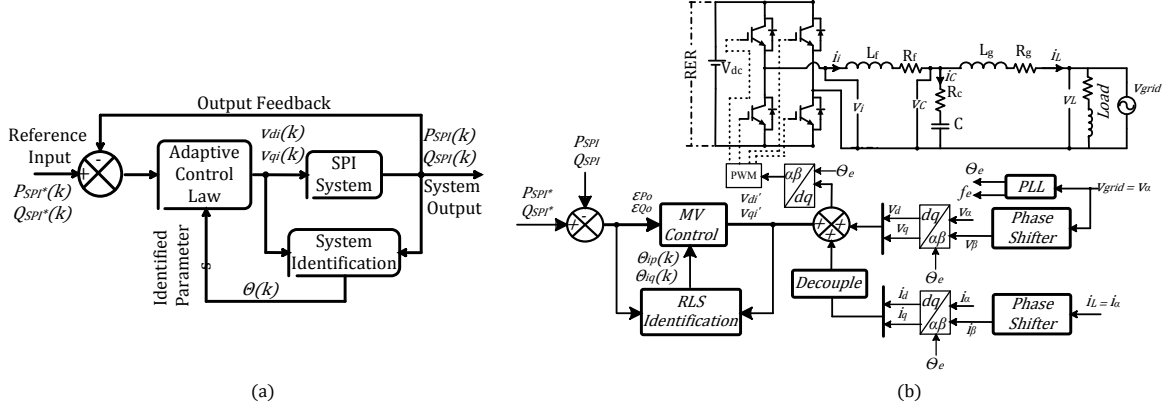
Figure 3.23: Proposed adaptive control framework for grid-connected SPI. a) General Schematic b) Proposed Implementation.

Similarly, the minimum variance control law for reactive power control is given by,

$$v'_{invq}(k) = (a_1 \epsilon_{Q_o}(k) + a_2 \epsilon_{Q_o}(k-1) + a_3 \epsilon_{Q_o}(k-2)$$

$$-b_1 v'_{qi}(k-1) - b_2 v'_{qi}(k-2))/b_0 \qquad (3.31)$$

where $\epsilon_{Q_o}(k) = Q^*_{inv}(k) - Q_{inv}(k)$. Q^*_{inv} is the reference reactive power to be delivered to the grid and Q_{inv} is the actual reactive power delivered. Fig. 3.23a represents the overall control structure proposed in this work for active and reactive power control of single-phase grid-connected inverter. The system identification sampling time and controller sampling time used in this work are provided in the Appendix.

3.9   Controller Performance Comparison

The adaptive minimum variance controller performance validation was carried out on a single-phase grid-connected inverter, in a one/single machine infinite bus (OMIB/SMIB) setup as shown in Fig. 3.24. This is to provide a proof of concept for the adaptation of active and reactive power control on one single-phase inverter. This proof of concept paves way for scaling to a larger system to perform various tests with a real grid model. The performance comparison of the controller is based on digital simulation. The simulation results presented are with the non-linear switching model
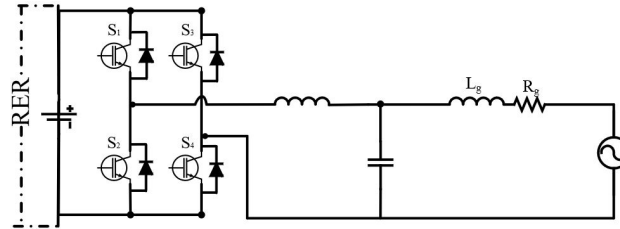
Figure 3.24: Single machine infinite bus test system for the SPI.

of the inverters for the different types of controllers compared. The linearized model was primarily used to simplify the control design.

3.9.1   Proof of Concept: Machine Infinite Bus

The DC module consists of a Photovoltaic (PV)-Battery system rated for 1.5 kW and 1000 V DC with the AC side connected to a constant voltage source or infinite bus at 230 V. The comparative studies are performed for the PI and the adaptive controller based on active and reactive power tracking capability under varying grid conditions.

3.9.1.1   Case 1 for OMIB: Active and Reactive Power tracking with arbitrary references

Fig. 3.25 and Fig. 3.26 compares the active and reactive power reference tracking performance of the proposed controller with the conventional PI controller. PI controller for the single-phase inverter has been tuned based on the system state-space model presented in (3.11) and (3.12). The controller is optimized to have an overshoot of less than 20% for step changes and with a settling time of 0.1 seconds. It can be observed from Fig. 3.25 and Fig. 3.26, that the proposed controller has a better dynamic response in terms of less overshoot and lower settling time as compared to the conventional PI-based control. Also, note that the proposed controller did not assume prior knowledge of the system parameters as opposed to the PI controller which required prior knowledge of the system parameters for proper controller tuning. The results show that the proposed system identification-based control can be a better
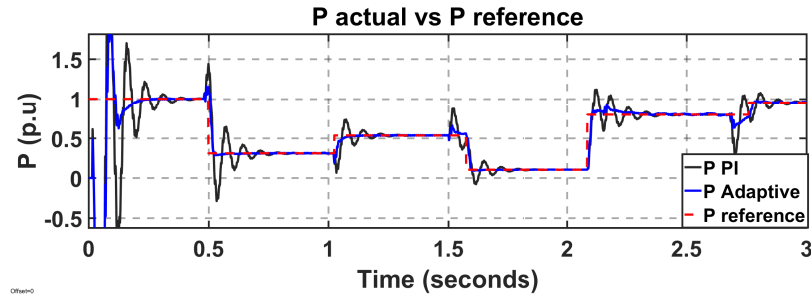
Figure 3.25: Case 1 for OMIB: Active power tracking performance comparison.
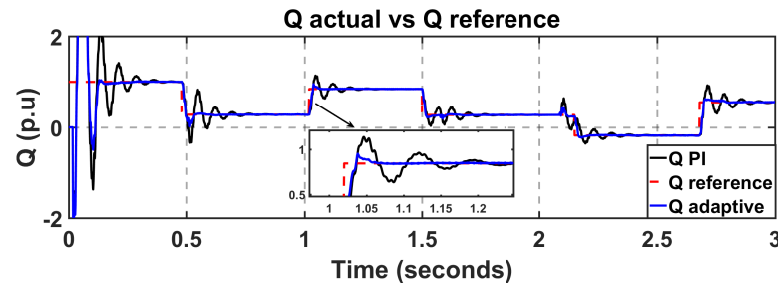
Figure 3.26: Case 1 for OMIB: Reactive power tracking performance comparison.

alternative to the existing vector control scheme for the SPI.

3.9.1.2 Case 2 for OMIB: Controller performance during voltage sag

Fig. 3.27 presents the active and reactive power graphs with a presence of voltage sag on the grid at the 1.5-second mark. The voltage sag is on the grid side, which is a 10 cycle sag that lowers the grid voltage from 0.99 p.u. to 0.8 p.u. When the sag occurs, the low voltage ride-through capability of the inverter tries to keep tracking the power output reference. Observation from the figure shows that the capability of the adaptive technique is comparable to the PI control. Active power overshoot with the conventional PI control is much larger compared to the adaptive controller and shows better convergence to the setpoint during and after the sag.

3.9.1.3 Case 3 for OMIB: Controller performance with measurement noise

Adaptive control is dependent on the measurement of the system's input and output data. Any variations and noise in the measurements can cause the controller to malfunction and compromise the power tracking capability. Therefore, a test is
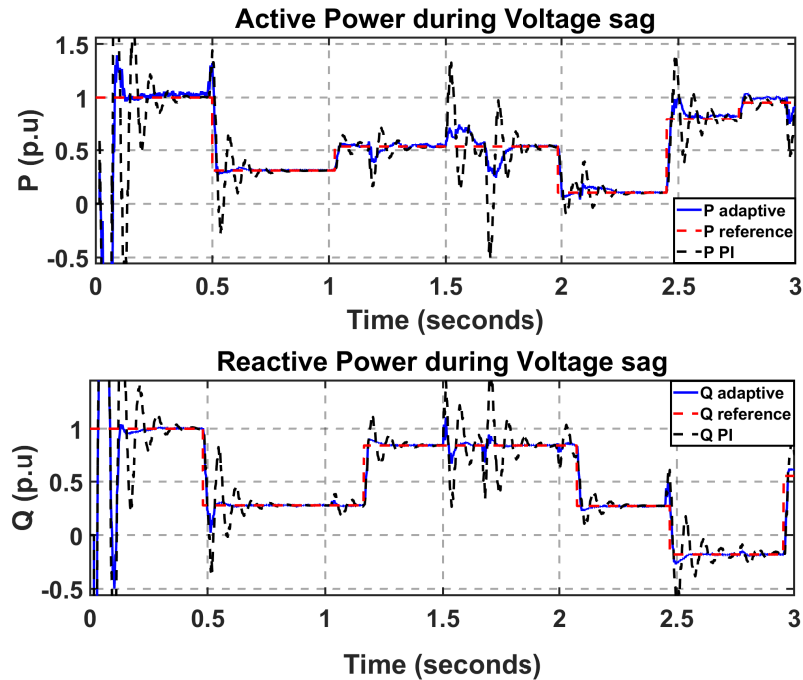
Figure 3.27: Case 2 for OMIB: Active and reactive power comparisons during voltage sag.
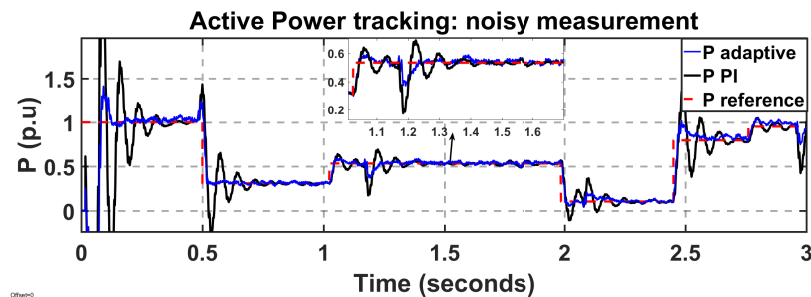
Figure 3.28: Case 3 for OMIB: Active Power comparisons when feedback noise is introduced.

performed in the presence of the noise in the measurements. Fig. 3.28 and Fig. 3.29 shows the active and reactive power tracking or the PI and adaptive controller in the presence of the measurement noise. The minimum variance adaptive controller has a better steady-state tracking performance than that of the conventional PI in the presence of measurement noise. This feature is crucial as the feedback measurements can include noises coming from inverter switching, fast changes from the load and, generation sources like PV.
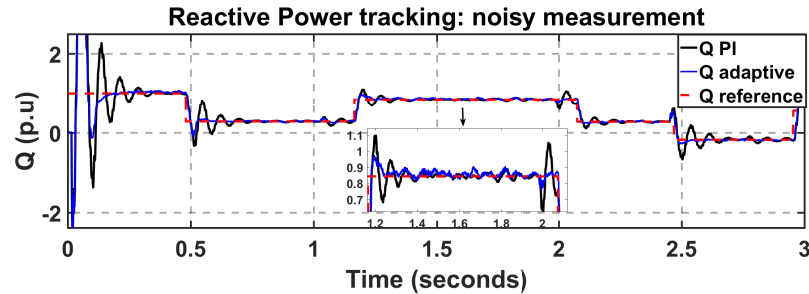
Figure 3.29: Case 3 for OMIB: Reactive power comparison when feedback noise is introduced.

3.9.2   Scalability: Study with IEEE 123 Bus system

The scalability of the proposed architecture is tested using a modified IEEE 123 Node Test Feeder (see Fig. 3.30). The power distribution system from [92] is modified to include DER connected SPI's as indicated in Fig. 3.30. The nature of this system is that it is inherently unbalanced. So the application chosen is power and voltage balancing. The dq- based SPI controller with the proposed architecture is connected to bus 21 (inverters 504, 505, and 506), bus 42 (inverters 501, 502 and 503) and bus 97 (inverters 507, 508 and 509) on all the Three-Phases (total nine inverters). The inverters have a power rating of 50 kW at 2.4 kV. The power balancing is based on (32) and (33). For comparison purposes, two controllers are used. First, PI controllers are used with re-tuned best parameters based on the same process discussed in Section II. C. Also, a PR controller is designed for comparison purposes. The PR controller is based on the basic controller formulation shown in [93]. The control signals were adapted to the control architecture shown in Fig. 3.23 for a clear comparison in the $\alpha\beta$ reference frame. In the following section, the simulation results showcased are for inverter 501. This is because, the other inverters (502-509) portray a similar dynamic response to the changes provided, as seen in the following cases.

**DER Connection- 1 SPI per phase on node 21, 42 and 97 of 50 KVA rating
(Details as shown in Figure 1)**
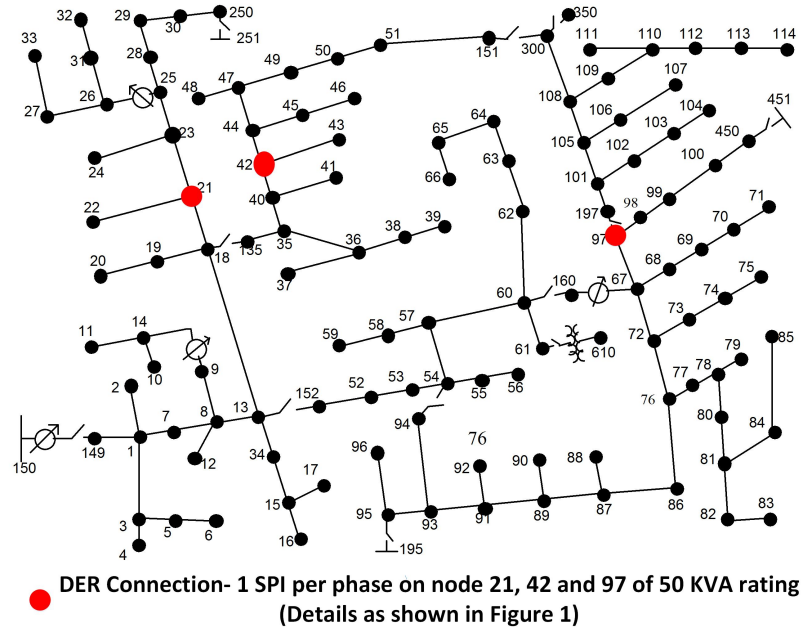
Figure 3.30: Modified IEEE 123-bus system.

3.9.2.1   Case 1 for Scalability Studies: Active and reactive power tracking with DERs attached to the 123-Bus system

Two sub-cases are illustrated in this case. In Case 1a, the tracking ability of active and reactive power of the proposed controller compared to PI gains tuned based on SMIB is illustrated. Fig. 3.31 compares the tracking performance of the PI, PR, and adaptive controllers. Inverter 501 attached to bus 42 is taken as the reference. It can be seen that PI and PR control for the SPI's active and reactive power control is comparable in tracking the references provided to the outer loop. However, when connected to IEEE 123 bus system their performance deteriorated. The adaptive control, on the other hand, has a better performance comparatively. Quantitative comparisons are shown in Table. 3.9. In Case 1b, active and reactive power tracking are compared with PI gains based on IEEE 123-bus system configuration (see Fig. 3.32). It can be seen that the proposed adaptive control architecture has similar characteristics but faster convergence, lower under and overshoot, and flexibility of implementation to any generic inverter topology. This is also exemplified by the

results in Table 3.9.
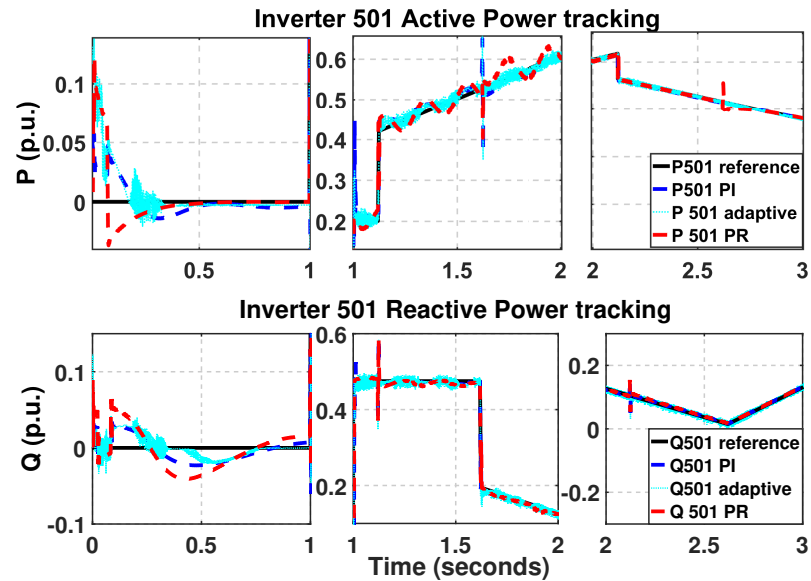
Figure 3.31: Case 1a: System scalability: Active power tracking performance comparisons with PR and re-tuned PID parameters.

Table 3.9: Performance Analysis of Case 1 and Case 3 in Scalibility Studies (5.4.2)

Controller	Steady State %error P	Steady State %error Q	% Improvement w.r.t OMIB PI control
Case 1b			P & Q
OMIB PI	15%	10%	
PI	3.6%	5%	76% 50%
PR	4%	5.6%	73% 44%
Adaptive	3%	4.2%	80% 58%
Case 3			P & Q
PI	1.35%	3.5%	91% 50%
Adaptive	1.26%	3%	65% 70%

3.9.2.2   Case 2 for Scalability Studies: Active and reactive power tracking during

voltage sag

Fig. 3.33 shows the active and reactive power comparison during the presence of a grid voltage sag where the grid voltage goes from 0.99 p.u. to 0.8 p.u at 2.5 secs. It can be observed that the adaptive controller has a good low voltage ride-through
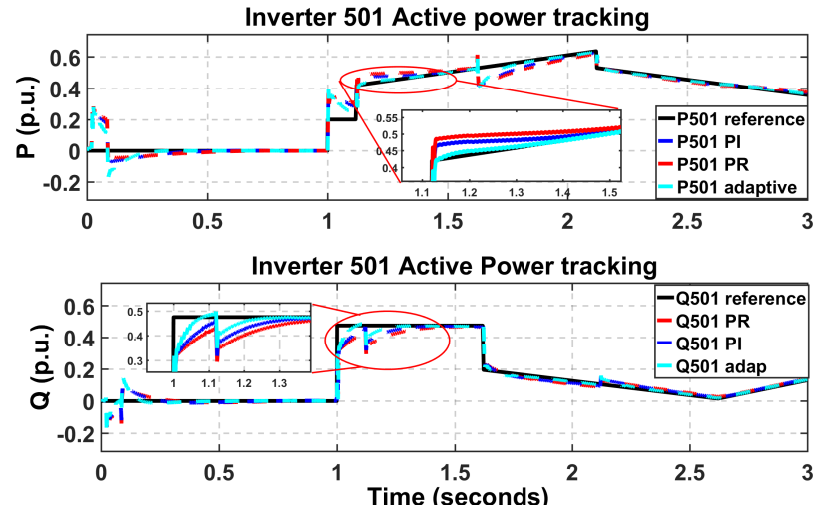
Figure 3.32: Case 1b: System scalability: Active power tracking performance comparisons with PR and re-tuned PID parameters.

capability and shows better convergence to the setpoint once the sag is cleared.

3.9.2.3   Case 3 for Scalability Studies: Active and reactive power tracking under oscillatory reference change and voltage sag

Fig. 3.34 shows the tracking performance of the PI and proposed controller under random oscillatory reference and voltage sag conditions similar to that of Case 2. In this case, even though the active power tracking is comparable with the PI controller, the proposed architecture shows better performance in active and reactive power tracking.

Table II summarizes the quantitative analysis of controller performance compared to PI and PR controllers. It can be seen that the proposed architecture shows superior performance when compared to other controllers.

3.10   Application to Unbalanced three-phase Systems

Reactive power generation by inverters is a valuable commodity for the grid, and controlling the inverter output powers can help quench some of the issues related to voltage dynamics. In this section, the focus is on utilizing the proposed architecture to mitigate the power unbalance and improve voltage dynamics and deviations from
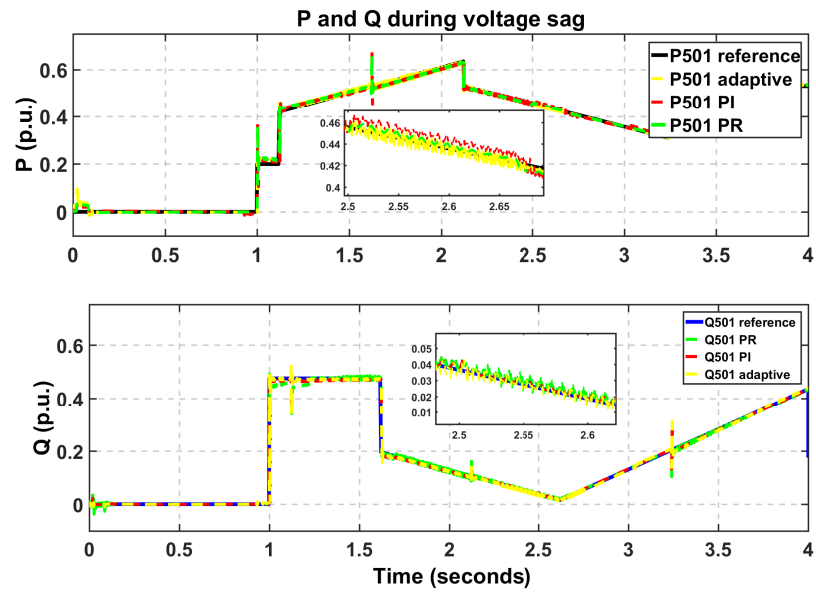
Figure 3.33: Case 2: System scalability: Active and reactive power tracking comparisons during voltage sag with PR and re-tuned PID parameters.
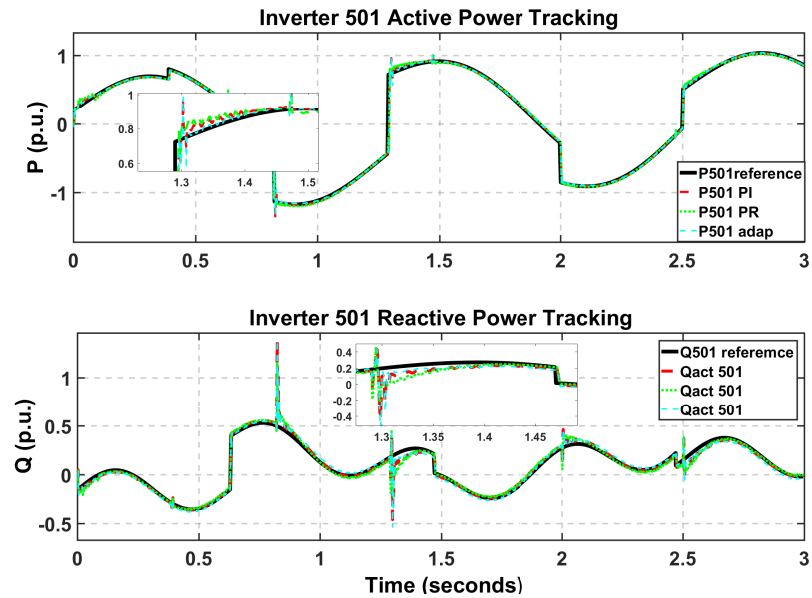
Figure 3.34: Case 3: System scalability: Active and reactive power tracking comparisons during voltage sag with varying reference PR and re-tuned PID parameters.

the nominal voltage. The application of inverter control in unbalanced systems is performed using the OPAL-RT RT-lab setup as shown in Fig. 3.35. Here the IEEE 123 bus system is simulated in the OP4510 real-time simulator, which in the future will provide a base setup for Power Hardware In the Loop (P-HIL) simulations. The following cases in the next section are performed in the RT-lab testbed.
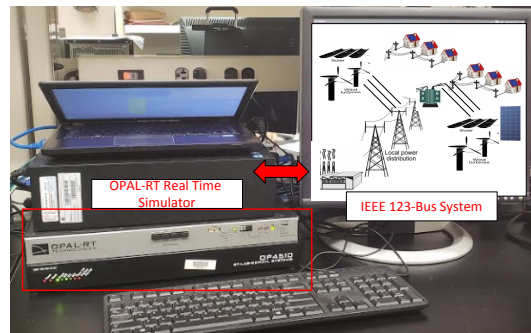
Figure 3.35: Real-time hardware test bed for studying IEEE 123-bus system.

3.10.1 Case 1 Unbalanced Application: Phase Power Balancing With Adaptive Controlled SPIs

For this study nodes 42, 21, and 97 have single-phase grid-tied inverters as shown in Fig. 3.30. These inverters can control the output active and reactive powers flowing out of the GCIs. To control or dictate the power generation, the references are created by using the upstream power. For this purpose, buses 42, 21, and 97 have power meters connected, which measures active power and voltage. Here, P_a, P_b and P_c, Q_a, Q_b and Q_c are the active and reactive power flowing through each phase. The setpoint is the average power calculated using (32) and (33). Here P_{inva} and Q_{inva} represents active and reactive power output of the inverter attached to phase a and P_{aref} and Q_{aref} are power references for the same inverter. Similarly, these references can be generated for the inverters on the other two phases as well. For the following
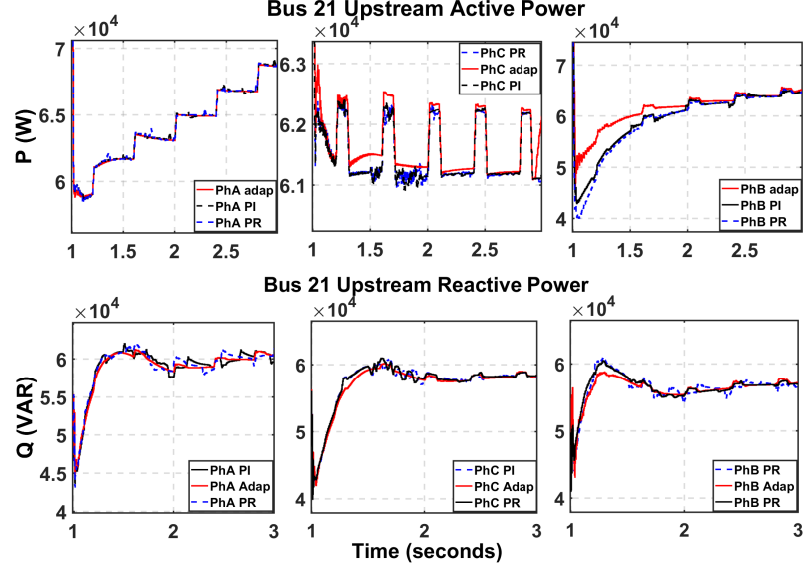
Figure 3.36: Case 1 for unbalanced application: Bus 21 active and reactive power balancing capability comparisons.

cases, the inverters start to participate at the 1-second mark of simulation time.

$$\frac{(P_a + P_b + P_c)}{3} - P_{inva} = P_{aref} \tag{3.32}$$

$$\frac{(Q_a + Q_b + Q_c)}{3} - Q_{inva} = Q_{aref} \tag{3.33}$$

When the GCIs intervene, the active and reactive powers seen upstream converge and stabilize the average value of the active and reactive power respectively. It can be seen that the phase power is not balanced. In Fig. 3.36, 'P PI' and 'P adapted' curves show the upstream powers when the powers are supported with SPIs. Please note that simulation results in Fig. 3.36 only show bus 21 results, as the other two buses show similar behavior. It can be seen that the power from the adaptive controlled SPIs shows better tracking and balancing as opposed to PI. This can further help in regulating the voltage, as removing power unbalance from the system improves the overall system's stability. The adaptive controller from Fig. 3.36, has a smoother transition towards balancing out the upstream reactive powers than the PI controller. This steady-state error does not show in the traditional active and reactive

Table 3.10: Performance Analysis of Case 1 in Application to Unbalanced three-phase System Section

Controller	Steady State %error P	Steady State %error Q	% Improvement w.r.t PI control
Inverters at Bus 42			P & Q
PI	1.84%	3.43%	
Adaptive	0.6%	1.2%	71% 65%
PR	2.1%	3.8%	
Inverters at Bus 21			
PI	2%	2.42%	
Adaptive	0.56%	0.89%	72% 63%
PR	2.3%	4%	
Inverters at Bus 97			
PI	1.72%	2.6%	
Adaptive	0.68%	0.91%	60% 65%
PR	2%	3%	

power tracking but when there is a supervisory or an extra controller drove setpoint generation, the performance deteriorates as it can be observed.

3.10.2 Case 2 Unbalanced Application: Voltage Unbalance Mitigation

In this case, the voltage is monitored and corrected by the inverter at the point of common coupling (PCC). The error generated by the measured voltage with the required reference is provided to the reactive power loop of the inverter. The voltage control loop has a PI controller that takes the voltage error as the input and generates the corresponding q-axis current reference for the inner loop. The reactive power generation depends on the d-axis voltage and the q-axis current at the LC-filter. The required reactive power for complete mitigation or balancing voltage might be different or higher than the rating of the inverter, but having the GCI help regulate the voltage up to the rated capacity of the GCI is the main objective here. Our single-phase DER inverter system is rated for 50kW, therefore when there is no active power demand, theoretically, the reactive power support by the GCI can be up to 50kVAR.
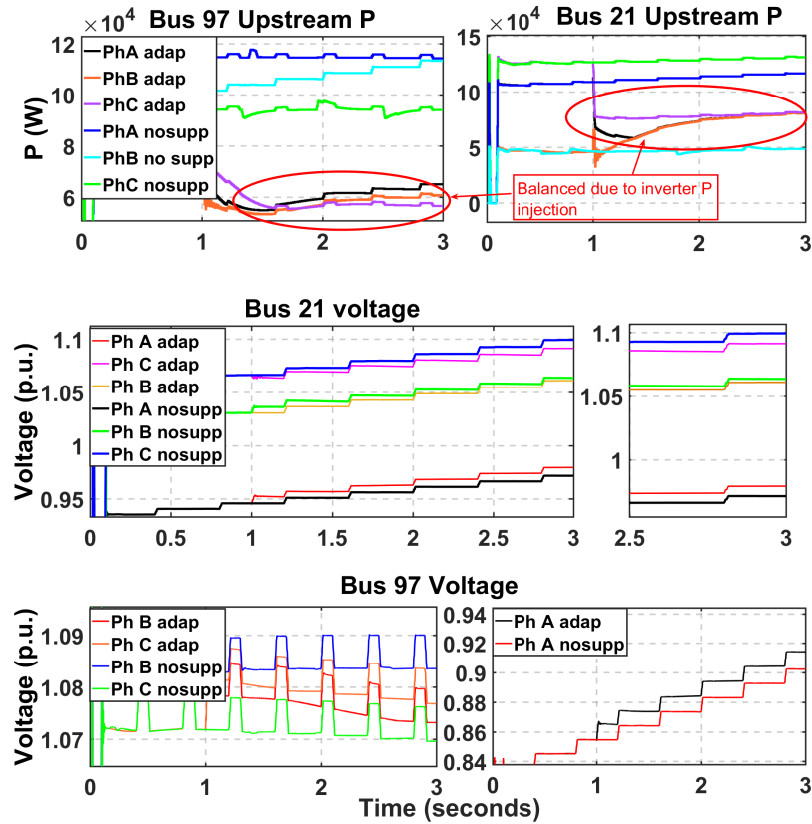
Figure 3.37: Case 2 for unbalanced application: Bus 21 and 97 upstream Active-Reactive Power and Voltage after voltage balancing provided by the inverter and their respective Bus voltages.

It can be seen from Fig. 3.37 that the proposed architecture can improve the voltage very effectively. Table 3.11 shows the qualitative improvement when compared to the PI controller. It can be seen that a minimum of 3% overall improvement in the voltage can be attained.

3.11 Summary

This chapter first presents a unified control topology for the single-phase inverter-based DERs. The traditional switching between two control modes for GC and SA modes of the MG is eliminated. Secondly, a seamless transfer algorithm is explored with manual and auto override options for the end-user. Lastly, power and voltage unbalance mitigation methodology is provided utilizing an adaptive minimum variance control.

Table 3.11: Performance Analysis of Case 2 in Voltage Unbalance Mitigation Section (5.5.2)

Control	Steady State Voltage %error	% Improvement w.r.t PI control
Bus 21		
PI	0.29%	
Adaptive	0.28%	3.4%
Bus 42		
PI	0.2%	
Adaptive	0.185%	7%
Bus 97		
PI	0.25%	
Adaptive	0.24%	4%

Initially, the seamless transfer algorithm is evaluated and put up against different frequency and voltage-related excursions. The efficiency and clearing times for the algorithm are seen to abide by the IEEE 1547.2018 regulations. In the second half, the single-phase inverter model in the grid following mode and the proposed controller design is illustrated. The adaptive control shows better dynamic performance and noise rejection capability than the conventional PI control for a single machine infinite bus system (SMIB). The proposed controller can adapt to the system topology change, unlike the PI controller, whose gains have to be re-tuned depending on the system. The control architecture is simple and allows flexible active and reactive control for the single-phase inverter. Second, the chapter presents a method to help mitigate the unbalanced nature of the three-phase system through the contribution of these SPIs. Using the active and reactive power control ability of the SPIs, the line power unbalances are mitigated completely. Lastly, this chapter presents the power and voltage balancing method using the SPI's readily available reactive power to minimize the voltage error and improve the system's voltage profile in conjunction with the active line power balancing. The overall advantage and novelty are that the proposed architecture can be used for multiple coordinated point active and reactive power

support for the power distribution system.

CHAPTER 4: Multiple SPI Management using adaptive droop framework

Chapter 3 ventured into the contribution of the local controllers once the secondary level control or reference generation provides a set point for multiple MGs in a distribution network. In this Chapter, a secondary level control framework is formulated for the reference set point generation for local controllers within one MG or multiple MGs. Traditional droop has often been implemented in the past as a power management technique in islanded conditions, but this framework is not applicable when the R/X ratio is varying or high. There is a need for identification-based power management that can dynamically adjust the power references on the local controllers' output according to the objective, i.e., voltage-frequency control in SA mode, power, and voltage-frequency regulation in GC mode. Therefore, An Alternating Direction Method of Multipliers (ADMM) approach is proposed to evaluate multiple inputs and multiple-output (MIMO) transfer function. ADMM provides the sensitivities between the input and output, which can be utilized for formulating different reference set-points for different MGs or inverters based on the mode of operation.

4.1   Introduction

Parallel connection and control of multiple inverters are an important area of research in current microgrid technology. Traditionally placing capacitors at the nodes was considered the ideal method for voltage control, but this becomes impractical with large-scale inverter-controlled devices in the power distribution system. When a large number of DERs are placed in a system, the supply-demand characteristic changes and integration of these inverters with the grid become difficult. Grid-connected inverters have the primary task of controlling the active and reactive power flowing

into the grid, keeping the voltage and frequency constant at the Point of Common Coupling (PCC) [94]. There is a potential of mitigating any variation in the voltage and frequency locally by absorbing or supplying the appropriate power (active and reactive power) [95] by utilizing LV and MV grid-connected inverters. This is done generally based on P-ω and Q-V droop equations, which is for HV transmission networks [96]. Few papers have discussed strategies to find droop controllers for different types of inverters [97]. For this, the knowledge of the R/X ratio needs to be known, and the droop gains can vary depending on the scale of the source and the network. An adaptive droop control method evaluation the decoupling matrix online has been proposed [98]. This can work for various X/R ratios, but different power scaling of the DERs is still an issue. Using the variations in the voltage and frequency (ΔV,Δf) in conjunction with the impedance matrix, we can generate the required demand from the inverter or source (ΔP,ΔQ). This chapter explores this concept which is then implemented on modified or universal droop control and adaptive PI-based modified droop control. The approach uses an impedance matrix to couple the effect of change in voltage and frequency to generate ΔP and ΔQ for outer loop control. Even though there are various apparent advantages of renewable energy integration, several significant issues need to be addressed with the growing integration of renewable sources in distribution networks. One major issue is the voltage imbalances in the power distribution network with higher penetration of Single-Phase and Three-Phase inverter-based energy resources. If the consumer end actively contributes towards regulating the system (via injecting active and reactive power), much of the voltage and power balance issues can be mitigated [4]. Management of grid and control of power inverters is the key to voltage improvement. Control of Single-Phase inverters (SPIs) for these modes have been explored [5, 6, 7, 8, 9], but it still proves to be a difficult task due to the varying grid requirements. Three-Phase power distribution systems especially with high penetration of DERs (Three-Phase and Single-Phase)

Figure 4.1: Introductory figure for droop control strategy.

suffer from unbalancing loading, voltage sags, and power quality issues. Earlier research work has been performed for solving these problems by placing compensating devices such as capacitor banks (also, aided by power electronic elements) [10], series compensation devices [11], and voltage support using power output of the converters [12]. However, the use of power electronic equipment and penetration has been increasing in such a drastic way that these methods prove costly. There is a notion that with the already existing inverters in the system or consumer-end inverters, most of the problems can be mitigated to a large extent [13, 14]. Reactive power generation by inverters is a valuable commodity for the grid, and dynamically controlling the inverter output powers (active and reactive power) can be a great way to manage local voltage or frequency changes [15].

Challenges of managing multiple Single-Phase inverters are mainly, a) there should be a way to dynamically sense the effect of multiple inverter control inputs at multiple

output relevant output locations, and b) there should be a coordinated approach to manage multiple Single-Phase inverters. Droop-based control has been explored in the past, providing a passive form of power-sharing for voltage and frequency regulation. This eliminates the necessity of having active communication links between the sources and provides accurate power-sharing in micro-grid systems. The idea is taken from traditional power system control, generally based on P-ω and Q-V droop equations, which is applicable for HV transmission networks. Few papers have discussed strategies to find droop controllers for different types of inverters (L-,R- and C-inverters), that work for more general cases. A universal droop control has also been explored in [99, 100]. However, these approaches need prior knowledge of the R/X ratio of the power network. As opposed to fixed measurements, online estimation has been suggested by perturbing the voltage magnitude and measuring the power output variations. This can work for various X/R ratios, but sensing with different power ratings can be an issue.

4.2   Main Contributions

The main contributions of this chapter can be summarized as follows:

- Formulated an impedance matrix that provides the universal droop formulae. The cross-coupling between power and V-f are all-encompassing of different R/X ratios of the line and inverter filters.

- With earlier works creating virtual impedance-based droop control to compensate for either a dominantly capacitive network or inductive network, and having the pre-existing knowledge of the line impedances, this chapter provides ADMM based droop control that identifies the system impedance matrix online to have proper power-sharing amongst the DER interconnecting devices.

- Mathematical formulation for sequence extraction for three-phase systems to its single-phase components are provided in this chapter. This forms the basis

of sequence-based control for SPI in three-phase microgrids.

- Sequence-based SPI controller architecture is presented that has an advantage of suppressing negative sequence components and eliminating current and voltage spikes during transitioning between GC to SA mode and vice versa during harsh voltage sag and frequency sag excursions.

4.3 Analyzing dq- frame inverter model for power management

Control in dq- reference frame is advantageous because of the possibility of getting infinite gain and zero steady-state error at the fundamental frequency as the signals are dc signals. Inverter modeling in dq- frame has been studied and explored in the past [101, 6, 102, 103]. Using Park's transformation once the dq- components are extracted for the current and voltage signals, we can create the control architecture for active and reactive power control as follows:

$$\frac{d}{dt}\begin{bmatrix} I_d \\ I_q \end{bmatrix} = \begin{bmatrix} Dq \\ Dq \end{bmatrix}\frac{V_{dc}}{L} + \begin{bmatrix} 0 & -(\omega) \\ (\omega) & 0 \end{bmatrix} \cdot \begin{bmatrix} I_d \\ I_q \end{bmatrix} - \begin{bmatrix} I_d \\ I_q \end{bmatrix}\frac{1}{L}(R_l + Z) - \begin{bmatrix} v_d \\ v_q \end{bmatrix}\frac{1}{L} \quad (4.1)$$

$$\frac{d}{dt}\begin{bmatrix} v_d \\ v_q \end{bmatrix} = \begin{bmatrix} I_d \\ I_q \end{bmatrix}\frac{1}{C} - \begin{bmatrix} v_d \\ v_q \end{bmatrix}\frac{1}{CZ}\begin{bmatrix} 0 & -(\omega) \\ (\omega) & 0 \end{bmatrix} \cdot \begin{bmatrix} v_d \\ v_q \end{bmatrix} \quad (4.2)$$

where v_d, v_q, i_d and i_q are the d- and q- axis capacitor and inductor's voltages and currents; Vdc is the DC-link voltage, R_l, Z L and C are the inverter output filter's element values. Utilizing (4.1) as the inner loop and the outer loop can be implemented as active and reactive power control loop by using:

$$P = (v_d i_d + v_q i_q) = v_d i_d \quad (4.3)$$

$$Q = (v_d i_q + v_q i_d) = v_d i_q \quad (4.4)$$
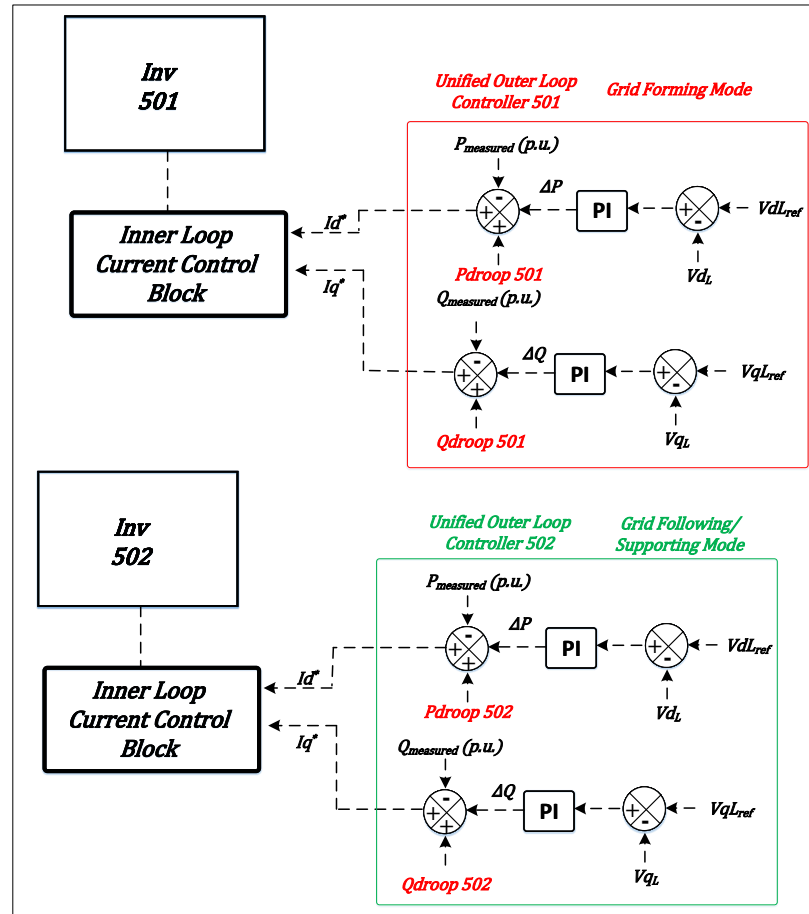
Figure 4.2: Unified Controller adapted to fit the droop control architecture.

These equations (4.3) and (4.4) generate the required current references for inner loop for active and reactive power control of the inverter. Fig. 4.2 shows the controller architecture which can be written as

$$\frac{Pref + \Delta P}{v_d} = i_{dref} \tag{4.5}$$

$$\frac{Qref + \Delta Q}{v_d} = i_{qref} \tag{4.6}$$

4.3.1 Modification on traditional droop equations

Utilizing the traditional equations for power flows, the inverter active (P) and reactive (Q) power can be expressed as:

$$P = \left(\frac{V_i V_g cos(\delta - \delta_g)}{Z} - \frac{V_g^2}{Z} \right) cos(\theta) + \frac{V_i V_g sin(\delta - \delta_g)}{Z} sin(\theta) \tag{4.7a}$$

$$Q = \left(\frac{V_i V_g cos(\delta - \delta_g)}{Z} - \frac{V_g^2}{Z} \right) sin(\theta) - \frac{V_i V_g sin(\delta - \delta_g)}{Z} cos(\theta) \tag{4.7b}$$

Where, V_i is the inverter voltage output across the filter capacitor, V_g is the grid voltage, δ is the inverter voltage angle, δ_g is grid voltage angle, Z is the impedance between the grid and inverter, and θ is the impedance angle.

We can rewrite (4.7a) and (4.7b) with respect to the grid impedance as:

$$P = \left(\frac{V_i V_g cos(\delta - \delta_g)}{Z} - \frac{V_g^2}{Z} \right) \frac{R}{Z} + \frac{V_i V_g sin(\delta - \delta_g)}{Z} \frac{X}{Z} \tag{4.8a}$$

$$Q = \left(\frac{V_i V_g cos(\delta - \delta_g)}{Z} - \frac{V_g^2}{Z} \right) \frac{X}{Z} - \frac{V_i V_g sin(\delta - \delta_g)}{Z} \frac{R}{Z} \tag{4.8b}$$

$$P = Q'\frac{R}{Z} + P'\frac{X}{Z} \tag{4.9a}$$

$$Q = Q'\frac{X}{Z} - P'\frac{R}{Z} \tag{4.9b}$$

Where,

$$P' = \frac{V_i V_g (\delta - \delta_g)}{Z} \tag{4.10a}$$

$$Q' = \frac{V_i V_g}{Z} - \frac{V_g^2}{Z} \tag{4.10b}$$

We can represent the active and reactive power P and Q in a more general equation that can work with any grid impedance ratio; equation (4.11) shows the same. Here

P' and Q' are the generalized active and reactive powers that alter according to the X/R ratio of the network.

$$
\begin{bmatrix} P \\ Q \end{bmatrix} = \begin{bmatrix} X/Z & R/Z \\ -R/Z & X/Z \end{bmatrix} \cdot \begin{bmatrix} P' \\ Q' \end{bmatrix} \tag{4.11}
$$

or,

$$
\begin{bmatrix} P' \\ Q' \end{bmatrix} = \begin{bmatrix} X/Z & -R/Z \\ R/Z & X/Z \end{bmatrix} \cdot \begin{bmatrix} P \\ Q \end{bmatrix} \tag{4.12}
$$

using (4.10a) and (4.10b) and implementing it in (4.12) we can get the relation between voltage and angle with the AC power. This is shown by:

$$
(\delta - \delta_g) = \frac{1}{V_i V_g}(XP - RQ) \tag{4.13a}
$$

$$
(V_i - V_g) = \frac{1}{V_g}(RP + XQ) \tag{4.13b}
$$

Linearizing (4.13b):

$$
V_{oi} = V_g - K\frac{\omega_c}{s + \omega_c}(RP_o + XQ_o) \tag{4.14a}
$$

$$
(V_{oi} + \Delta V_i) = V_g - K\frac{\omega_c}{s + \omega_c}[(RP_o + XQ_o) - (R\Delta P + X\Delta Q)] \tag{4.14b}
$$

$$
\begin{bmatrix} P \\ Q \end{bmatrix} = T. \begin{bmatrix} P' \\ Q' \end{bmatrix} \tag{4.15}
$$

This can be written as

$$
f_o - f = -k_f(P'_o - P') \tag{4.16}
$$

$$
V_o - V = -k_v(Q'_o - Q') \tag{4.17}
$$

We use the predetermined impedance matrix to couple the frequency and voltage
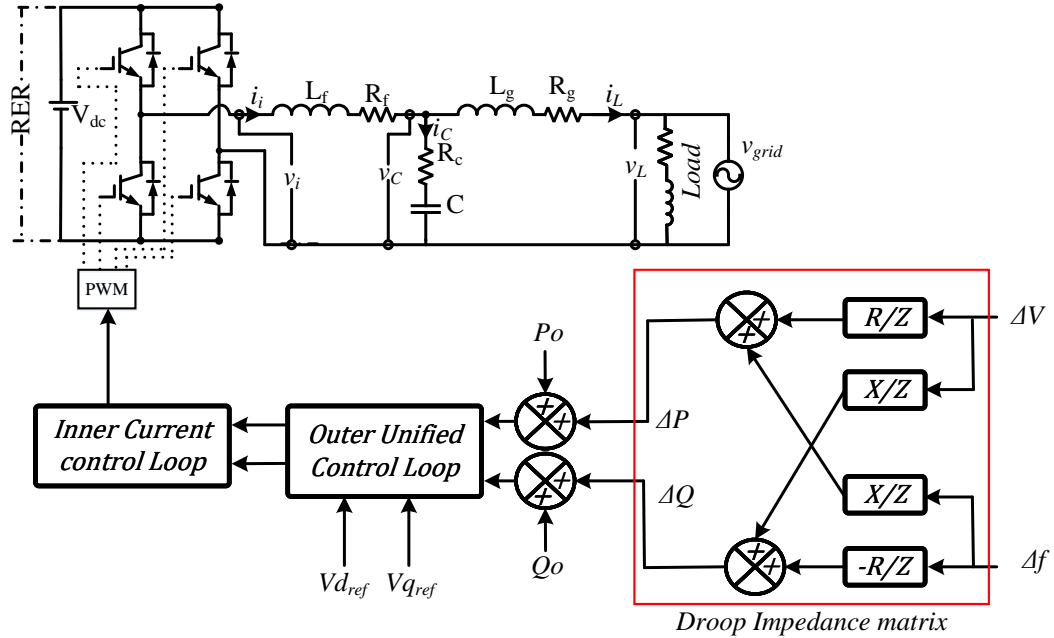
Figure 4.3: Modified droop with dq- control

changes with the additional active and reactive power reference (ΔP, ΔQ). Linearizing (4.11) and substituting (4.16) and (4.17),

$$
\begin{bmatrix} \Delta P' \\ \Delta Q' \end{bmatrix} = \begin{bmatrix} X/Z & R/Z \\ -R/Z & X/Z \end{bmatrix} \cdot \begin{bmatrix} \Delta P \\ \Delta Q \end{bmatrix}
\tag{4.18}
$$

$$
\begin{bmatrix} \Delta P \\ \Delta Q \end{bmatrix} = \begin{bmatrix} X/Z & -R/Z \\ R/Z & X/Z \end{bmatrix} \cdot \begin{bmatrix} \Delta(V/Kv) \\ \Delta(f/Kf) \end{bmatrix}
\tag{4.19}
$$

Determining the gains for the active and reactive power set-points can either be done by the traditional equations as mentioned above or by identifying the droop gains or sensitivity between the powers and the voltage-frequency at the PCC. Gain identification can be done by an adaptive framework or utilizing the earlier discussed framework of the Alternate Direction Method of Multipliers (ADMM).

4.3.2   ADMM based MIMO identification

The ADMM algorithm utilizes the inputs and outputs of the MIMO plant to generate individual transfer functions for each input and output combination. This assimilates the relationship of one output to every input. It is an optimization algorithm that combines advantages of dual ascent method and method of multipliers. It attempts to solve problem as shown in (5.6) where primal variable is split into two parts, x and z.

$$\begin{aligned} \text{minimize} \quad & f(x) + g(x) \\ \text{subject to} \quad & Ax + Bz = c \end{aligned} \tag{4.20}$$

Similar to the method of multiplier approach, an augmented Lagrangian can be formed as shown in (5.7) and thus the algorithm consists of an x-minimization step, a z-minimization step, and a dual variable update step as discussed in [104, 105] and shown in (5.8), (5.9) and (5.10).

$$L_\rho(x, z, y) = f(x) + g(x) + y^T(Ax + Bz - c) + \frac{\rho}{2}||Ax + Bz - c||^2 \tag{4.21}$$

$$x^{k+1} := \underset{x}{\operatorname{argmin}} L_\rho(x, z^k, y^k) \tag{4.22}$$

$$z^{k+1} := \underset{z}{\operatorname{argmin}} L_\rho(x^{k+1}, z, y^k) \tag{4.23}$$

$$y^{k+1} := y^k + \rho(Ax^{k+1} + Bz^{k+1} - c) \tag{4.24}$$

$$\begin{bmatrix} \Delta P_{501} \\ \Delta Q_{501} \end{bmatrix} = \begin{bmatrix} G11 & G12 \\ G13 & G14 \end{bmatrix} \cdot \begin{bmatrix} \Delta V \\ \Delta F \end{bmatrix} \tag{4.25}$$

$$\begin{bmatrix} \Delta P_{502} \\ \Delta Q_{502} \end{bmatrix} = \begin{bmatrix} G21 & G22 \\ G23 & G24 \end{bmatrix} \cdot \begin{bmatrix} \Delta V \\ \Delta F \end{bmatrix} \tag{4.26}$$
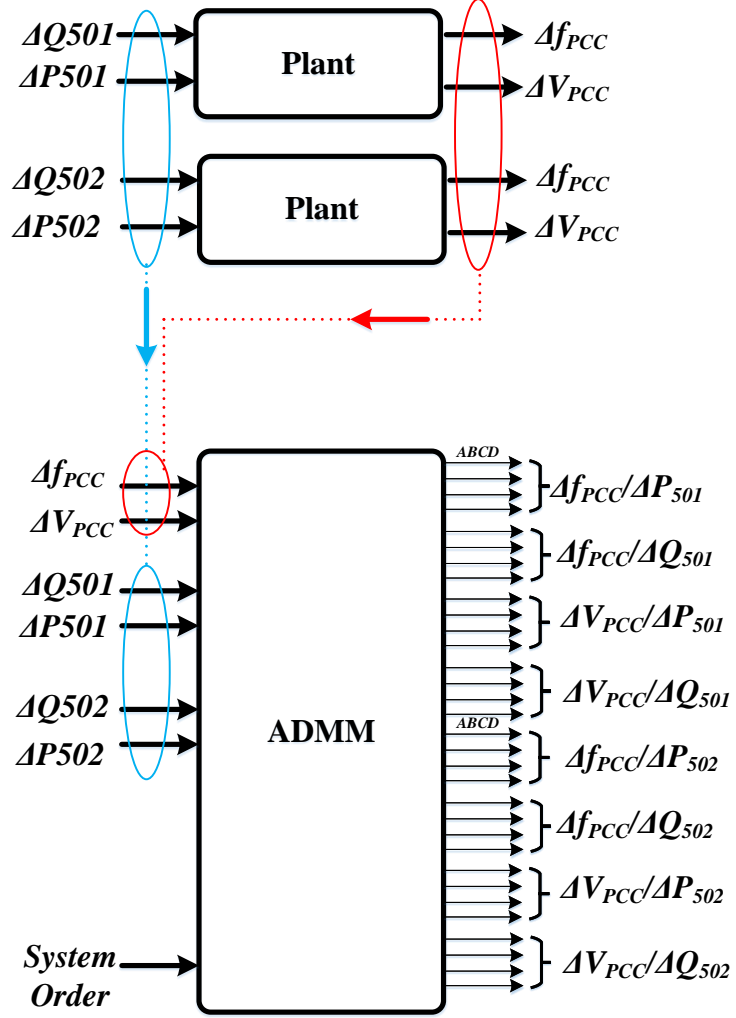
Figure 4.4: ADMM based identification of a MIMO system such as the droop impedance matrix

$$
\begin{bmatrix} \Delta P_{503} \\ \Delta Q_{503} \end{bmatrix} = \begin{bmatrix} G31 & G32 \\ G33 & G34 \end{bmatrix} \cdot \begin{bmatrix} \Delta V \\ \Delta F \end{bmatrix} \tag{4.27}
$$

$$
G_{11} = \frac{\Delta P_{501}}{\Delta V} = \frac{b_0^{501} + b_1^{501} z^{-1} + \dots + b_k^{501} z^{-k}}{1 + a_1^{501} z^{-1} + a_2^{501} z^{-2} + \dots + a_k^{501} z^{-k}} \tag{4.28}
$$

$$
G_{12} = \frac{\Delta P_{501}}{\Delta F} = \frac{b_0^{502} + b_1^{502} z^{-1} + \dots + b_k^{502} z^{-k}}{1 + a_1^{502} z^{-1} + a_2^{502} z^{-2} + \dots + a_k^{502} z^{-k}} \tag{4.29}
$$
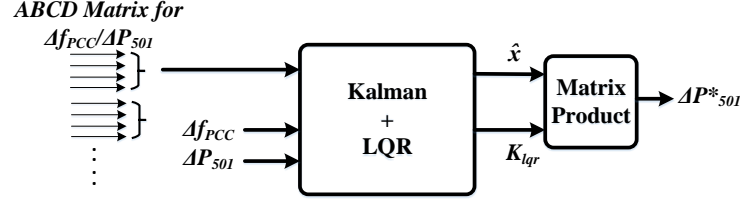
Figure 4.5: Kalman LQR utilized for generating the droop set points

$$G_{13} = \frac{\Delta Q_{501}}{\Delta V} = \frac{b_0^{503} + b_1^{503} z^{-1} + ... + b_k^{503} z^{-k}}{1 + a_1^{503} z^{-1} + a_2^{503} z^{-2} + ... + a_k^{503} z^{-k}} \qquad (4.30)$$

$$G_{14} = \frac{\Delta Q_{501}}{\Delta F} = \frac{b_0^{503} + b_1^{503} z^{-1} + ... + b_k^{503} z^{-k}}{1 + a_1^{503} z^{-1} + a_2^{503} z^{-2} + ... + a_k^{503} z^{-k}} \qquad (4.31)$$

where b_0, b_1...,b_k are the numerator coefficients of the transfer functions and $a_1,a_2...a_k$ are the denominator coefficients of the transfer functions. ADMM method uses least squares method to first estimate the individual transfer functions and reach a global consensus problem. Then a global consensus optimization problem can be formulated as:

$$\min_{a^{501}..a^{503}} \frac{1}{2} ||[P][a] - [B] + [P_x][b]||^2 \qquad (4.32)$$

where a is a vector of all the denominator coefficients and b is the vector of all the numerator coefficients. Also, B is the matrix of the current samples of P_{50x}, P is the matrix of the previous samples of P_{avg} and P_x are the previous samples of P_{50x}. The objective is to make $a^{501}=a^{501}=a^{501}=$z for a global consensus problem, so the numerator and denominator coefficients are calculated iteratively till the objective is achieved.

4.3.3   Kalman Estimation and LQR Controller Design

After the transfer function identification, the ABCD matrices is generated using a Kalman filter and LQR [106]. As shown in Fig. 5.5, $Y1$ and $U1$ are the plant input

and output. The plant state and measurement equations can be written as

$$x[n + 1] = Ax[n] + BP_{50x}[n] \tag{4.33a}$$

$$P_{avg} = Cx[n] \tag{4.33b}$$

$$\hat{x}[n + 1] = A\hat{x}[n] + BP_{50x}[n] \tag{4.34a}$$

$$P = APA' + Q \tag{4.34b}$$

$$K = \frac{PC'}{CPC' + R} \tag{4.34c}$$

where P is the error covariance matrix, K is the Kalman gain, R and Q are the output and input noise covariance matrix, respectively. Further, the measurement residual is calculated, the state and error covariance matrix estimate is updated, which can be written as (4.35).

$$residual = P_{50x} - C\hat{x}[n] \tag{4.35a}$$

$$\hat{x}[n + 1] = A\hat{x}[n] + K * residual \tag{4.35b}$$

$$P = (I - KC)P' \tag{4.35c}$$

The discrete time quadratic problem is then to minimize is

$$\sum (\hat{x}^T Q_1 \hat{x} + P_{50x}^T R_1 P_{50x}) \tag{4.36}$$

The unique stabilizing solution can be given by the control

$$K = (R_1 + B^T X B)^{-1} B^T X A \tag{4.37}$$
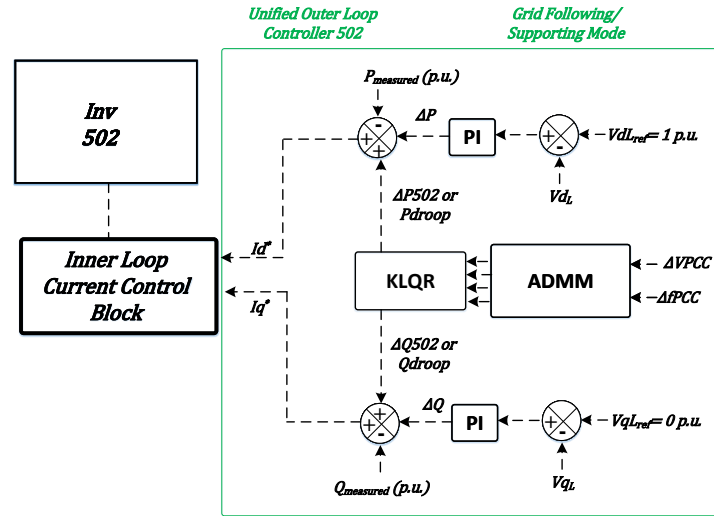
Figure 4.6: Grid supporting inverter control architecture with ADMM in the loop
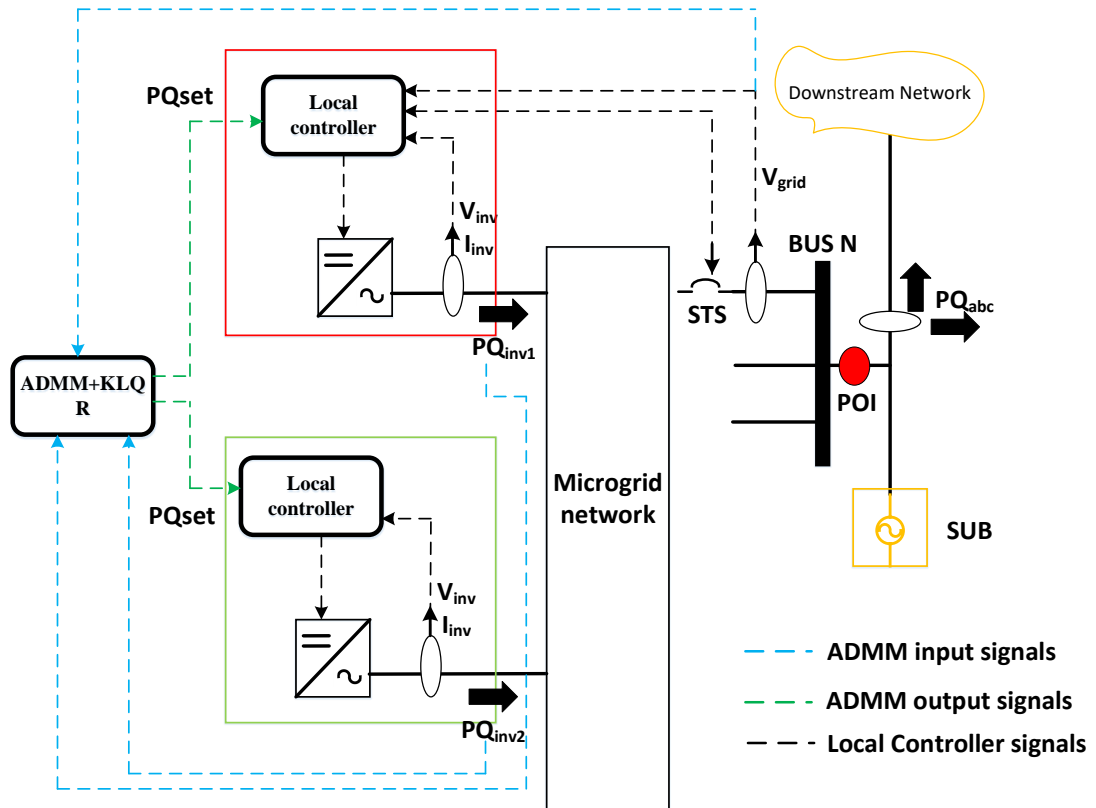
Figure 4.7: Modified droop with dq- control

Table 4.1: Rated power and voltage for Inverters 501 and 502

Inverter	Power (kVA)	Voltage (kV)	Bus	Phase Connected
Inv 501	2	2.4	45	A
Inv 502	2	2.4	46	A
MG	3.7	2.4	45,45A,46,46A	A

4.4 Simulation result

The two inverters are labeled as 501 and 502, and the proposed controller is tested for stand-alone and grid-connected modes. The outer loop of the two inverters is of the unified control loop topology, as discussed in the earlier chapter. The inverters are connected on Bus 45 and 46 of the 123 bus system. The two cases provided here are for grid-connected mode and stand-alone mode for the microgrid. The system is modified to fit or be comparable to the sizing of the DERs; hence an additional 3.7 MVA load is provided on the MG. Two cases are simulated using this topology, Stand Alone (SA) mode and Grid-Connected (GC) mode. The power-sharing between the inverters is presented for both the cases in the following section.

Case 1 Stand-Alone mode: The two inverter connections are described in Table 5.1, and the inverters, in this case, are operating in the stand-alone mode where the unified controller architecture for one is working in grid forming mode with the additional ΔP and ΔQ set to zero and the other inverter with the outer loop power set-points being acquired from the ADMM based controller.

Fig. 4.8 shows the power-sharing between the inverters during the SA mode of operation. The MG loading keeps changing throughout the simulation time (values shown in the figures) and it can be observed that the grid-following inverter shares the power with the grid-forming inverter coequally. The same cannot be said for the reactive power, shown in Fig. 4.9. However, due to the appropriate reference generation the voltage deviation from 1 p.u. does not exceed 0.2 p.u. and the MG maintains a stiff voltage and frequency profile, shown in Fig. 4.10 and 4.11 respectively.
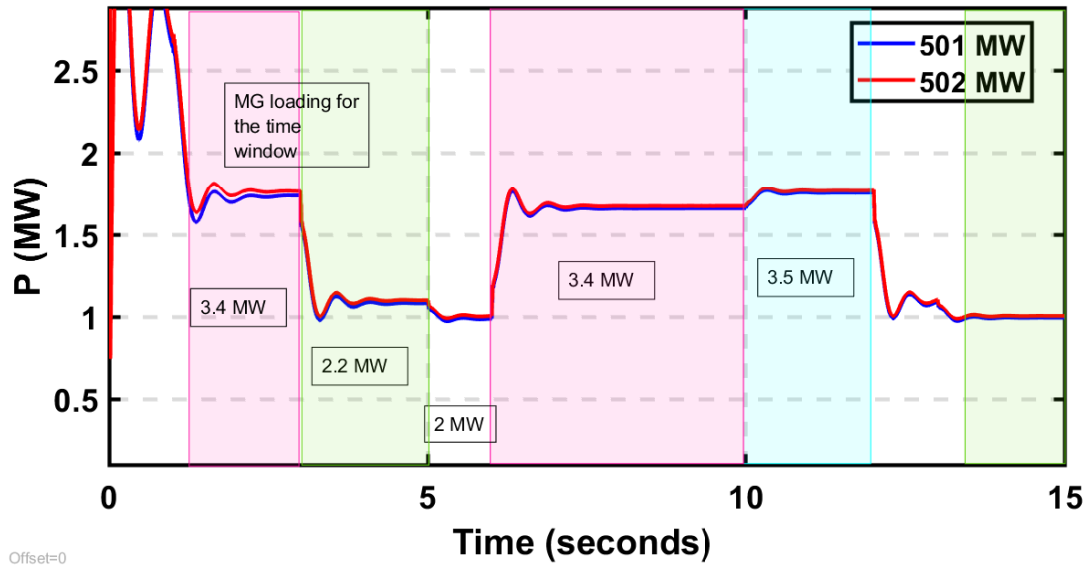
Figure 4.8: Active Power sharing between 501 and 502 during SA mode of operation of the MG
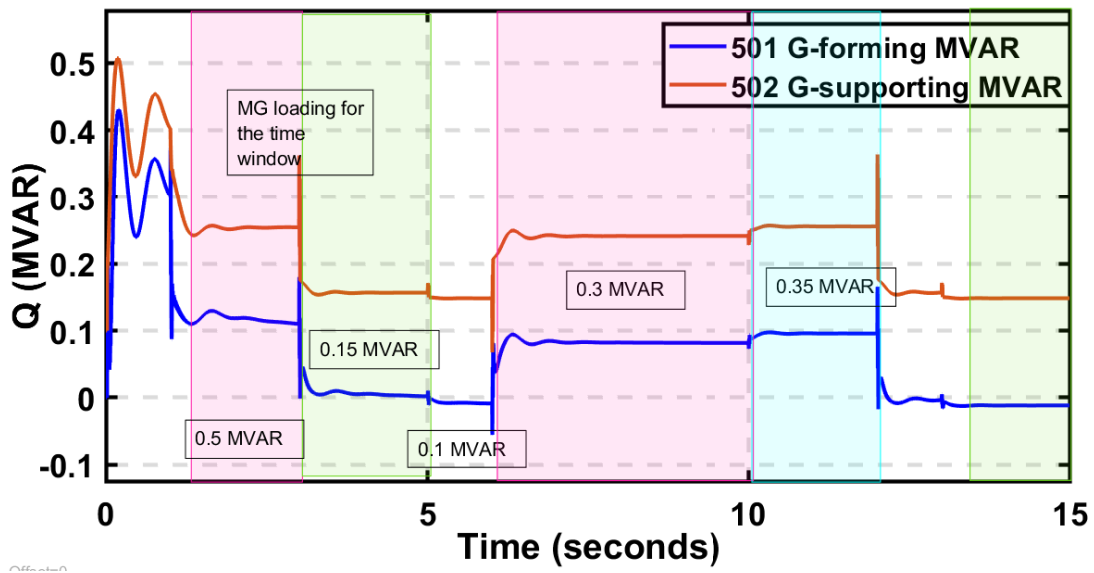
Figure 4.9: Reactive Power sharing between 501 and 502 during SA mode of operation of the MG

Case 1 Grid-Connected mode: In the grid-connected mode, one inverter works as a grid following inverter as the ADMM input to this inverter is zero, and the other works as a supporting inverter due to ΔP and ΔQ to the outer loops coming from the ADMM algorithm-based controller.
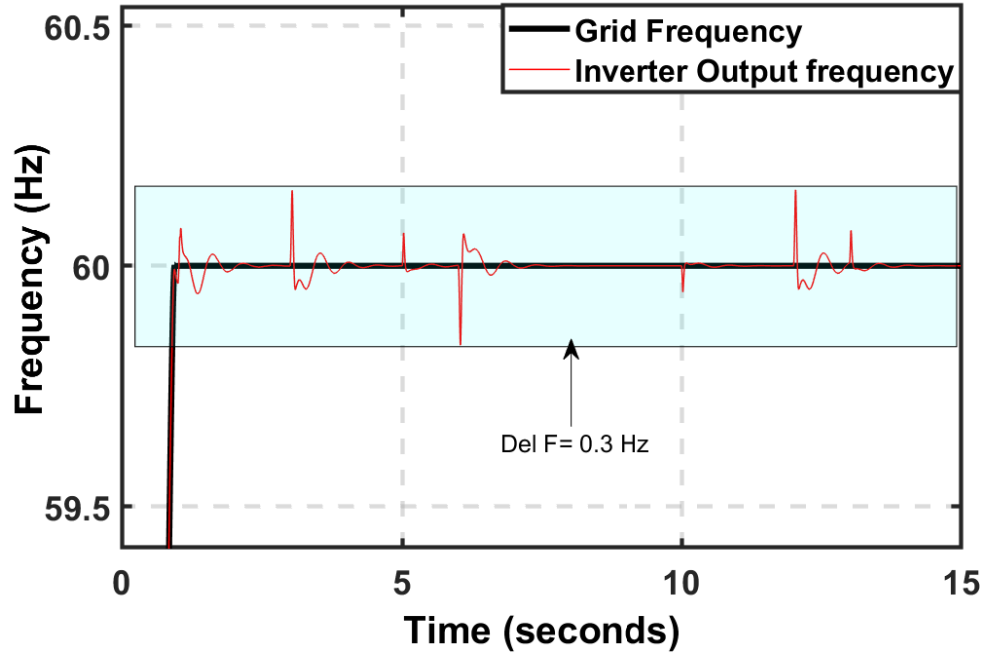
Figure 4.10: Frequency comparison of the MG POI and the grid side during SA mode of operation of the MG
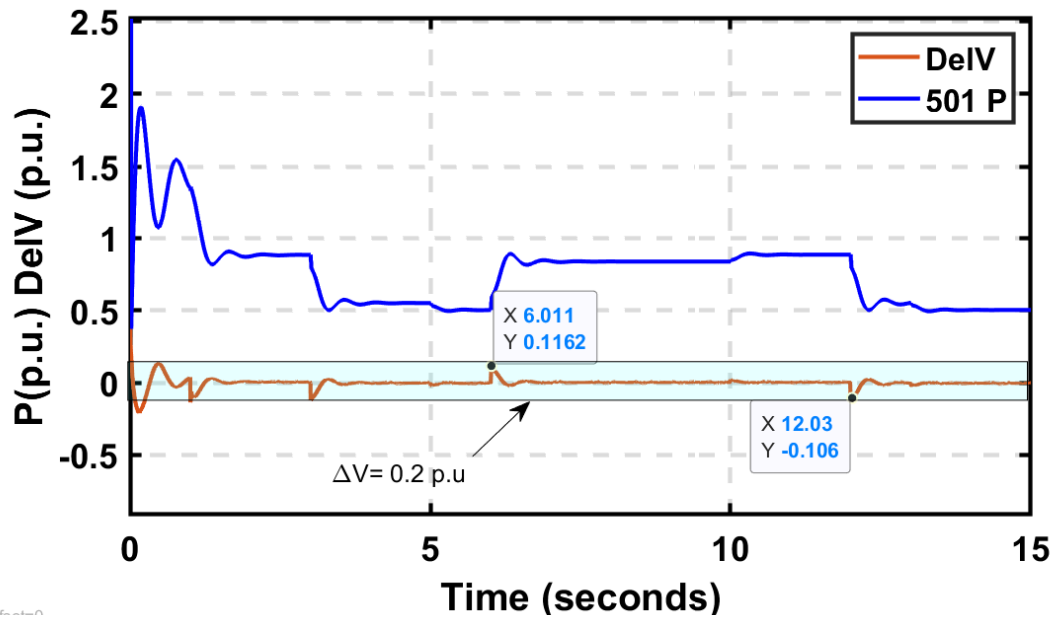
Figure 4.11: Voltage fluctuations during SA mode of operation with step load changes.

Fig. 4.12 and 4.13 show the active and reactive power tracking capability of the grid-following inverter during the the grid-connected mode of operation. This is similar to the chapter 1 results. Fig. 4.14 and 4.14 are the active and reactive power

Grid Following Inverter 501 Active Power
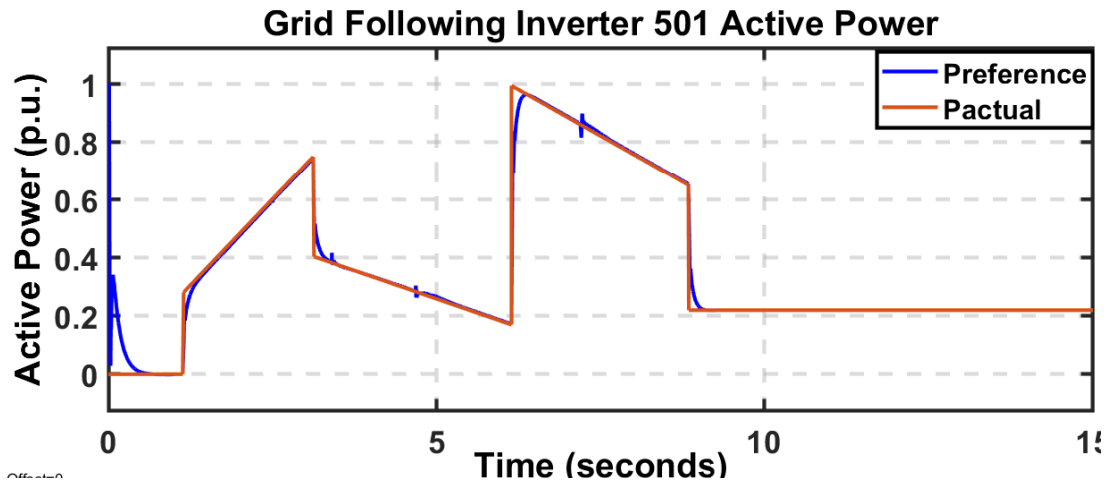
Figure 4.12: Active Power tracking for the grid following inverter.

Grid Following Inverter 501 Reactive Power
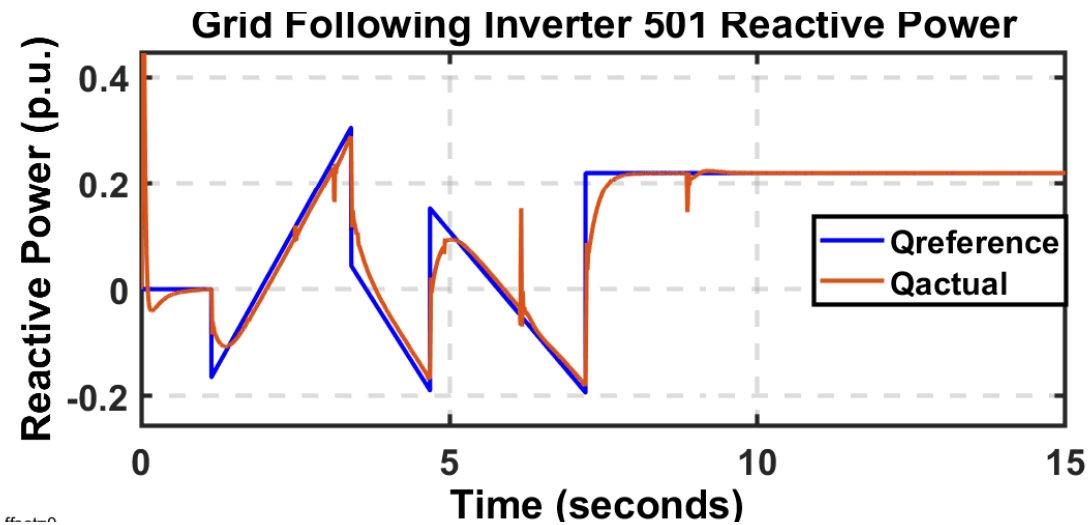
Figure 4.13: Reactive Power tracking for the grid following inverter.

tracking for the grid-supporting inverter. The power references are generated by the addition of normal reference set-points plus the ADMM control ouput.

4.5 Sequence Components base Control of Multiple Single Phase DER based Microgrids

There is an increase in interest and demand for research towards the decentralization of power generation in recent times. This has brought grid-forming inverters and the concept of micro-grids to the main stage. Especially with renewable resources garnering attention, there is an obligation towards control topologies not
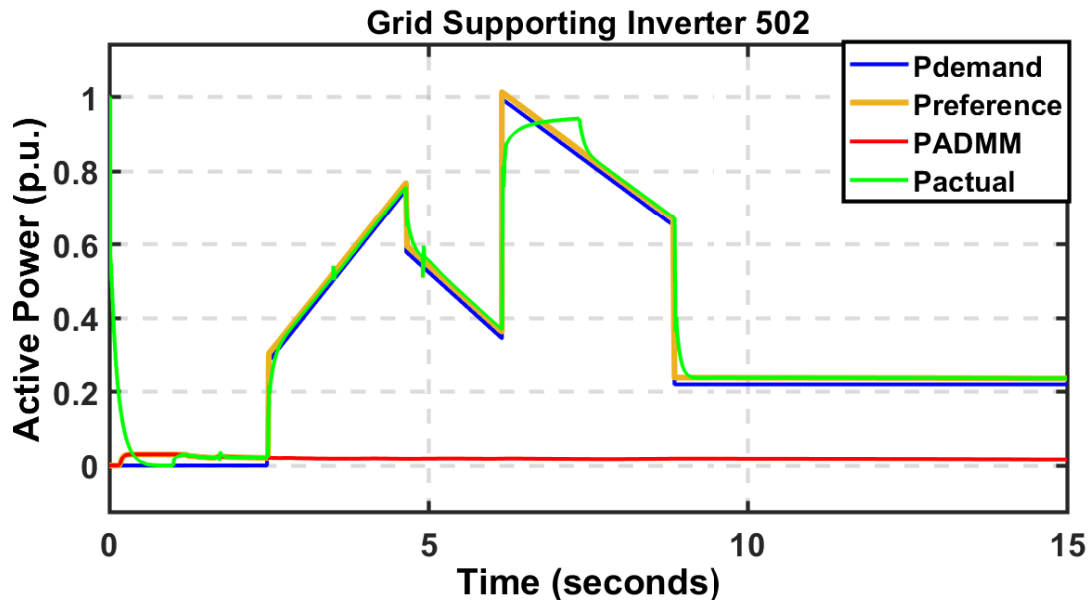
Figure 4.14: Active Power tracking for the grid supporting inverter.
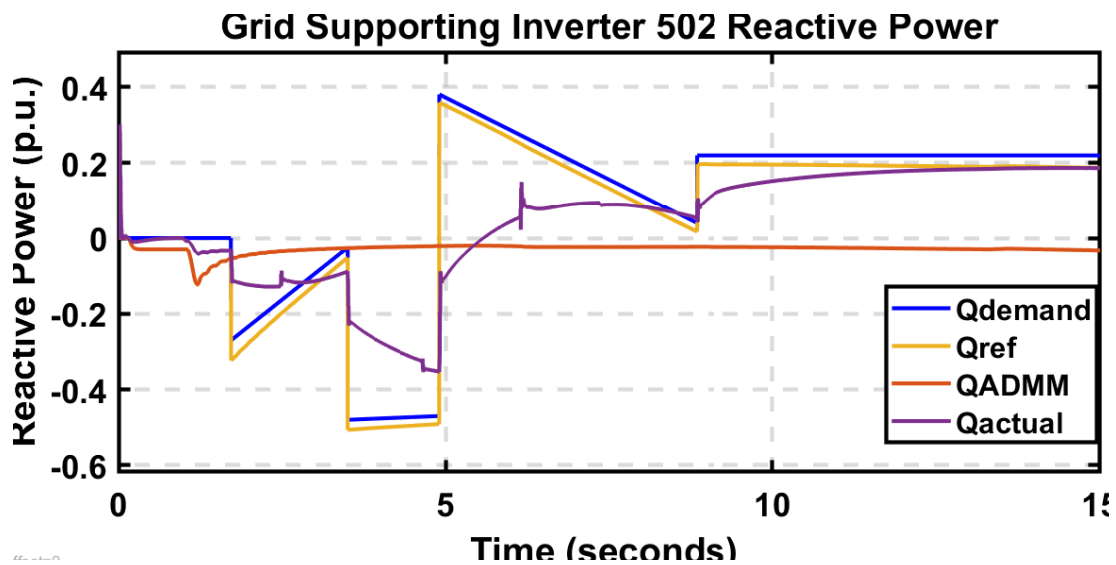
Figure 4.15: Reactive Power tracking for the grid supporting inverter.

only for Three-Phase inverters but Single-Phase Inverters (SPI) as well. Distributed Generation (DG) has numerous benefits such as back-up power for resiliency applications when EPS is down, peak load shaving, and other grid ancillary applications [107, 108, 109, 110]. For micro-grid applications, these DERs/DGs are sometimes the only available energy source available within the island and previous works have discussed off-grid or island-mode of operation for the inverters interconnecting the
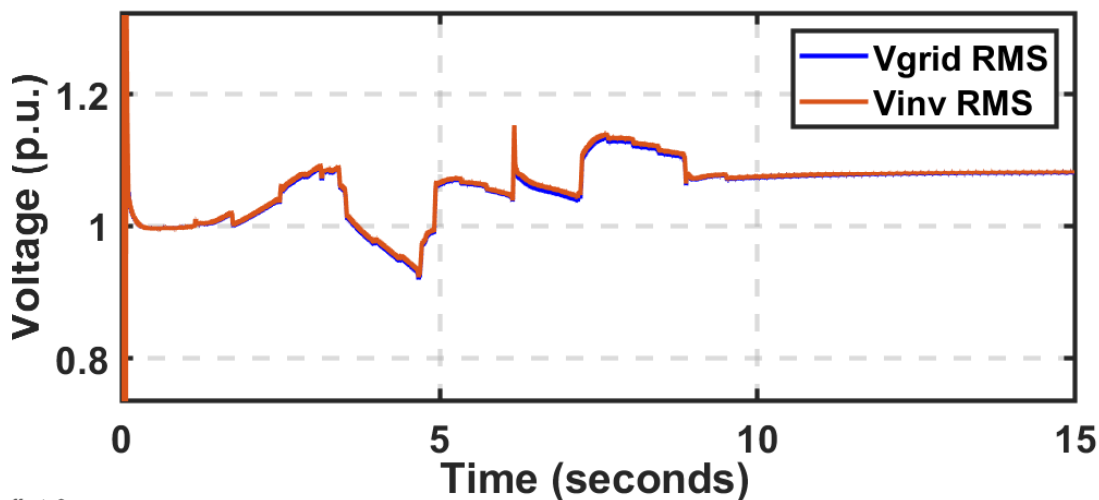
Figure 4.16: Point of Interconnection voltage
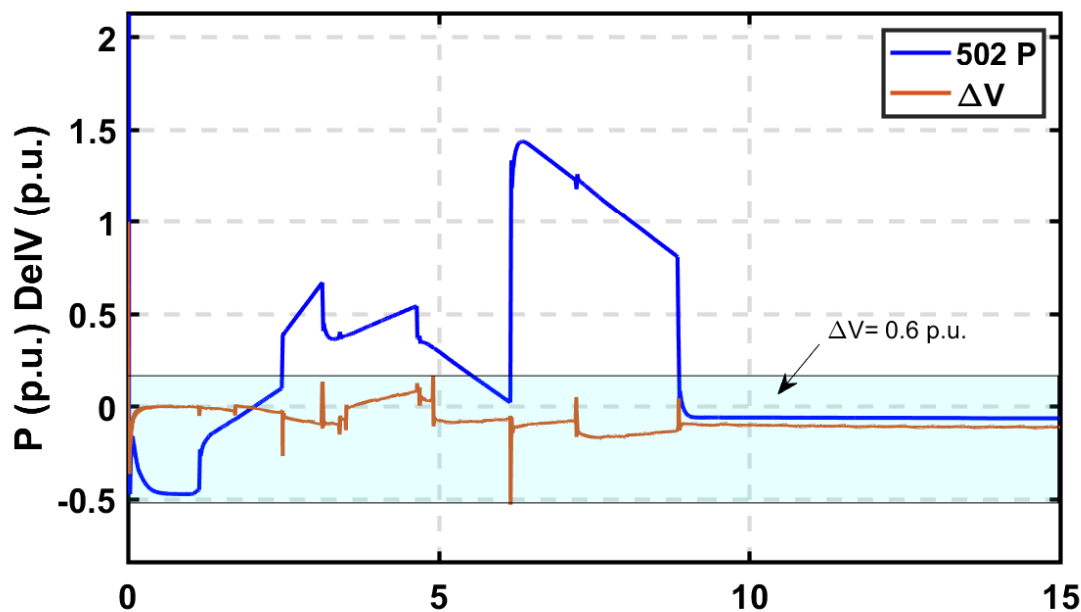
Figure 4.17: Modified droop with dq- control

critical loads to the DERs in detail [111, 112, 113, 114, 115]. These DERs are often connected to the local loads using an inverter; it can either be a three-phase or a single-phase inverter. Extensive research has been done on three-phase micro-grids with Three-Phase Inverters (TPIs) for voltage and frequency-based controls and current control-based grid-connected operating modes. SPIs, on the other hand, have been very rarely investigated as the primary source of power in three-phase and single-

phase micro-grids because of the output power capability limitation. Although, with the emergence of medium and low voltage micro-grids, Single-Phase Inverter systems (SPIs) are quickly gaining popularity.

A topic that needs more investigative efforts is controls of SPIs for low voltage (LV) three-phase micro-grids. Three-phase Inverters (TPIs) participate in balanced power control and injection in microgrids, whether grid-connected or islanded, and do not participate in unbalancing compensation or mitigation. SPIs have the capability to provide compensation for unbalance loading (i.e. negative and zero sequence) for both modes of operations (i.e. grid-connected and islanded) [116, 117]. In this paper, the authors investigate the effect of positive-, negative- and zero-sequence-based control on SPIs implemented in a three-phase micro-grid system. The controller architecture is that of the local dqframe-based control which either controls the symmetrical components (positive-, negative- and zero-sequence) of the output current (during grid-connected mode) or the same sequence components of the inverter output voltage and frequency (during islanded-mode). The advantage of doing this is to compensate for the unbalance presence in the circuit by utilizing the local controllers only and not depend on external communication or supervisory level power management loops to generate the set-points for the local/primary controllers. This methodology's other advantage is to curtail or mitigate negative sequence current injection into the grid during the grid-connected mode and during the transitioning between islanded/Stand Alone (SA) mode and Grid-Connected mode (GC).

The modification to the *dq*-frame control presented in this paper enables the inverter to operate in the three modes (grid supporting, grid forming, and grid feeding) with a seamless transfer strategy for Single-Phase grid-tied inverter using a Synchronous Reference Frame Phase Lock Loop (SRF-PLL). The modified SRF-PLL is responsible for the synchronization process, and the input to the PLL depends on the mode of operation of the inverter. The design and modeling of the proposed con-

troller and the individual components accomplishing the seamless transfer and grid interfacing modes are described in the paper. The contribution and major advantages of this work are:

- Negative sequence current damping during the grid-connected mode of operation.

- Better current amplitude regulation during transitioning between Grid-Connected (GC) and Stand Alone (SA) modes compared to traditional dq-domain based current control.

- Active participation from the inverters to mitigate power unbalances in the system.

- Flexibility in the operation of different modes due to the unified structure of the control architecture.

to provide a unified control topology capable of seamless transitioning between grid-connected and stand-alone mode of operation of the inverter and insight into the controller performance for different grid types and conditions.
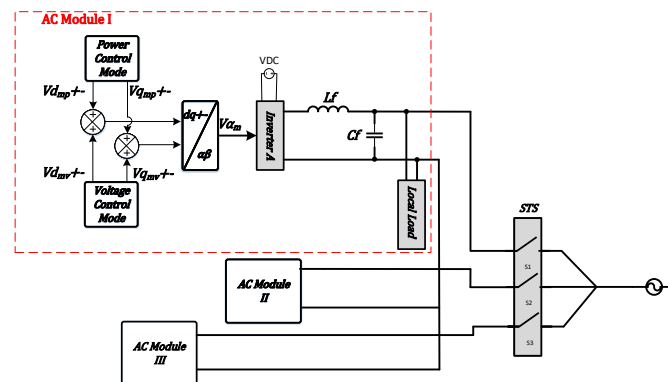
Figure 4.18: SPI based micro-grid connected to the utility via STS

4.5.1 System Description

This section discusses the proposed SPI positive and negative sequence-based dq-domain controller, sequence extraction process for the single-phase systems and the

seamless transfer algorithm for the GC to SA and SA to GC transition. The overall structure of the micro-grid (MG) is that of a balanced three-phase system where loads are attached at the PCC of the SPIs, the STSs are at the end of the MG or Point Of Interconnect (POI).

4.5.2 Single-Phase Inverter Based Micro-grids in a Three-Phase System

The grid-tied SPI configuration that is capable of grid-connected and islanded-mode operations is shown in Fig.4.18. The DC-module consists of a PV-battery system that serves as the source of power to the AC-module (i.e., inverter), connected to an LC-filter, local load, and eventually the STS that connects the DER to the utility/grid. The LC-type filter is chosen over the L-type filter for higher attenuation of harmonics. The LCL-type filter has a high resonant peak and contributes significantly to the series and parallel resonant frequency of the system when multiple inverters are involved [118].

The control system for the SPI shown in Fig. 4.18 is based on the dq-control strategy the authors used in [119], where the inner current loop is based on controlling the dq-frame current and the outer loop is responsible for controlling the voltage (for islanded-mode) and power (for grid-connected mode). The selection of the mode was done via a switch that allowed

4.5.2.1 Grid Connected Mode Control Topology

The grid-connected inverter is a current source when viewed from the grid side, and it is the inverter output current that is regulated by the current control loop. From Fig. 4.18 one can understand that power control mode is to be discussed for grid-connection as the voltage control is unnecessary for grid-connected inverters. Therefore, with Fig. 4.18 as a reference, the internal elements of individual inverter control architecture can be viewed as in Fig. 4.19. For this mode of operation, other than current measurements, the grid side voltage and phase sensing are essential

as the *dq*-axis transformation is dependent on this. The equations representing the dynamics of the output current and voltage can be written as:

$$\frac{d\,id_p}{dt} = \frac{-R_f}{L_f}id_p + \omega_o iq_p + \frac{1}{L_f}(Vcd_p) \tag{4.38}$$

$$\frac{d\,iq_p}{qt} = \frac{-R_f}{L_f}iq_p - \omega_o id_p + \frac{1}{L_f}(vq_p) \tag{4.39}$$

$$\frac{d\,Vcd_p}{dt} = \omega_o Vcq_p + \frac{id_p}{C_f} - \frac{Vcd_p}{C_f} \tag{4.40}$$

$$\frac{d\,Vcq_p}{dt} = -\omega_o Vcd_p + \frac{iq_p}{C_f} - \frac{Vcq_p}{C_f} \tag{4.41}$$

The controller equations therefore can be written as:

$$Vd_{mp} = \frac{d\,id_p}{dt} + \omega_o Liq_p + Vcd_p \tag{4.42}$$

$$Vq_{mp} = \frac{d\,iq_p}{dt} + \omega_o Lid_p + Vcq_p \tag{4.43}$$

Where Vd_{mp} and Vq_{mp} are the control signals generated from the inner current control loop. Writing the equations 4.43 in discrete domain such that the signals Vcd_p, Vcq_p, id_p and iq_p are constant during one sampling period, the controller equations can be re-written as:

$$
\begin{aligned}
Vd_{mp} = kp_{id}(i^*d_{p,k} - i^*d_{p,k}) + \frac{1}{T_i}\sum_{m=0}^{k-1}[i^*d_p - i^*d_p] \\
- \omega_o L\frac{i^*q_{p,k} + iq_{p,k}}{2} + Vcd_{p,k}
\end{aligned}
\tag{4.44}
$$

$$
\begin{aligned}
Vq_{mp} = kp_{iq}(i^*q_{p,k} - i^*q_{p,k}) + \frac{1}{T_i}\sum_{m=0}^{k-1}[i^*q_p - i^*q_p] \\
- \omega_o L\frac{i^*d_{p,k} + id_{p,k}}{2} + Vcq_{p,k}
\end{aligned}
\tag{4.45}
$$

Where $i^*d_{p,k}$ and $i^*q_{p,k}$ are the current references for the inner loop current control. Using 4.46 the reference current signals can be generated using active and reactive power demand, initiated by the end user, obtainable DER power or utility.

$$P_{inv} = v_{Ld}i_{Ld}$$
$$Q_{inv} = v_{Ld}i_{Lq}$$

(4.46)

The control strategy used in this section involves an active and reactive power control loop as the secondary outer loop and current control as the primary inner loop, as shown in Fig. 4.19. The active power is linked with the d-axis component of the inverter output current and reactive power with the q-axis component. The dq-axis components of the current are acquired from the Park's transformation block with the phase angle estimated from the SF-PLL. The active and reactive power calculation
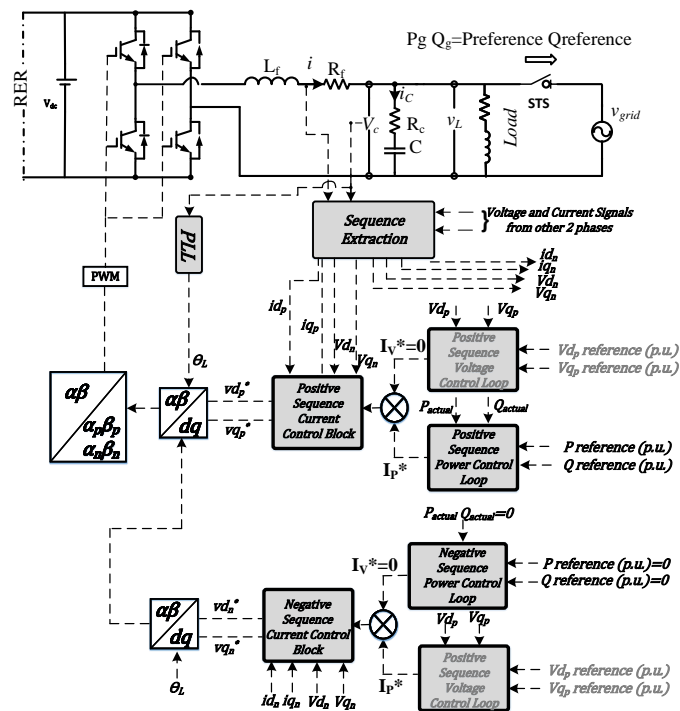
Figure 4.19: Grid connected inverter and controller architecture.

is performed using the equations, where the dq-axis signals of inverter output voltage and current are utilized to evaluate the output powers. This serves as the feedback

signal to the outer power control loop. This loop aims to provide efficient active and reactive power tracking and zero steady-state error during normal grid conditions.

4.5.2.2   Stand Alone Mode Control Strategy

The inverter control topology is a dual loop controller for sequence-based control action; the outer loop regulates the voltage across the capacitor, and the inner loop regulates the inductor current. PI controllers can quickly achieve zero steady-state error for the dq-axis components of the measured filter voltage and current at the inverter output. Hence, they are utilized for the Stand Alone (SA) or islanded-mode of operation. SA mode requires the inverters to 'form the grid' for the local loads. Hence the necessity/priority is given to provide a constant rated voltage and frequency at its terminals. The control architecture for the SA mode of operation of the inverter utilized in this section is described in Fig. 4.20.
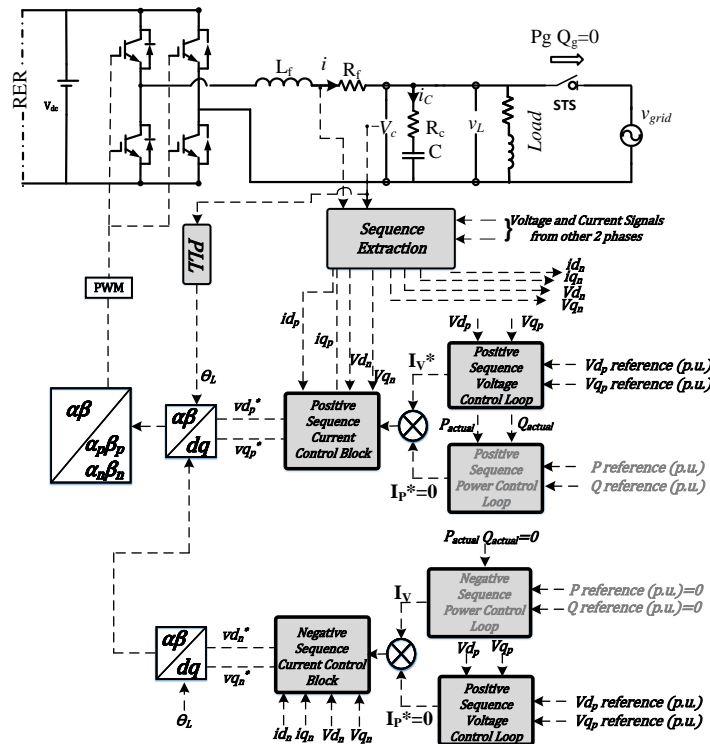
Figure 4.20: Stand Alone inverter and controller.

During the SA mode of operation, the contribution of the GC-mode outer loop is

brought to zero. In other words, the output of the active and reactive power control loop does not contribute towards controlling the inverter output current via the inner control loop.

4.5.2.3 Symmetrical Component Extraction for Single-Phase Inverter based Micro-grids

Thus section explores the sequence extraction for voltages and currents measured at the output filter of single-phase inverters. Three-phase signals are mandatory for sequence extraction, and multi-inverter (single-phase) based micro-grids are short-handed on the number of signals required for the symmetrical transformation. The load allocation and planning for the micro-grid are done so that the phases are balanced, making the transformation process simpler. The voltage and current signals on the output of the inverters are taken as feedback signals for the positive and negative sequence-based dq-control framework. In order to accomplish this, we first assume the ABC signals as:

$$I_A(t) = \sqrt{2}I\,cos\theta(t)$$

$$I_B(t) = \sqrt{2}I\,cos(\theta(t) - 2\pi/3) \tag{4.47}$$

$$I_C(t) = \sqrt{2}I\,cos(\theta(t) + 2\pi/3)$$

Where I is the RMS value of the signal, I_A, I_B, and I_C are the ABC signals, The first step towards extraction of symmetrical components is the transformation from ABC to alpha-beta-zero domain. This can be done by,

$$\begin{bmatrix} I_\alpha \\ I_\beta \\ I_0 \end{bmatrix} = \frac{2}{3} \begin{bmatrix} 1 & -1/2 & -1/2 \\ 0 & \sqrt{3}/2 & -\sqrt{3}/2 \\ 1/2 & 1/2 & 1/2 \end{bmatrix} \cdot \begin{bmatrix} I_A \\ I_B \\ I_C \end{bmatrix} \tag{4.48}$$

The simplification of the alpha component,

$$I_\alpha = \frac{2}{3}\left(\sqrt{2}I\,cos\theta(t) - \frac{\sqrt{2}}{2}\left(I\,cos(\theta(t) - \frac{2\pi}{3}) \right. \right.$$

$$\left. \left. + I\,cos(\theta(t) + \frac{2\pi}{3}) \right) \right)$$

$$I_\alpha = \frac{2}{3}\left(\sqrt{2}I\,cos\theta(t) - \frac{\sqrt{2}}{2}I\left(2\,cos(\theta(t))cos\left(\frac{2\pi}{3}\right) \right) \right) \tag{4.49}$$

$$I_\alpha = \frac{2I}{3}\left(\frac{2\sqrt{2}\,cos\theta(t) + \sqrt{2}\,cos\theta(t)}{2} \right) \tag{4.50}$$

$$I_\alpha = \sqrt{2}I\,cos\theta(t) \tag{4.51}$$

Similar simplifications for beta component can be done arriving at,

$$I_\beta = \sqrt{2}I\,sin\theta(t) \tag{4.52}$$
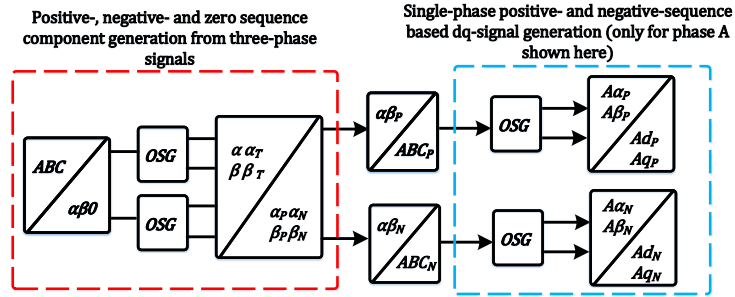
Figure 4.21: Sequence extraction block for single-phase systems in dq-domain

Generating the symmetrical sequence components in the alpha-beta-zero domain can be accomplished by utilizing the Orthogonal Sequence Generator (OSG) technique. OSG is a method wherein the original signal is shifted by 90°. Original signals in the $\alpha\beta0$ domain after passing through the OSG can then be utilized to create the

symmetrical components,

$$I_{\alpha P} = \frac{1}{2}\left[I_\alpha - I_{\beta_T}\right]$$

$$I_{\alpha N} = \frac{1}{2}\left[I_\alpha + I_{\beta_T}\right]$$

$$I_{\beta P} = \frac{1}{2}\left[I_{\alpha_T} + I_\beta\right]$$

$$I_{\beta N} = \frac{1}{2}\left[I_{\alpha_T} - I_\beta\right]$$

(4.53)

Where $I_{\alpha P}, I_{\alpha N}, I_{\beta P}$ and $I_{\beta N}$ are the positive and negative sequence components of the alpha and beta signals, respectively. I_{α_T} and I_{β_T} are the orthogonal signals for the alpha and beta signals, respectively.

$$I_{\alpha_T} = I_\beta = \sqrt{2}I\, sin\theta(t)$$

$$I_{\beta_T} = \sqrt{2}I\, sin\left(\theta(t) - \frac{\pi}{2}\right)$$

$$I_{\beta_T} = -\sqrt{2}I\, cos\theta(t)$$

(4.54)

$$I_{\alpha P} = \frac{1}{2}\left[\sqrt{2}I\, cos\theta(t) + \sqrt{2}I\, cos\theta(t)\right]$$

$$I_{\alpha P} = \sqrt{2}I\, cos\theta(t)$$

$$I_{\beta P} = \frac{1}{2}\left[\sqrt{2}I\, sin\theta(t) + \sqrt{2}I\, sin\theta(t)\right]$$

$$I_{\beta P} = \sqrt{2}I\, sin\theta(t)$$

(4.55)

$$I_{\alpha_N} = \frac{1}{2}\left[\sqrt{2}I\,cos\theta(t) - \sqrt{2}I\,cos\theta(t)\right]$$

$$I_{\alpha_P} = 0$$

$$I_{\beta_N} = \frac{1}{2}\left[\sqrt{2}I\,sin\theta(t) - \sqrt{2}I\,sin\theta(t)\right]$$

$$I_{\beta_P} = 0$$

(4.56)

Once the positive and negative sequence components (in the $\alpha\beta 0$ domain) are formulated, they can be transformed into the ABC-domain as shown below,

$$\begin{bmatrix} I_{A_P} \\ I_{B_P} \\ I_{C_P} \end{bmatrix} = \begin{bmatrix} 1 & 0 & 1 \\ -1/2 & \sqrt{3}/2 & 1 \\ -1/2 & -\sqrt{3}/2 & 1 \end{bmatrix} \cdot \begin{bmatrix} I_{\alpha_P} \\ I_{\beta_P} \\ I_{0_P} \end{bmatrix}$$

(4.57)

$$I_{A_P} = \sqrt{2}I\,cos\theta(t) + I_0$$

(4.58)

$$I_{B_P} = -\frac{1}{2}\sqrt{2}I\,cos\theta(t) + \frac{\sqrt{3}}{2}\sqrt{2}I\,sin\theta(t)$$

$$I_{B_P} = \sqrt{2}I\,cos\left(\theta(t) - \frac{2\pi}{3}\right)$$

(4.59)

$$I_{C_P} = -\frac{1}{2}\sqrt{2}I\,cos\theta(t) - \frac{\sqrt{3}}{2}\sqrt{2}I\,sin\theta(t)$$

$$I_{C_P} = \sqrt{2}I\,cos\left(\theta(t) + \frac{2\pi}{3}\right)$$

(4.60)

The disadvantage of a single-phase system is that dq-transformation and other three-phase transformations are difficult to compute as there is only one signal available. Although, work has been done to generate a virtual orthogonal signal that modifies

single-phase phase systems or signals into the $\alpha - \beta$-domain signals. These signals can then be utilized to form dq components for stationary-frame-based controllers. The following equations can show this,

$$I_{A_P} = I_{A\alpha_P}$$
$$I_{A\alpha_P} = \sqrt{2}I\,cos\theta(t) \tag{4.61}$$

$$I_{A\beta_P} = I_{A\alpha_P} + 90°$$
$$I_{A\beta_P} = \sqrt{2}I\,cos(\theta(t) - \pi/2) = \sqrt{2}I\,sin\theta(t) \tag{4.62}$$

So the dq-frame signals for phase A can be written as:

$$I_{Ad_P} = \left[I_{A\alpha_P}\,cos\theta(t) + I_{A\beta_P}\,sin\theta(t)\right]$$
$$I_{Aq_P} = \left[-I_{A\alpha_P}\,sin\theta(t) + I_{A\beta_P}\,cos\theta(t)\right] \tag{4.63}$$

$$I_{Ad_P} = \left[I_{A\alpha_P}\,cos\theta(t) + I_{A\beta_P}\,sin\theta(t)\right]$$
$$I_{Aq_P} = \left[-I_{A\alpha_P}\,sin\theta(t) + I_{A\beta_P}\,cos\theta(t)\right] \tag{4.64}$$

Finally, simplifying the equations the d-axis corresponds to the amplitude of the current signal:

$$I_{Ad_P} = \sqrt{2}I$$
$$I_{Aq_P} = 0 \tag{4.65}$$

4.5.2.4   Seamless Transfer Algorithm Modifications

Grid voltage waveforms are balanced during normal operating conditions, but during an anomaly, three-phase voltages can be unbalanced, or detection of positive-sequence voltage component becomes an issue, and hence it affects the inverter synchronization/ process. For three-phase inverters, techniques have been devised for detecting the fundamental positive-sequence voltage that aids the generation of a proper synchronization signal [120, 121]. For single-phase inverters, one phase voltage (L-N) signal is sufficient for PWM generation and synchronization capability. Although, in a three-phase micro-grid architecture, the STS operation will work concurrently in all the Three-Phases.
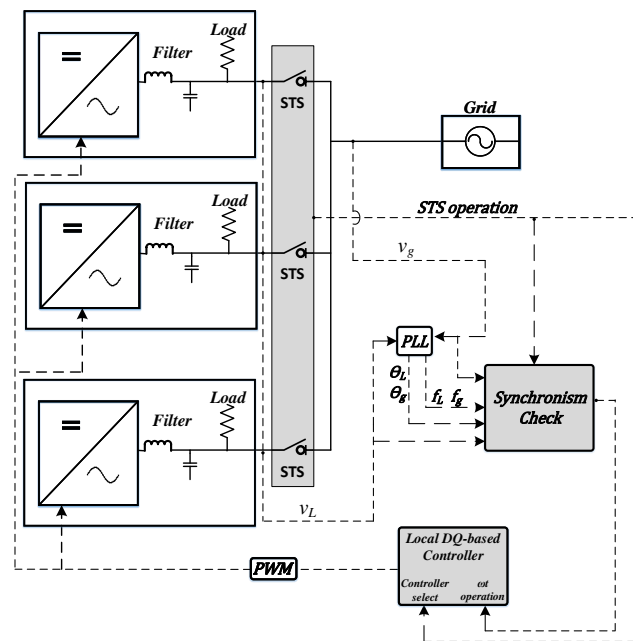
Figure 4.22: Transfer Control Architecture on the SPI

The seamless transfer operation is dependent on the PLL and the transfer decision block as shown in Fig. 4.23. Grid connection and disconnection are performed via the STS switch, which is controlled by the seamless transfer decision block which works in tandem with the SRF-PLL to generate the appropriate synchronization and

STS status signal. The sequence of operation for disconnection and re-connection is discussed in the coming subsections where the two types of transitions will be discussed, namely, transfer from grid-connected to stand-alone mode and transfer from stand-alone to the grid-connected mode.

<div align="center">Grid Connected to Stand Alone Mode</div>

Anomalous behavior on the grid, such as grid voltage sag/swell and faults, will cause the transfer decision block to trip the STS and protect the critical local loads and the inverter from any form of aberrant operation. To avoid the potential escalation of anomalous operation of the inverter, the PLL switches to a stand-alone mode of operation. For a successful grid operation, as discussed previously, the PLL takes a 0 reference for the q-axis voltage comparison with the inverter rather than the grid side q-axis voltage as reference (all the signals are per unitized). The detailed sequence of events can be illustrated as:

- Seamless transfer decision block acquires the grid side voltage signal and checks for the frequency and voltage for normal operating conditions. It evaluates the RMS value and the 60Hz frequency operation every $50\mu s$.

- If the normalcy check fails the synchronization status switches the PLL operation from GC mode to SA mode of operation. Phase A PLL reference is switched from v_{qg} to zero. This will neutralize the sudden jump of the phase angle provided by the PLL and causes the PWM for phase A voltages to operate $\omega_o t$. For the other two MGs, the phase angle is provided $120°$ apart. This will allow the three-phase MG to have positive sequence components of voltage and current measurement signals.

- The control mode changes from power regulation (or current regulation) to voltage control mode, in which, current references generated from the outer power loop (I_P^*) are set to zero. Current references, in this case, are provided

by the outer voltage control loop (I_V^*).
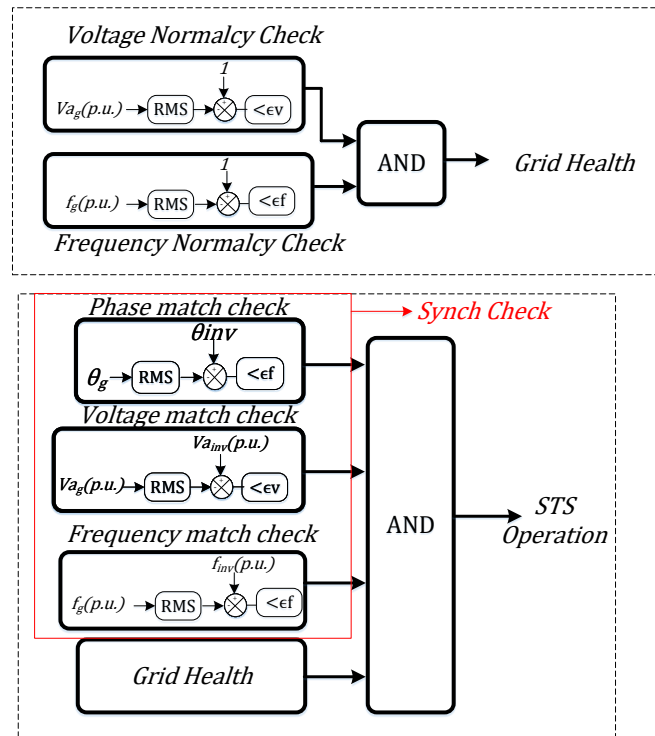
Figure 4.23: Seamless transfer decision block

4.5.2.5   Transition from Off-Grid to Grid-Connected Mode

The removal of the fault or anomaly will cause the voltage/frequency deviation to go away; however, grid connection cannot be attempted without synchronization of all the DERs in the three phases. For synchronization to occur, inverter voltage and grid voltage magnitude, frequency, and phase must match for all three phases, and then the error between the two should be minimal and as presented in Table 3.2. The sequence of events for the transition from stand-alone mode to grid-connected mode can be explained as:

- Transfer decision block constantly monitors the grid side voltage signal and checks for the frequency and voltage RMS value for normal operating conditions. It evaluates the RMS value and the 60Hz frequency operation every 50μs.

- If the grid side voltage and frequency are within normal operating range as described by IEEE 1547, the decision block generates the appropriate 'synchronization status' signal for the PLL, commanding the inverter output phase lock with the grid side phase angle.

- Inside the PLL, the q-axis reference voltage signal changes from 0 to grid side v_{qg} which compares to the q-axis voltage of the inverter v_q. This action leads to the generation of ωt for the PWM such that the inverter output phase begins to match the grid side phase angle.

- Outer loop voltage control and PLL maintains the inverter output voltage and frequency as close to the rated value.

- if the grid and inverter side signals pass the match check blocks described in Fig.4.23, then the STS is triggered, allowing the micro-grid to transition from SA mode to GC mode.

4.5.3   Simulation Results

Verifying the validity of the proposed controller with the seamless transfer operation, different simulation cases were performed using Simulink.

Case 1: Frequency Sag The AC module utilized for these simulation cases is a synchronous generator that can simulate a frequency/voltage sag. The three-phase MG is presented in Fig. 4.22, where each SPI is attached to one of the system's Three-Phases. Frequency sag excursion is created such that it causes the system frequency to sag to 0.95 p.u. or 0.05 p.u. asâfor 57Hz at T= 10.03sec. According to section3.4, the microgrid should be able to disconnect with the local EPS or the grid within 0.16 seconds. The controller was created to allow maximum ride through. Therefore a 0.16-second ride-through can be seen in Fig.4.24 where the breaker trip signal is generated at 10.19 seconds which is 0.16seconds after the frequency sag excursion is acknowledged.
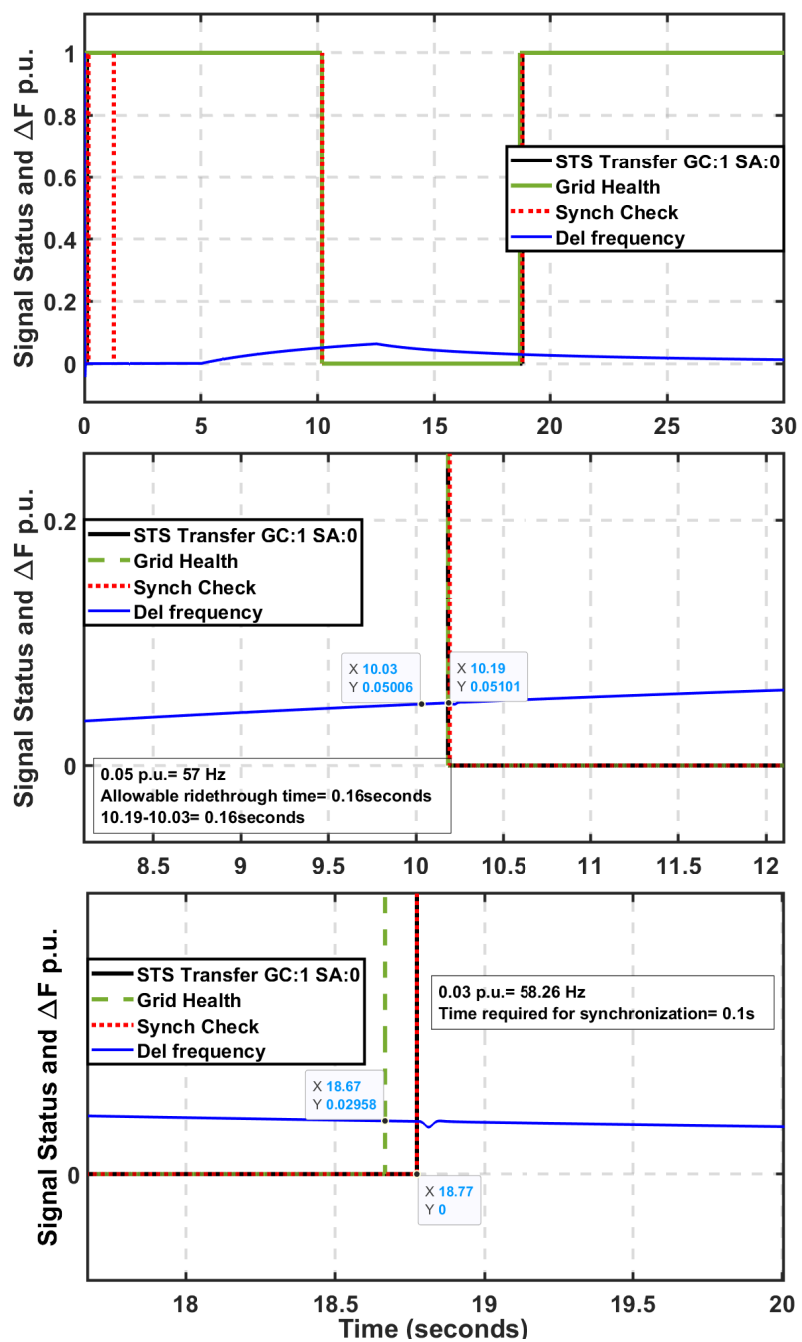
Figure 4.24: Seamless transfer checks and breaker operation during frequency sag on grid side.

Re-connection back to the grid involves frequency, amplitude, and phase checks, where the inverter controller is modulated. The instantaneous inverter voltage latches to the grid, as shown in Fig 4.25. During the time frame described as **island-mode: Grid Synchronization**, the inverter controller adjusts its PLL to synchronize the inverter output voltage to the grid.
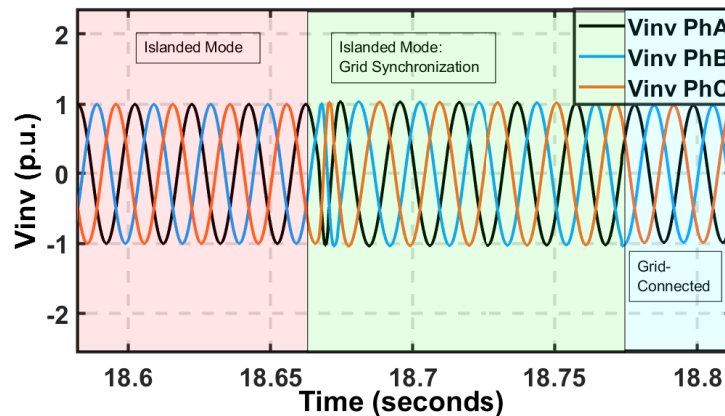
Figure 4.25: Inverter voltage during re-synchronization back to the grid

Sequence components of the inverter output voltage and current show that during the frequency sag excursion no negative sequence component of voltage and current were generated. Fig. 4.26, 4.27 and 4.28 show the generated sequence components of inverter voltages in the $\alpha\beta$- and dq-frame.

Sequence components of the currents shown in Fig. 4.30 and 4.31 give an insight into the efficacy of sequence generation blocks explained in earlier sections and the ability of the inverters to control the sequence components as one unit. Fig. 4.29 shows the three-phase current output measured on the PCC of each inverter, and one can observe that during the transitions, the negative sequence components are kept at a minimum.

Case 2: Voltage Sag Utilizing the generator, a step change on the grid-side voltage was provided instead of gradual voltage sag. This was done to observe the difference in the negative sequence components for a harsh voltage deviation; Fig. 4.32 shows the grid and inverter RMS voltage (per unit) overlapped with the grid health and breaker
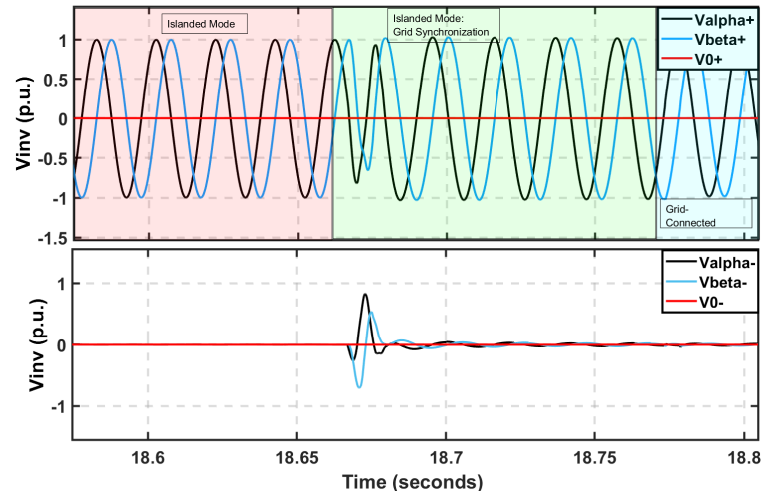
Figure 4.26: Positive and negative sequence alpha beta components during grid connection
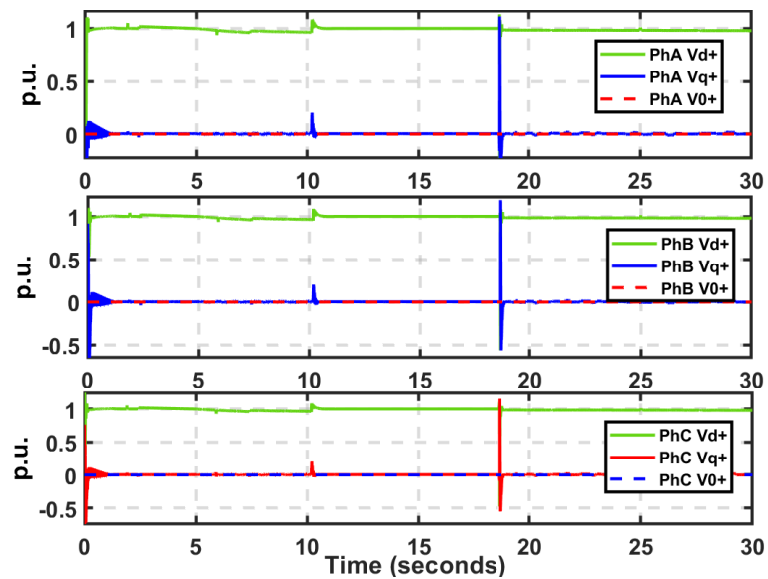
Figure 4.27: Positive sequence components of inverter output voltages in DQ-frame during frequency sag excursion.
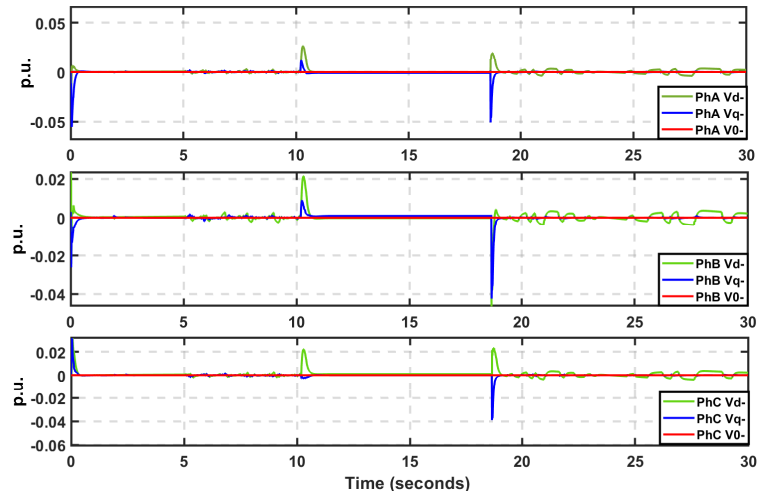
Figure 4.28: Negative sequence components of inverter output voltages in DQ-frame during frequency sag excursion.
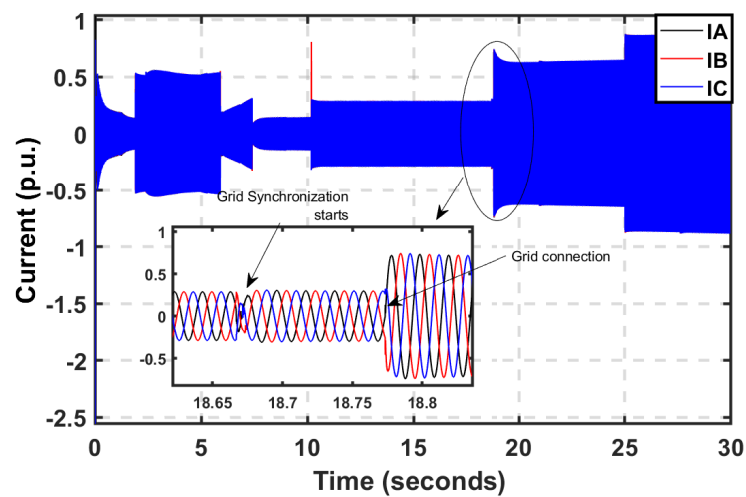
Figure 4.29: Inverter output current for all Three-Phases during the frequency sag excursion.
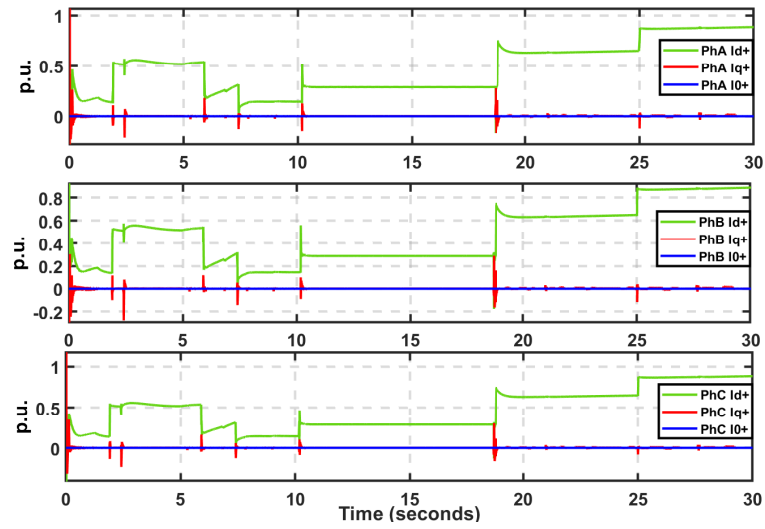
Figure 4.30: Positive sequence components of inverter output current in DQ-frame during frequency sag excursion.
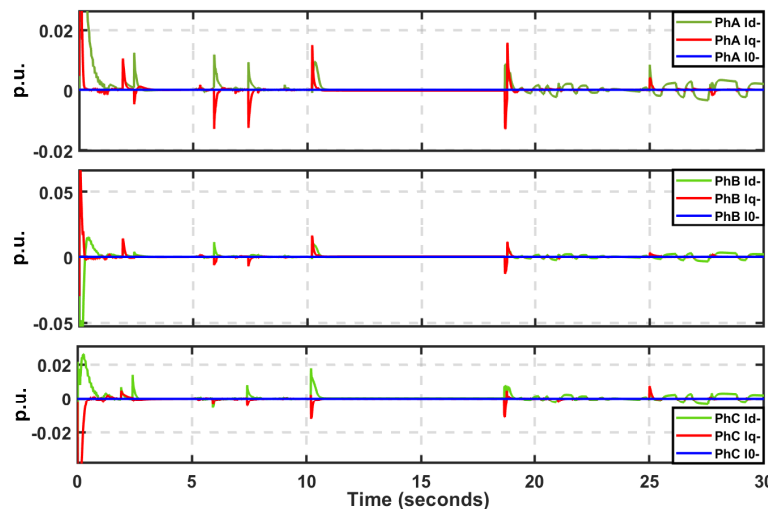
Figure 4.31: Negative sequence components of inverter output current in DQ-frame during frequency sag excursion.

status signals. What can be observed is that the local controllers allow the inverter to ride through for 0.16 seconds, and during the disconnection, the inverter immediately returns to its normal operating voltage with a 120% overshoot and achieves a steady-state value of 1 p.u. within 1 second.
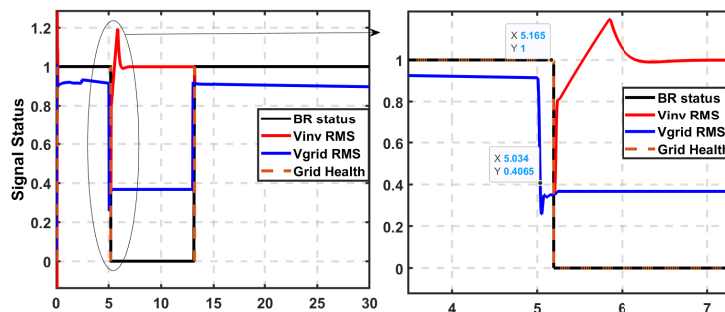
Figure 4.32: Grid health monitoring and breaker status during voltage sag excursion.
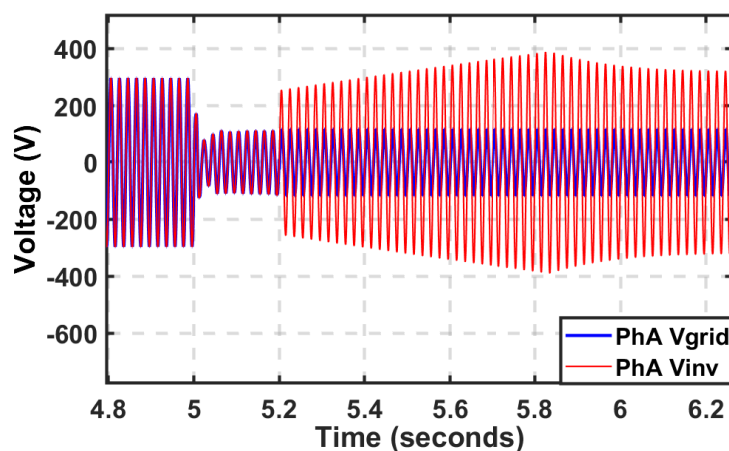
Figure 4.33: Phase A grid and inverter voltage during inverter transition from grid-connected to stand alone mode for voltage sag on the grid side.

Similar to frequency sag excursion, the positive sequence values are coequal to the actual rated values of the inverter. Fig. 4.35,4.36 and 4.37 showcase the results of the voltage component generation blocks, and these signals are eventually sent to the local controllers for negative sequence quenching. An observation can be made that a small negative sequence voltage component is observed at 0.01 p.u. steady-state value.
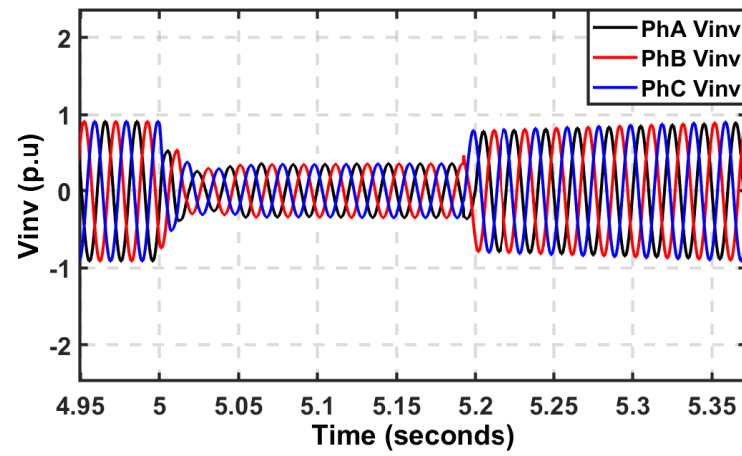
Figure 4.34: Three-phase inverter output voltage response for voltage sag excursion.
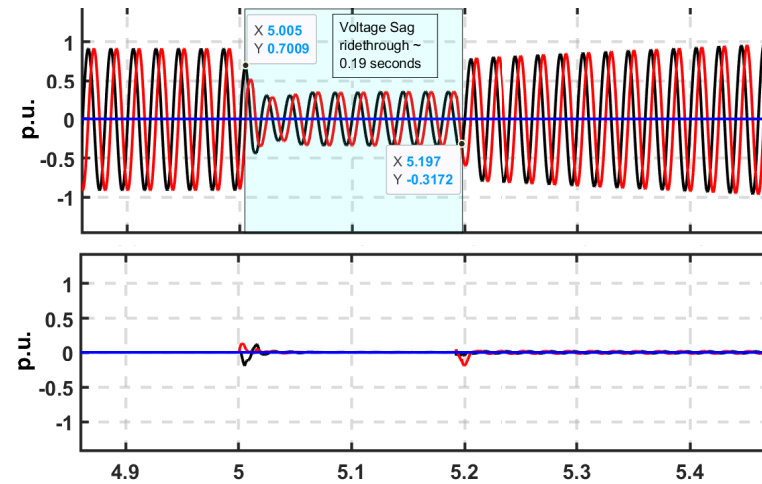
Figure 4.35: Alpha-Beta frame sequence components of inverter output voltage during voltage sag excursion.
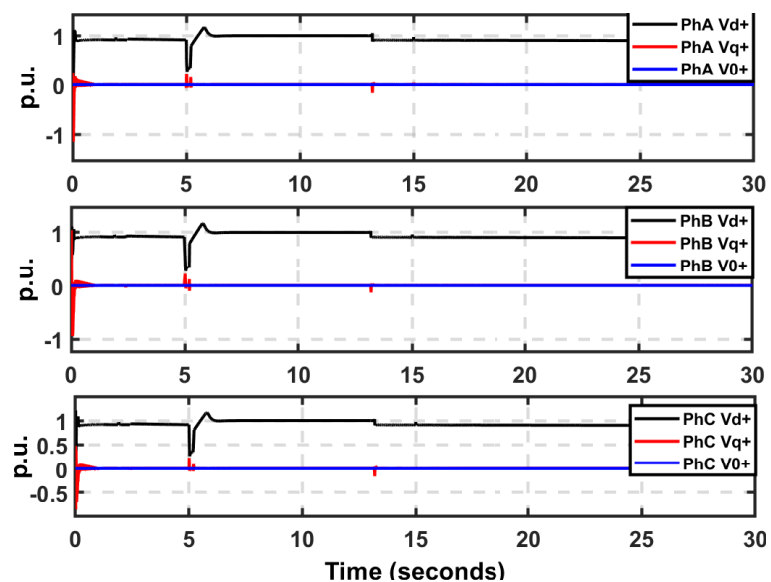
Figure 4.36: Positive sequence DQ-frame components of inverter output voltage during voltage sag excursion.
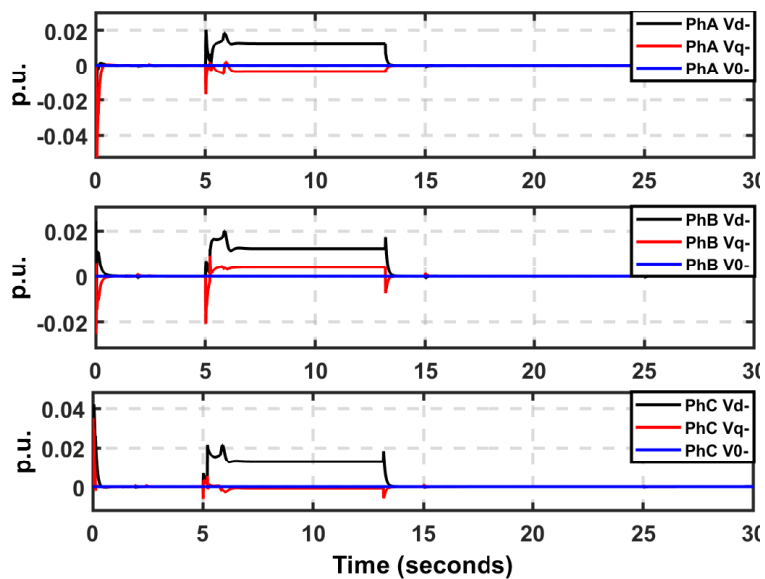
Figure 4.37: Negative sequence DQ-frame components of inverter output voltage during voltage sag excursion.

Similarly, the current components are shown in Fig. 4.38 and 4.39. During a harsh voltage jump, the negative sequence component for the inverter output current overshoots up to 0.1 p.u. Although, due to the control action, this negative sequence component is quenched within 0.2 seconds.
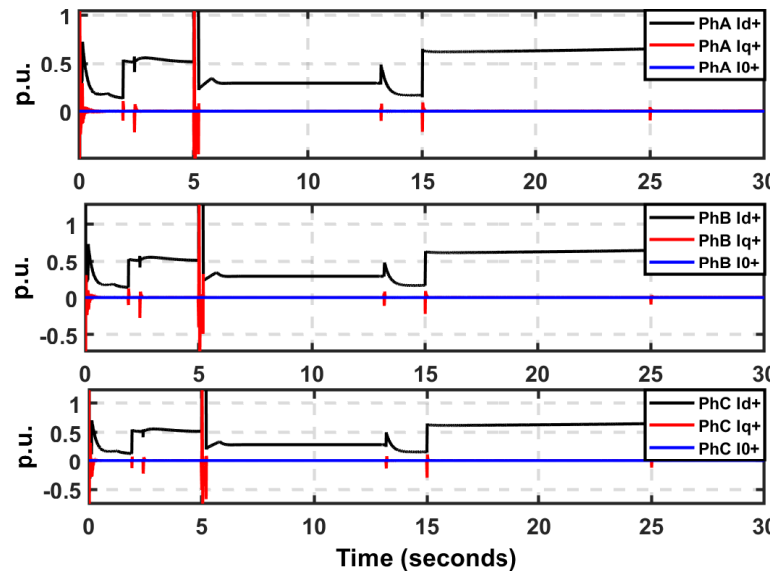
Figure 4.38: Positive sequence DQ-frame components of inverter output current during voltage sag excursion.

4.6   Summary

In this chapter, a secondary level controller is explored based on the droop impedance matrix for LV and MV distribution networks. ADMM is utilized here to identify the system impedance matrix and eventually provide reference set-points for the local controller for active and reactive power. To test the control performance, two inverters in a SMIB system were utilized to simulate GC and SA mode of operation. In SA mode, one inverter forms the grid, and the other inverter was made to follow. Simulation studies then performed showcased that the inverters shared the active power coequally while maintaining the system voltage and frequency at the rated value. In SA mode, ΔV was less than 0.2 p.u. for 1.4 MW step load change and Δf was kept within 0.3 Hz. Similarly, the control architecture functionality was tested out for GC
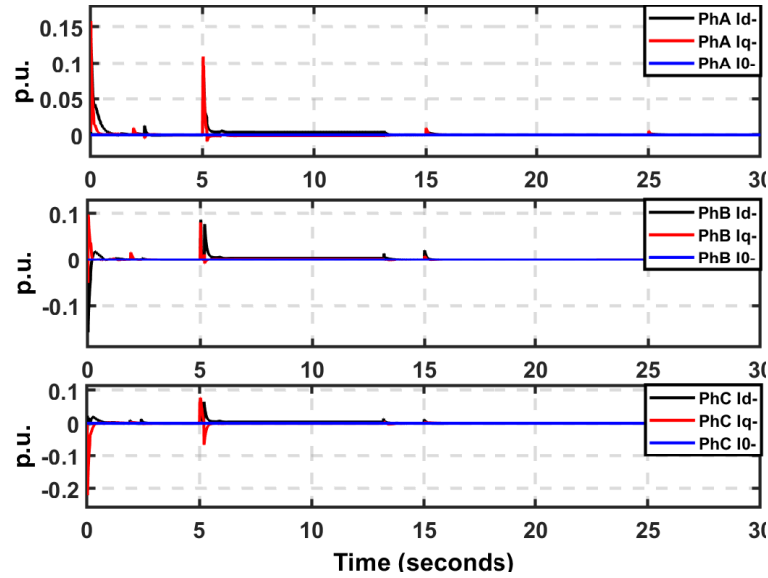
Figure 4.39: Negative sequence DQ-frame components of inverter output voltage during voltage sag excursion.

mode where grid-following and supporting features were tested. The second half focuses on the contributions by Single-Phase Inverters (SPIs) in three-phase micro-grid systems. A novel unified control architecture for single-phase inverters in three-phase micro-grid systems is presented that utilizes voltage and current sequence components for the grid current and inverter output voltage control during grid-connected and stand alone mode of operation respectively. Mathematical framework was presented to generate postive-negative-zero sequence based dq-axis signals for each phase and eventually utilized by individual SPI for active-reactive power control for GC mode and voltage and frequency control for SA mode of operation. One advantage that this form of control strategy is that the negative sequence components can be quenched utilizing the sequence based controllers presented in this chapters. The sequence based controller was evaluated for SA and GC mode separately and eventually simulated in tandem with the earlier formulated seamless transfer alogrithm for SPIs.

CHAPTER 5: Multiple Microgrid Management using Novel Adaptive controller framework

In the previous chapter, power management strategy for muliple DER within the same MG structure was investigated. Traditional droop application fails for different network configurations and R/X ratios, hence an adaptive framework was proposed that identified system parameters for finer power sharing between the DERs. The local controller formulated in the previous chapter is encapsulated in the 'DER' framework in this chapter where multi-MG control and power management strategies are explored.

5.1   Introduction

This chapter presents an ADMM based multiple-input multiple-output (MIMO) identification method to generate individual transfer functions relating to inverter output power (active (P) and reactive (Q)) which are input control sources and voltages (V) of the locations in the power grid. Transfer functions generated by the MIMO identification can imbibe the sensitivity of powers concerning voltage perturbation [122]. A Kalman estimator and linear quadratic regulator (LQR) based optimal controller is designed to find the optimal active and reactive power support from the inverter to manage the powers and voltage. The whole architecture is formulated based on the active and reactive power droop concept.

Different coordination or optimal control schemes have been explored earlier to allow the inverter to dispatch reactive powers [123, 124, 125, 126]. Most of the solutions can control the voltage only at the inverter nodes or utilize the feedback data for localized regulation or control. ADMM based identification offers an architecture

that is capable of changing the point of interest to a "non-local" bus or a node away from the PCC of the inverters. Other works on compensation devices like capacitor bank placement, series compensation devices, STATCOMS have been explored in the past [127, 128, 129]. However, these methods are not the most economical solutions for the "ever-changing" distribution networks. The availability of reactive powers in distributed inverters can prove to be a valuable commodity and can be utilized for various voltage and frequency regulation applications[130].

The proposed method has the following advantages:

- Dynamic MIMO architecture based on the identification of the transfer functions ($P_{unbalance}$/P, P/V and Q/V) can change with varying operating conditions accurately determining input/output changes.

- Optimal control framework can coordinate with multiple inverters providing dynamic set points.

- The approach is scalable, independent of X/R ratios, and works for a larger system with different inverter capacities.

5.2   Main Contributions

The main contribution of the work presented in this chapter are as follows:

- Optimal control framework can coordinate with multiple inverters providing dynamic set points.

- Power management of multiple SPI-based (multi-phase) microgrids has been presented in this chapter that utilizes the universal droop control strategy to generate the active and reactive power references for the local controllers.

- ADMM based secondary controller architecture is utilized to accurately identify and generate active and reactive power set-points showcased for cases like power unbalance mitigation in distribution networks, and local bus voltage regulation.
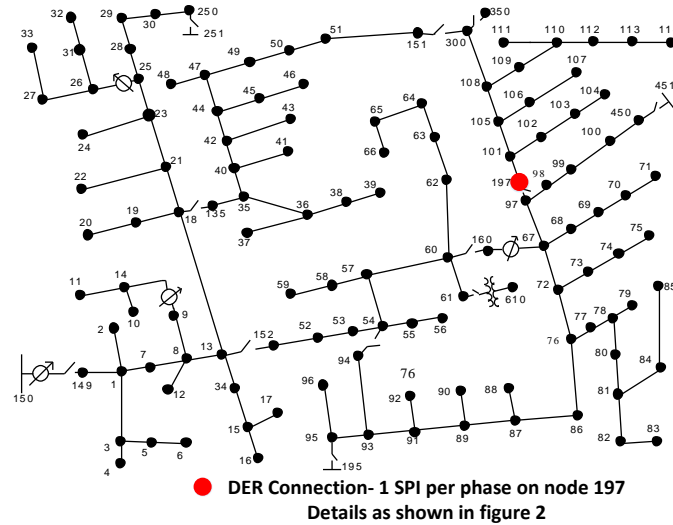
Figure 5.1: DER connection on the IEEE 123 Bus system.

- Higher-order ADMM is provided in the chapter that improves the Volt/Var dynamics and has a better response to voltage deviations at the point of interconnection of the MG.

- The approach is scalable, independent of X/R ratios and works for larger system with different inverter capacity.

5.2.1   System Configuration

The simulation study and modeling are performed using the MATLAB/Simulink platform. Inverters and controllers, including the DC-module, AC-module of the renewable energy source (RES), and the IEEE 123 bus system, are modeled. The PV-battery system, including their respective DC-DC converters, make up the DC-module. The DC-module is interfaced with the grid using the H-bridge inverter and is responsible for supplying the active power to the grid sideload. The reactive power circulates between the source and the load, and their generation is credited to the inverter (switches and diodes)[7]. Table. 5.1 shows the ratings of the SPIs used in this chapter.

The methodology is validated on the IEEE 123 node test feeder system as shown

Table 5.1: Rated power and voltage for Inverters 510, 502 and 503

Inverter	Power (kVA)	Voltage (kV)	Bus	Phase Connected
Inv 501	50	2.4	197	A
Inv 502	50	2.4	197	B
Inv 503	50	2.4	197	C

in Fig. 5.1. This system is inherently unbalanced with weak downstream buses. The system's inherent dynamics are captured by the proposed control, and based on the calculated sensitivity, active power management, and voltage regulation is achieved. The proposed controller can be applied to areas with devices that can improve power quality and voltage profile. Bus 197 on the IEEE 123 bus system shows promise for these conditions, and the data from the power flow conclude that this is one of the weaker buses in the system. Thus, three Single-Phase inverters are placed in each phase of the particular bus to provide power and voltage support for every phase independent of the other.

5.2.2   Proposed Control Architecture and Power Flow Management

To control the active and reactive power flowing out of the inverter a *dq-* based controller is implemented [9]. Subsequent sub-sections will provide the details on the dq-axis model of the grid-connected inverter topology and how the ADMM and LQR based controller can be used for power-sharing with multiple inverters.

5.2.3   Single-Phase Inverter Connections and Signal Flow

Fig. 5.2 shows the connections of the three Single-Phase inverters in the distribution network. DQC in the figure represents the DQ-frame-based active and reactive power control. The three inverters ($501, 502$ and 503) set-points are provided by the utility generally, but the references are based on the universal droop control methodology in this chapter. The ADMM algorithm optimizes the additional dynamics or correction (see Fig. 5.2), where the P_{50x} (x representing any of the three inverters) are the power output of the inverters used by DQC to generate the droop control reference. The
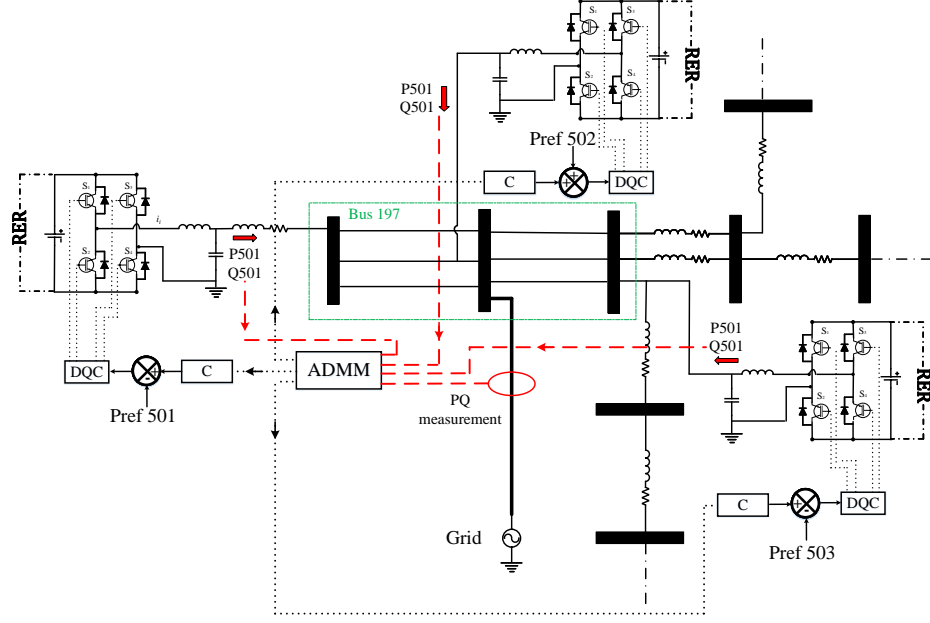
Figure 5.2: Single-Phase inverter connections with the ADMM based supervisory controller.

additional ΔP_{50x}, is the output of the ADMM algorithm. The extra power needed to satisfy the unbalance and voltage deviation is provided by the proposed joint ADMM and LQR algorithm. The inputs to the ADMM as shown in Fig. 5.2 are the upstream and individual power flowing from the SPIs.

5.2.4 Universal Droop controller

Traditional droop equations work well for high voltage power networks where the R/X ratio is low, but in distribution networks with the unbalanced network, traditional droop fails [131]. This chapter sees a utilization of modified droop equations to provide active and reactive power references to SPIs. Equations (5.1), (5.2) and (5.3) represent the active and reactive power from the three inverters (501, 502 and 503) respectively. In these equations, the R is the line resistance, X is the line reactance and Z is the lime impedance.

$$
\begin{bmatrix} P'_{50x} \\ Q'_{50x} \end{bmatrix} = \begin{bmatrix} X/Z & R/Z \\ -R/Z & X/Z \end{bmatrix} \cdot \begin{bmatrix} P_{50x} \\ Q_{50x} \end{bmatrix} \tag{5.1}
$$

$$\begin{bmatrix} P'_{50x} \\ Q'_{50x} \end{bmatrix} = T. \begin{bmatrix} P_{50x} \\ Q_{50x} \end{bmatrix} \tag{5.2}$$

where

$$T = \begin{bmatrix} X/Z & R/Z \\ -R/Z & X/Z \end{bmatrix} \tag{5.3}$$

The traditional droop equation can be written as:

$$f_o - f = -k_p(P'_{50xo} - P'_{50x}) \tag{5.4}$$

$$V_o - V = -k_q(Q_{50xo} - Q'_{50x}) \tag{5.5}$$

where f_o and V_o are the base system frequency and voltage respectively, and k_p and k_q are the respective droop gains for the same. We use the predetermined impedance matrix to couple the frequency and voltage changes with the additional active and reactive power reference (P'$_{50x}$, Q'$_{50x}$). Here, x is a generalization that can either be 1,2, or 3, depending on the inverter.

5.2.5 ADMM Based MIMO transfer function identification

ADMM is an optimization algorithm that combines advantages of dual ascent method and method of multipliers. It attempts to solve problem as shown in (5.6) where primal variable is split into two parts, x and z.

$$\begin{aligned} \text{minimize} \quad & f(x) + g(x) \\ \text{subject to} \quad & Ax + Bz = c \end{aligned} \tag{5.6}$$

Similar to the method of multiplier approach, an augmented Lagrangian can be formed as shown in (5.7) and thus the algorithm consists of an x-minimization step, a z-minimization step, and a dual variable update step as discussed in [104, 105] and

shown in (5.8), (5.9) and (5.10).

$$L_\rho(x, z, y) = f(x) + g(x) + y^T(Ax + Bz - c) + \frac{\rho}{2}||Ax + Bz - c||^2 \qquad (5.7)$$

$$x^{k+1} := \underset{x}{\mathrm{argmin}} L_\rho(x, z^k, y^k) \qquad (5.8)$$

$$z^{k+1} := \underset{z}{\mathrm{argmin}} L_\rho(x^{k+1}, z, y^k) \qquad (5.9)$$

$$y^{k+1} := y^k + \rho(Ax^{k+1} + Bz^{k+1} - c) \qquad (5.10)$$

Using (5.3), one can determine the active and reactive power reference for the DQC, as shown in Fig. 5.2. Here, the changes in the active and reactive power (ΔP_{50x} and ΔQ_{50x}) are captured by the ADMM identification.
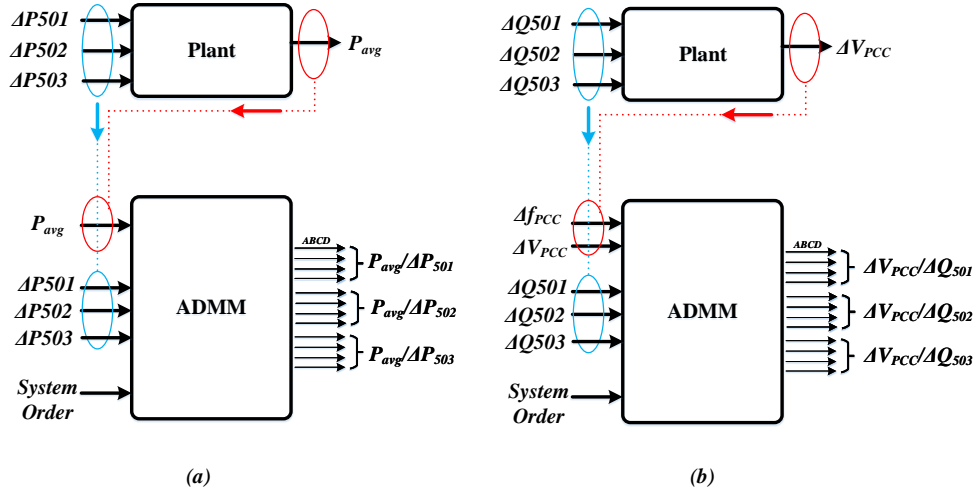
Figure 5.3: The ADMM based MIMO transfer function identification block.

$$\begin{bmatrix} P'_{50x} + \Delta P'_{50x} \\ Q'_{50x} + \Delta Q'_{50x} \end{bmatrix} = T. \begin{bmatrix} P_{50x} \\ Q_{50x} \end{bmatrix} + T. \begin{bmatrix} \Delta P_{50x} \\ \Delta Q_{50x} \end{bmatrix} \qquad (5.11)$$

$$T. \begin{bmatrix} \Delta P_{50x} \\ \Delta Q_{50x} \end{bmatrix} = \begin{bmatrix} \Delta Pref_{50x} \\ \Delta Qref_{50x} \end{bmatrix} \Big\} ADMM\ output \qquad (5.12)$$
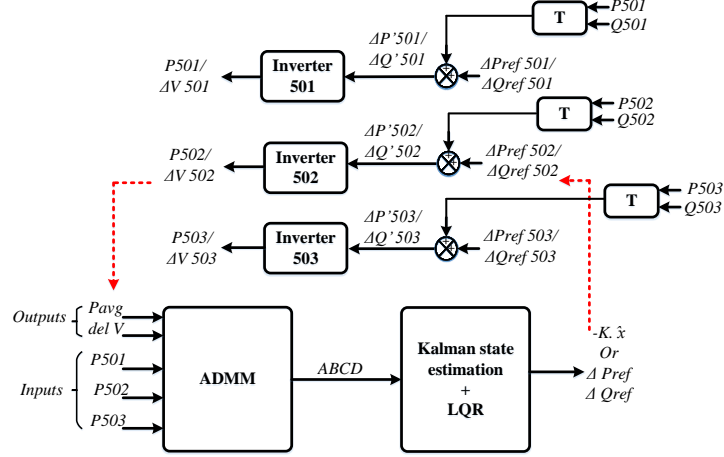
Figure 5.4: Supervisory active and reactive power sharing control based on power unbalance and voltage deviation.

As shown in Fig. 5.3, the ADMM algorithm utilizes the inputs and outputs of the MIMO plant to generate individual transfer functions for each input and output combination. This assimilates the relationship of one output to every input.

5.2.5.1 Active Power Identification for Power Unbalance Mitigation

Then the MIMO transfer function for power balancing with the individual inverter powers can be written as

$$
\begin{bmatrix} P_{avg} \end{bmatrix} = \begin{bmatrix} G_1(z) & G_2(z) & G_3(z) \end{bmatrix} \begin{bmatrix} P_{501} \\ P_{502} \\ P_{503} \end{bmatrix} \tag{5.13}
$$

where P_{avg} is the power required from the inverters in order to balance the Three-Phase upstream powers and P_{501}, P_{502} and P_{503} are the active power output from inverter 501, 502 and 503 respectively. Based on the MIMO transfer functions, the individual transfer functions (G1, G2 and G3) can be represented as

$$
G_1 = \frac{P_{avg}}{P_{501}} = \frac{b_0^{501} + b_1^{501} z^{-1} + ... + b_k^{501} z^{-k}}{1 + a_1^{501} z^{-1} + a_2^{501} z^{-2} + ... + a_k^{501} z^{-k}} \tag{5.14}
$$

$$G_2 = \frac{P_{avg}}{P_{502}} = \frac{b_0^{502} + b_1^{502}z^{-1} + ... + b_k^{502}z^{-k}}{1 + a_1^{502}z^{-1} + a_2^{502}z^{-2} + ... + a_k^{502}z^{-k}} \qquad (5.15)$$

$$G_3 = \frac{P_{avg}}{P_{503}} = \frac{b_0^{503} + b_1^{503}z^{-1} + ... + b_k^{503}z^{-k}}{1 + a_1^{503}z^{-1} + a_2^{503}z^{-2} + ... + a_k^{503}z^{-k}} \qquad (5.16)$$

where b_0, b_1...,b_k are the numerator coefficients of the transfer functions and $a_1,a_2...a_k$ are the denominator coefficients of the transfer functions. ADMM method uses least squares method to first estimate the individual transfer functions and reach a global consensus problem. Then a global consensus optimization problem can be formulated as:

$$\min_{a^{501}..a^{503}} \frac{1}{2}||[P][a] - [B] + [P_x][b]||^2 \qquad (5.17)$$

where a is a vector of all the denominator coefficients and b is the vector of all the numerator coefficients. Also, B is the matrix of the current samples of P_{50x}, P is the matrix of the previous samples of P_{avg} and P_x are the previous samples of P_{50x}. The objective is to make $a^{501}=a^{501}=a^{501}=z$ for a global consensus problem, so the numerator and denominator coefficients are calculated iteratively till the objective is achieved.

5.2.5.2   Reactive Power Contribution for Voltage control

Similar technique, as discussed in the previous section, can be used to formulate the reactive power reference for the local inverter control for voltage support. Transfer function relating deviation in voltage with output reactive power from the three inverters (501,502 and 503) can be written as

$$\begin{bmatrix} \Delta V_{avg} \end{bmatrix} = \begin{bmatrix} G_1(z) & G_2(z) & G_3(z) \end{bmatrix} \begin{bmatrix} Q_{501} \\ Q_{502} \\ Q_{503} \end{bmatrix} \qquad (5.18)$$

where ΔV_{avg} is the average deviation of the bus voltage, and Q_{501}, Q_{502} and Q_{503} are the reactive power output of the Single-Phase inverters connected on bus 197. Individual component of the reactive power reference can be generated from the voltage deviation seen at the particular bus through the proposed controller and can be implemented for any bus on the system. The sensitivity of the reactive power output with the voltage deviation can be observed by the ADMM.
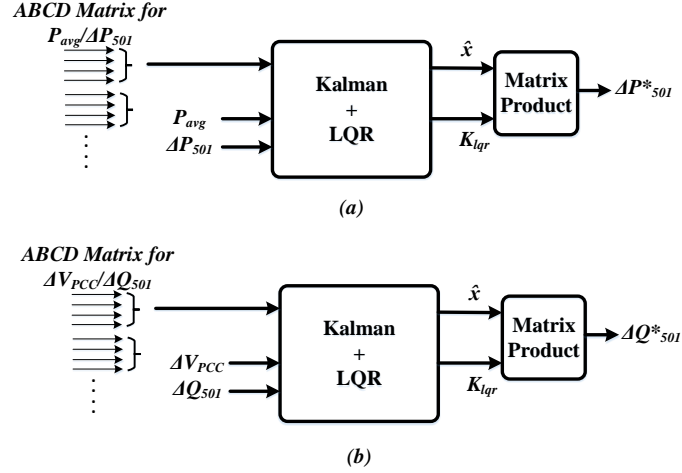
Figure 5.5: Kalman state estimation and LQR control block generating control outputs based on ABCD matrices from ADMM.

5.2.6   Kalman Estimation and LQR Controller Design

After the transfer function identification, the ABCD matrices are generated using a Kalman filter and LQR [106]. As shown in Fig. 5.5, $Y1$ and $U1$ are the plant input and output. The plant state and measurement equations can be written as

$$x[n+1] = Ax[n] + BP_{50x}[n] \tag{5.19a}$$

$$P_{avg} = Cx[n] \tag{5.19b}$$

$$\hat{x}[n+1] = A\hat{x}[n] + BP_{50x}[n] \tag{5.20a}$$

$$P = APA' + Q \tag{5.20b}$$

$$K = \frac{PC'}{CPC' + R} \tag{5.20c}$$

where P is the error co-variance matrix, K is the kalman gain, R and Q are the output and input noise co-variance matrix respectively. Further, the measurement residual is calculated, the state and error co-variance matrix estimate are updated which can be written as (5.21).

$$residual = P_{50x} - C\hat{x}[n] \tag{5.21a}$$

$$\hat{x}[n+1] = A\hat{x}[n] + K * residual \tag{5.21b}$$

$$P = (I - KC)P' \tag{5.21c}$$

The discrete time quadratic problem is then to minimize is

$$\sum(\hat{x}^T Q_1 \hat{x} + P_{50x}^T R_1 P_{50x}) \tag{5.22}$$

The unique stabilizing solution can be given by the control

$$K = (R_1 + B^T X B)^{-1} B^T X A \tag{5.23}$$

5.2.7   Local Controller for the Single-Phase Inverter

The local controller (DQC) as shown in Fig. 5.12, is represented in dq- reference frame

$$P = (v_d i_d + v_q i_q) = v_d i_d \tag{5.24}$$

$$Q = (v_d i_q + v_q i_d) = v_d i_q \tag{5.25}$$

The power references can then be given as

$$\frac{P'_{50x}}{v_d} = i_{dref} \tag{5.26}$$

$$\frac{Q'_{50x}}{v_d} = i_{qref} \tag{5.27}$$

where P'_{50x} and Q'_{50x} are the active and reactive power references provided by the ADMM and droop control as shown in Fig. 5.4. In Fig.5.4, $\Delta Pref_{50x}$ and ΔQ_{50x} are the additional power references provided by the ADMM based controller.

5.3   Simulation results

This section discusses the various simulation, performed utilizing a full detail model in the MATLAB/Simulink software. The simulation study was done on three cases to show the power-sharing between the inverters using the ADMM methodology:

- $Case1$: Active power-sharing using the upstream power flow to determine the contribution to be made by individual inverters to balance the upstream active power.

- $Case2$: Voltage deviation managed by the reactive power support provided by the inverters. Voltage dynamics at the PCC are observed by the controller, and appropriate reactive power set-points are derived.

- $Case3$: Both active and reactive power sharing by SPIs to perform active power balancing with voltage deviation mitigation via control of reactive power.

5.3.1   Case 1: Active Power Unbalance Correction

For this particular case, the inherent active power unbalance between the Three-Phases was mitigated by SPIs at bus 197. The dotted curves in Fig. 5.6 show the unbalance without inverter support. It can be seen that that PhA_{nosupp},PhB_{nosupp} and PhC_{nosupp} are clearly unbalanced. In the same figure, overall upstream powers of Bus 197, PhA_{ADMM}, PhB_{ADMM} and PhC_{ADMM}, converge after inverter support. Fig. 5.6, also shows the three inverter $(501, 502$ and $503)$ active and reactive power contribution. Reactive powers are zero because the references provided to the local converters are set to zero, and also, during no support, the active and reactive power
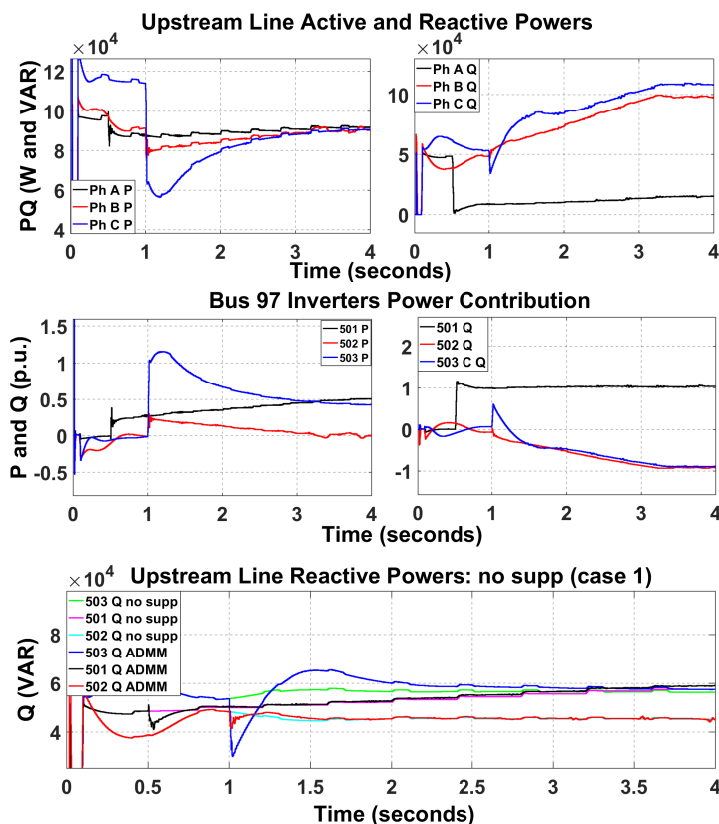
Figure 5.6: Case 1: Upstream line active and reactive powers and after active power balancing provided by the inverter.
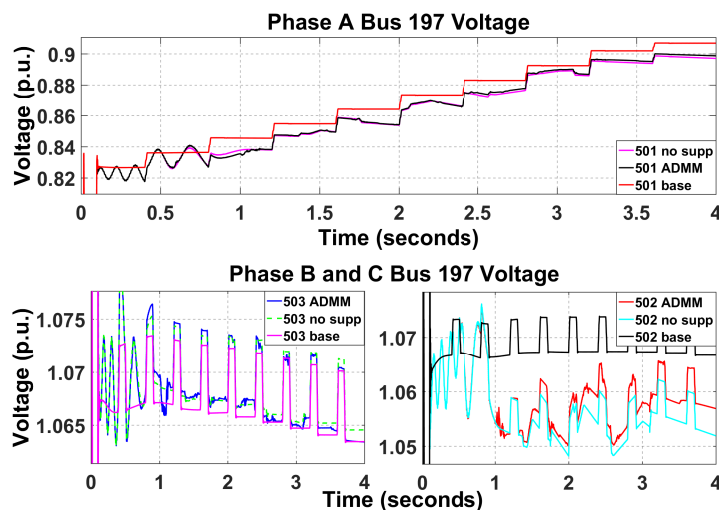
Figure 5.7: Case 2: Bus 197 voltages before amd after ADMM based support through reactive power injection.

references on the DQCs are zero. However, the active power contributions can be seen in Fig. 5.6.
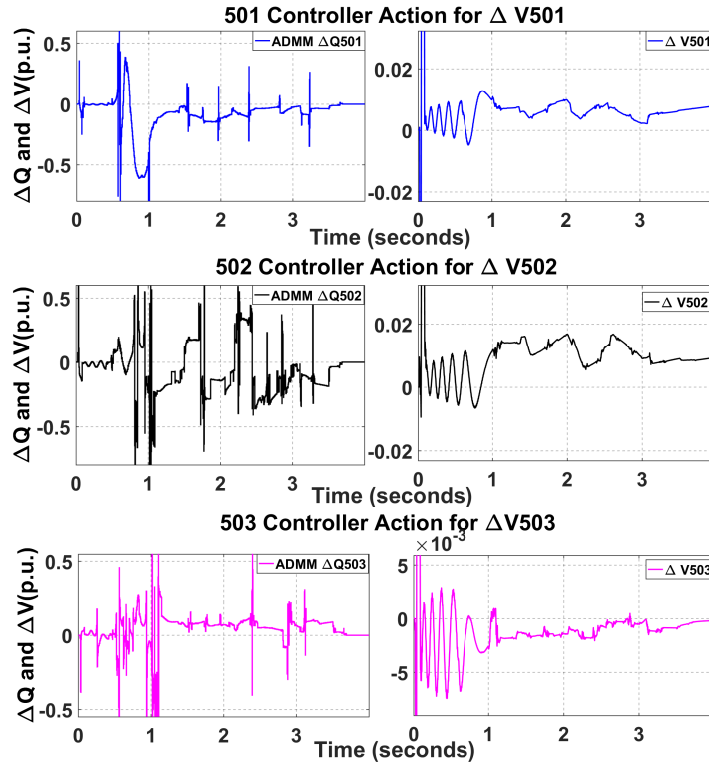
Figure 5.8: Case 2: ADMM controller action for voltage deviation mitigation.

5.3.2   Case 2: Voltage Deviation Mitigation

In case 2, several downstream loads were varied dynamically to create the voltage deviation on Bus 197. From Fig. 5.7, it can be observed that there are three instances on the bus voltage where there are no dynamics (501 base, 502 base, and 503 bases), load changing dynamics with no reactive power support from the inverter (501_{nosupp}, 502_{nosupp} and 503_{nosupp}) and mitigated voltage deviation through inverter support (501_{ADMM}, 502_{ADMM} and 503_{ADMM}). It can be seen that the reactive power support tries to mitigate the smaller voltage dynamics and the curves are closer to the base curves (501_{base}, 502_{base} and 503_{base}), via the controller action shown in Fig. 5.8. As the deviation increases in the positive direction, the ADMM controller action is to negate that by increasing the ΔQ_{50x} for the local controllers so more reactive power is injected into the system. The base curves are the voltage curves without any abrupt load changes and what one would see when there is no inverter participation.
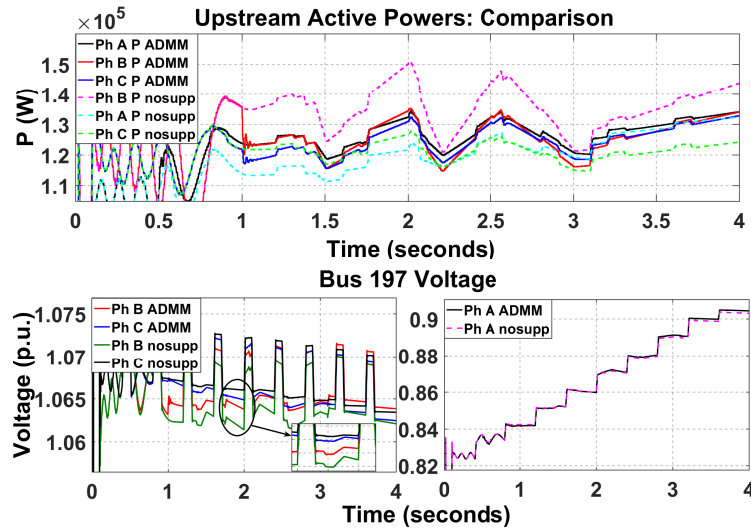
Figure 5.9: Case 3: Upstream active power balancing and bus 197 voltages before and after voltage support.

501_{nosupp}, 502_{nosupp} and 503_{nosupp} are the curves with load changes, but without any inverter participation. It can be seen that there are an abrupt voltage change and sag compared to the base case. Inverter contribution not only adds to the improvement of voltage profile on the bus but also to the other subsequent buses downstream. Full mitigation is not observed as the inverter power output is limited, and to observe thorough mitigation of the voltage deviation, a higher rated Distributed energy resource (DER) inverter should be available.

5.3.3 Case 3: Simultaneous Active Power Balancing and Voltage Deviation Mitigation

For the simulation setup, varying load conditions were developed for the downstream buses similar to case 2. The variation can be observed in upstream active power shown in Fig. 5.9, as compared to more steady active powers shown in Fig. 5.6. Bus 197 inverters (501, 502, and 503) are provided with additional ΔP_{50x} and ΔQ_{50x} from the ADMM algorithm, and Fig. 5.9 shows the resulting upstream power balancing waveforms with the voltage support. One can observe from Fig. 5.9 that the controller performs well for a varying load case, as the tracking for active power

for smaller dynamics can be difficult. The active power support from the inverters (501, 502, and 503) can be seen helping with the power balancing. It can be seen that the upstream phase B power is particularly deviating more than the other two phases when there is no inverter interjection. Furthermore, the reactive power support during the voltage deviation occurs simultaneously, as shown in Fig. 5.9.

5.4 Higher Order MIMO identification Based Power Management for Mulitple SPIs

The use of inverters to contribute towards improving the local power quality and voltage is a topic worth exploring because there is a clear intent of the need to increase DER penetration [132] in the power grid in general. In some parts of the world, there is already a higher level of DER penetration and prospects of having 20-30% penetration by 2023. Due to this "restructuring" of distribution networks, improved control for inverters based on supervisory control and multi-inverter control strategies need to be investigated. A novel approach for coordinated reactive power control strategy for multiple Single-Phase Inverters (SPIs- here grid-connected) using a higher-order Multiple Input Multiple Output (MIMO) identifications is proposed in this section. The proposed Single-Phase inverter control strategy includes a supervisory control which encapsulates the generation of reactive power references for local inverter controllers using a higher-order Alternating Direction Method of Multipliers (ADMM) technique. The architecture is based on dq-frame decoupled active and reactive power control for the SPIs. The main contribution is the high order identification technique that captures the sensitivity of the reactive power flow with respect to the voltage at the point of interest in the Distribution Network (DN). The results are tested on IEEE 123 bus system, and it is observed that the proposed architecture shows a higher percentage improvement in voltage control when compared to lower order identifiers.

This chapter is focused on designing an identification-based supervisory control

architecture based on ADMM. The chapter explores identification order and shows the effect of the order on controller output. The ADMM is utilized to identify the transfer function relating the deviation in voltage with the reactive power, and the controller action depends on the order, and the "accuracy" of the identification [133]. The proposed controller has the following advantages:

- MIMO transfer function identification is dynamic, so any changes to the system variables can be captured by the algorithm.

- This algorithm is flexible and thus gives a generic implementation quality for coordinated control of multiple devices.

- Nature and scaling of the devices are not an issue and the architecture lends itself to higher-order Kalman filter-based LQR control.

5.5   Higher Order ADMM Based Identification

Higher order ADMM identification is similar to the lower order ADMM, where the Langrangian formulation is the same. The transfer function however are of a higher order, which leads to a better representation and identification of the system as shown in (5.28).
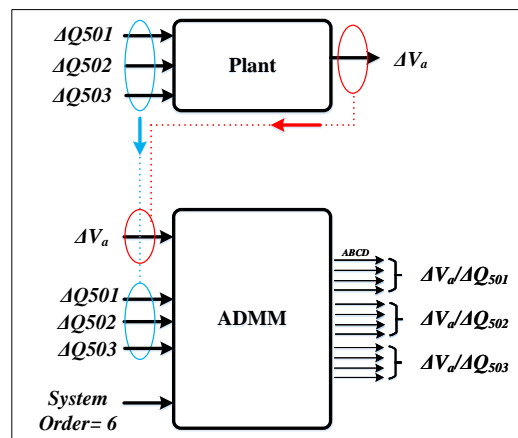
Figure 5.10: Measurement based transfer function identification using ADMM.
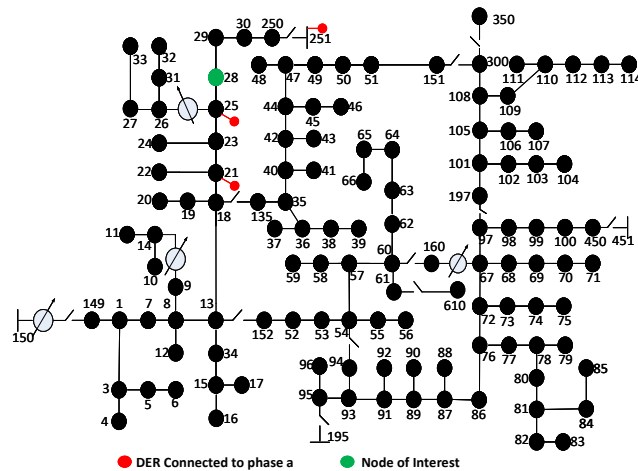
Figure 5.11: 123 Bus Distribution Test Feeder with SPIs.

A method of identifying transfer functions, as shown in Fig. 5.10, using ADMM is discussed in [134, 135]. For example, the MIMO transfer function relating deviation in voltage with output reactive power for a three inverters (1, 2, 3) set can be written as,

$$
\begin{bmatrix} \Delta V_a \end{bmatrix} = \begin{bmatrix} G_1(z) & G_2(z) & G_3(z) \end{bmatrix} \begin{bmatrix} Q_1 \\ Q_2 \\ Q_3 \end{bmatrix} \tag{5.28}
$$

where ΔV_a is the deviation of the bus voltage in phase a, and Q_1, Q_2 and Q_3 are the reactive power output of the Single-Phase inverters. Based on the MIMO transfer functions, the individual transfer functions (G_1, G_2 and G_3) can be represented as

$$
G_1 = \frac{\Delta V_a}{Q_1} = \frac{b_0^1 + b_1^1 z^{-1} + ... + b_k^1 z^{-k}}{1 + a_1^1 z^{-1} + a_2^1 z^{-2} + ... + a_k^1 z^{-k}} \tag{5.29}
$$

$$
G_2 = \frac{\Delta V_a}{Q_2} = \frac{b_0^2 + b_1^2 z^{-1} + ... + b_k^2 z^{-k}}{1 + a_1^2 z^{-1} + a_2^2 z^{-2} + ... + a_k^2 z^{-k}} \tag{5.30}
$$
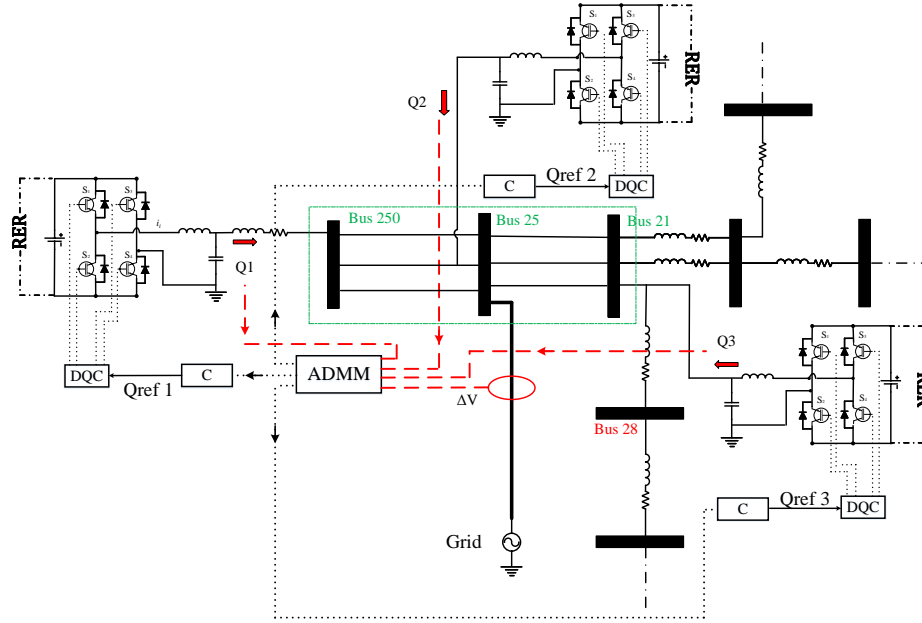
Figure 5.12: Single-Phase inverters with the ADMM based supervisory controller.

$$G_3 = \frac{\Delta V_a}{Q_N} = \frac{b_0^n + b_1^n z^{-1} + ... + b_k^n z^{-k}}{1 + a_1^n z^{-1} + a_2^n z^{-2} + ... + a_k^n z^{-k}} \tag{5.31}$$

where b_0, $b_1...,b_k$ are the numerator coefficients of the transfer functions and a_1, $a_2...a_k$ are the denominator coefficients of the transfer functions. Then a global consensus optimization in this problem can be formulated as:

$$\min_{a^1..a^n} \frac{1}{2}||[L][a] - [B] + [M][b]||^2 \tag{5.32}$$

where a is a vector of all the denominator coefficients and b is the vector of all the numerator coefficients. B is the matrix of the current samples of ΔV_a, L is the matrix of the previous samples of ΔV_a and M is the matrix of the current and previous samples of Q_x, $x = 1, 2, 3$.

5.5.1 Kalman based state estimation and LQR Control

The transfer functions identified using ADMM is converted to state-space matrices. Using this ABCD matrices and output measurement, a Kalman filter is utilized to

estimate states of the system (see Fig. 5.13). The state and measurement equations
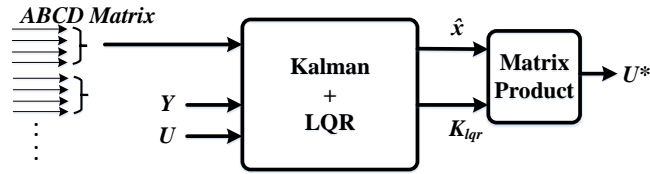
Figure 5.13: Kalman state estimation and LQR control block generating control outputs based on ABCD matrices from ADMM.

can be written as

$$x[n + 1] = Ax[n] + BU[n] \tag{5.33a}$$

$$Y = Cx[n] \tag{5.33b}$$

$$\hat{x}[n + 1] = A\hat{x}[n] + BU[n] \tag{5.34a}$$

$$P = APA' + Q \tag{5.34b}$$

$$K = \frac{PC'}{CPC' + R} \tag{5.34c}$$

P is the error covariance matrix, K is the Kalman gain, R and Q are the output and input noise co-variance matrix. For error reduction, a measurement residual is calculated, and the state and error covariance matrix estimates are updated, which can be written as (5.35).

$$residual = Y - C\hat{x}[n] \tag{5.35a}$$

$$\hat{x}[n + 1] = A\hat{x}[n] + K * residual \tag{5.35b}$$

$$P = (I - KC)P' \tag{5.35c}$$

The discrete time quadratic problem is then to minimize

$$\sum (\hat{x}^T Q_1 \hat{x} + U^T R_1 U) \tag{5.36}$$

For the LQR solution, the state transition matrix (A), input matrix (B), positive definite weights on states, and input vectors Q_1 and R_1 respectively are utilized to solve the discrete-time algebraic Riccati equation (DARE). The unique stabilizing solution and control signal can be given by

$$K = (R_1 + B^T X B)^{-1} B^T X A \tag{5.37}$$

$$U = -K * \hat{x} \tag{5.38}$$

Overall algorithm can be represented as follows.

Algorithm 1 Kalman estimation and LQR control signal generation

---
1: Initialize state variable x[n] and store ABCD matrices from the ADMM algorithm.

2: Calculate the Kalman gain (K) and co-variance matrices (P,Q_1 and R_1).
3: Calculate the residual matrix using the measurements Y.
4: Update the co-variance matrix.
5: Project state estimates.
6: Return to step 1.

5.6 System Configuration

The test system is the IEEE 123 bus distribution network, with SPIs connected to Phase A of the nodes 250, 25, and 21 as shown in Fig. 5.11. The SPI's DC module is the PV-battery system with their respective DC-DC converters and controllers (MPPT and DC-link voltage control). The AC module is an H-bridge inverter responsible for converting DC to AC and supplying active and reactive power to the grid. Table 5.2 shows the sizing of the inverters used for this study. Bus 28 is the point of interest for the proposed higher-order ADMM based control architecture. A voltage measurement unit at bus 28 feeds the RMS voltage data back to the supervisory controller. To generate voltage dynamics, a three-phase time-varying load is placed at bus 29, which has a maximum loading of 200kW. The active power set-point for the SPIs is 0.2 p.u. corresponding to 400 KW, which is assumed to be constant.
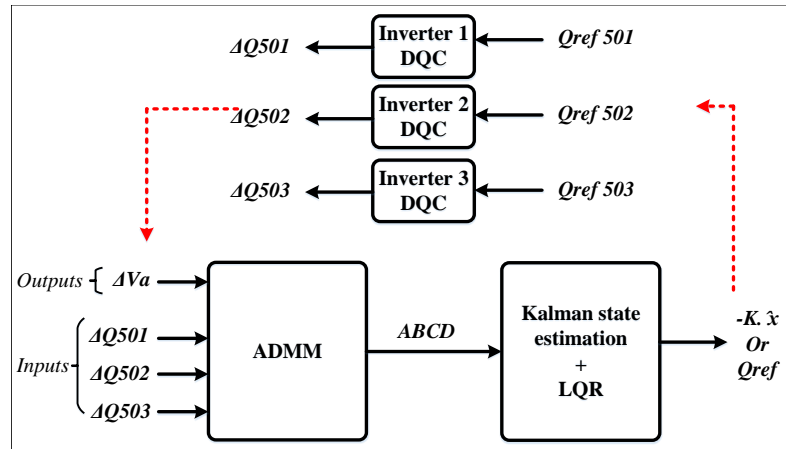
Figure 5.14: Supervisory reactive power control based on voltage deviation.

Fig. 5.12 shows the overall architecture and flow of signals of the proposed framework. Bus 28 is the node of interest for this particular study. The deviation observed at this node (ΔV) is provided as an input to the ADMM algorithm. The reactive power outputs from the SPIs (Q1, Q2, and Q3) acquired at the PCC are the other three signals required to formulate the transfer functions. After formulating the optimal control signals (Qref1, Qref2, and Qref3) for the respective voltage deviation, the signals are sent to the dqframe-based active and reactive power controller (DQC). Then, the appropriate PWM signals are generated and are provided to the switches of the SPIs. Fig. 5.14 represents how the single control architecture is designed based on ADMM.
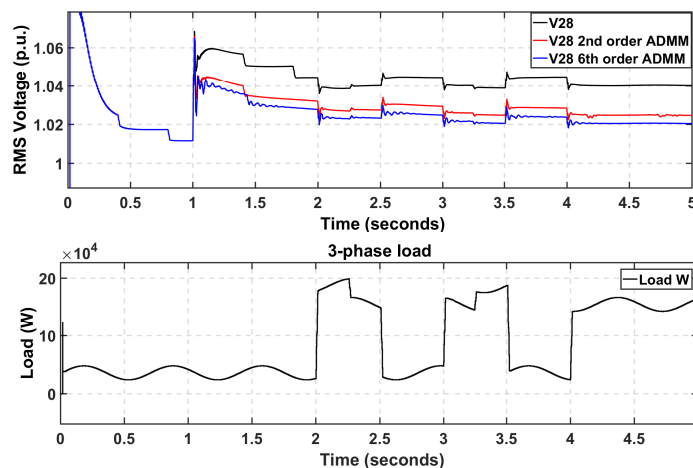
Figure 5.15: Bus 28 Voltage for the three cases.
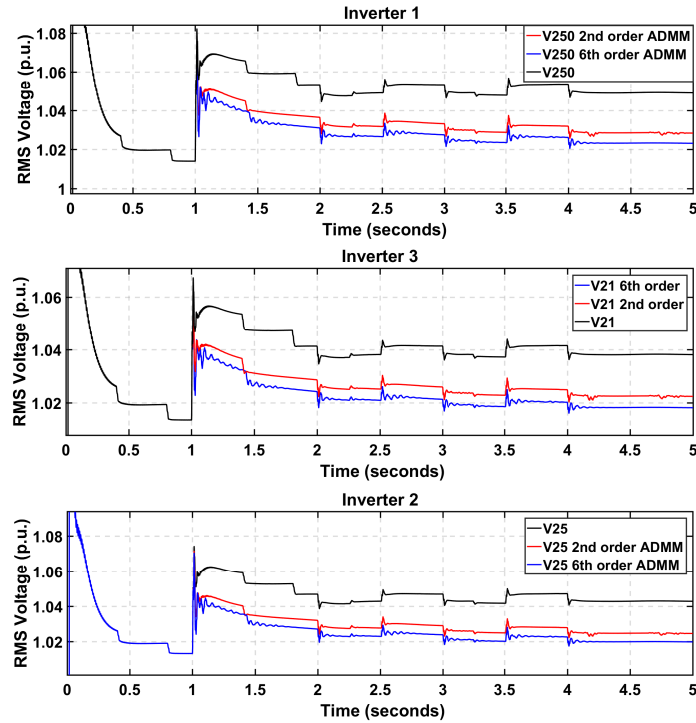
Figure 5.16: PCC voltages of the 3 inverter connections.
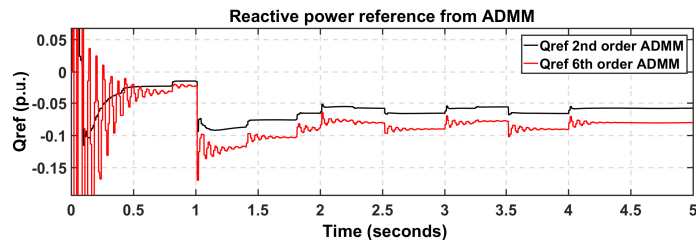
Figure 5.17: Reactive power references provided by the 2nd and 6th order ADMM identification.

5.7   Simulation Results and Discussion

The overall simulation setup and results are discussed here; the simulations are performed in the Matlab/Simulink platform. The inverters' dynamic model and the controllers are integrated into a power grid model with dynamically changing loads. The grid's legacy controllers, such as voltage regulators and their controllers, are modeled in detail.

Table 5.2: Rated power and voltage for Inverters 510, 502 and 503

Inverter	Power (MVA)	Voltage (kV)	Bus	Phase Connected
Inv 1	2	2.4	250	A
Inv 2	2	2.4	25	A
Inv 3	2	2.4	21	A

5.7.1   Simulation Setup

The cases performed for the system can be summarized as follows.

- The first set of results are produced by setting reactive power reference for the local inverter control to zero. As mentioned previously, the active power set-point remains at 0.2 p.u.

- Second set of results are created by utilizing the 2nd order ADMM identification and the corresponding reactive power injection through the Kalman and LQR control (Active power is 0.2 p.u.).

- Third set of results utilizes sixth-order identification from ADMM (active power 0.2 p.u.).

5.7.2   Results

During simulation, the local inverter controller is activated at one second. This can be observed in Fig. 5.15. The voltage rise at one second is attributed to the 0.2 p.u. (400kW) active power injection from the three inverters. The additional variations are due to time-varying three-phase loads. For the base case, when there is no inverter reactive power support, the voltage at the point of interest (bus 28) is seen to swell to 1.06-1.07 p.u. which is shown by the V28 (black) curve in Fig. 5.15. Similar voltage swells can be observed in Fig. 5.16, where the black curves (V250, V21, and V25, respectively) are the voltages for the base-case scenarios.

The effect of inverter reactive power contribution for voltage deviation mitigation achieved by ADMM can be seen in the red and blue curves in Fig. 5.15 and Fig.

Table 5.3: Voltage improvement based on the order of ADMM identification

Bus	2nd order %V improvement	6th order %V improvement
28	33	44
250	40	50
25	41	53
21	39	52

5.16. The tracking efficiency for the 2nd order and sixth-order identification-based controller is equally good. In conjunction with the K-LQR (Kalman and LQR) control, the voltage mitigation is very different. It can be observed that the higher-order identification and control has a more significant margin for control, as seen in Fig. 5.17. This is because the R and Q matrices were optimized for the inverters and not changed during the simulation studies. Any increment to these matrices, to provide higher Q injection or consumption, causes the system to go towards instability and the controller output (Qref for inverters) goes out of bounds. As summarized in Table 5.3, higher-order identification has more significant improvement in voltage deviation (44-52% improvement in bus voltages using the 6th order identification, whereas the 2nd order shows a 33-40% improvement in bus voltages).

5.8   Summary

The first half of the chapter presents an ADMM-LQR based dynamic coordinated control architecture for managing multiple SPIs in the power distribution system to aid the mitigation of power unbalance and voltage deviation in the power grid. Specific cases are presented, which can provide a proof of concept for the power-sharing voltage compensation capability of the proposed architecture. Firstly, the issue of power-sharing based on modified droop control has been discussed. This method utilizes an impedance transformation technique that generates the active and reactive power reference. The issue in accomplishing this is that preliminary knowledge of the gains or R/X ratio is required. This is overcome by modifying the active and reactive power reference generation via the ADMM MIMO identification technique.

Secondly, the MIMO architecture and transfer function generation using ADMM is discussed. This section also provides a detailed explanation of a coordinated optimal control framework based on the Kalman estimator and linear quadratic regulator that provides the modification for the power references for local inverter controllers. It is observed that the controller performs well during dynamic and changing conditions on the grid, and the upstream power balance and voltage management is performed very effectively as opposed to no control or base case. The second half evaluates a higher-order identification-based control architecture for grid-connected SPIs for Volt-VAR control. The reactive power injection and consumption are dependent on the precise identification of the transfer functions that relate to the deviation in the voltage for the point of interest of the DERs. It was shown that a higher-order ADMM K-LQR control architecture shows a better performance for voltage compensation. Compared to lower-order identification, there is an improvement of around 30 to 40 % in voltage deviation mitigation.

CHAPTER 6: Multiple Single-Phase DER Management

As discussed in the previous chapter, the contribution of single-phase DERs is to quench the ever-increasing energy demand seen in today's distribution networks. Single-phase inverter-based DERs provide the flexibility that is required in current networks to provide immediate local relief for energy demand, voltage/frequency regulation, and other reliability issues. Island formation capability of single and Three-Phase inverter-based DERs provides a way to decrease the overall System Average Interruption Duration Index (SAIDI) and System Average Interruption Frequency Index (SAIFI) of distribution systems. Control of one single-phase inverter-based DERs is already covered in the previous chapter; this chapter will focus on the different types of control architectures available on multiple single-phase DERs in a micro-grid.

6.1   Introduction

The impact of Distributed Energy Resources (DER) in MV and LV networks is continuously changing the system-level planning, analysis and operation. The current direction of research on integrating utility-scale DERs (1-5MW), but there is a dire need to formulate relevant model-based studies for integration of inverter-based DERs found in medium and low voltage networks. Therefore, the interaction of voltage controlling devices in traditional and modern distribution networks to the injection of power from the DERs. Typically voltage profile improvements in traditional distribution networks are realized by different voltage control devices such as substation transformers are equipped with on-load tap changers (OLTCs), Step Voltage Regulators (SVRs), fixed or adjustable capacitor banks, and power electronic-based compensators (SVC, STATCOMs).

However, with the recent advancements in inverter technology, grid-ancillary services are now a trend in low and medium-voltage networks. Various challenges in power and voltage management/control schemes are arising. There are two possible ways to solve this issue; either a coordinated optimized approach can be used for defining the optimal settings for voltage controlling devices and/or readily available reactive power from the DERs can be utilized to curb the over-utilization of the existing voltage regulators. The placement and sizing of the DERs serve a vital function in analyzing the potential problems faced by the voltage regulating units present in the distribution network. Issues related to Power quality and reliability arise from unplanned and random DER installations (eg. PV, BESS). For example, installations that occur at the far end of the feeder are more prone to voltage instability issues. Therefore, local efforts tackling voltage-related issues can be a way to get the most out of higher PV penetration in distribution networks.

Control methodologies such as Volt-var have been specified and implemented to mitigate such issues. However, these control functions operate based on the terminal voltage itself, whereas the OLTCs and SVRs are operated to regulate local and remote voltages. In conventional non-coordinated voltage control methods, higher penetration of PVs and other DERs can lead to misoperation (which can be excessive tap changes) or inaction of taps, leading to wear and tear of the device and cause instability in the network. The other issue is an existing one, which is bound to escalate with the increase in DER penetration; during low loading periods with high DER injection (over the generation of PV), reverse power flow can cause SVR runaway interactions with the PV/DER. These issues are a result of inappropriate regulator control settings. Therefore a proper coordination strategy or control between the different voltage controlling devices must be formulated for DMS and local controllers of the DERs. Coordinated response of the DERs based on the regulator actions can benefit the formation of a flat voltage profile. Optimization of OLTCs and

capacitor banks with the participation of smart inverters have been demonstrated in literature[136, 137]. Because the operation of OLTCs and SVRs, are based on locally measure voltage, a dynamic sensitivity-based control on smart inverters can help alleviate voltage issues locally in coordination with these devices. The advantage of sensitivity-based control is that the smart inverters' compensation does not have to be the immediate next bus or the PCC. A volt-var-based control framework is robust, but it does not allow the inverters to be flexible and prioritize grid-supporting features. This chapter's contribution will investigate the issues related to regulatory issues concerning the increasing PV penetration and how a sensitivity-based compensation from inverters can help alleviate these issues.

6.2   Main Contributions

The main contributions of this chapter are as follows:

- Issues with high penetrating DERs are identified in this chapter on the IEEE 123 Test Node Feeder. Depending on the DER placement in the network, the intensity of loading, and generation by the DER determine the efficacy of regulator operation and in some cases the clear violation of ANSI C84.1 voltage limit standards for buses downstream of the feeder.

- Volt/VAR support functionality is added to the SPI based microgrids (all types inclusive) by utilizing the ADMM control architecture to determine the sensitivity between the voltages of the node of interest or point of interest (POIn) (generally a weak bus or bus downstream), the PCC voltage and the reactive power injection by the MG.

- Volt/VAR capability of the inverters has shown to improve the overall voltage profile of the feeder and help regulators operate within the defined tap settings.

- Highest Density Index (HDI) of measured bus voltages show significant im-
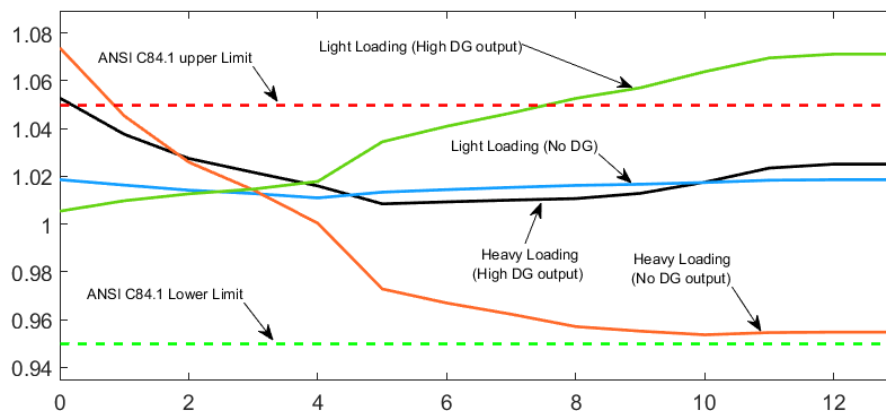
Figure 6.1: Effect of DER at end of the regulation zone.

provements when compared to no DER interference and DER Volt/VAR compensation results.

6.3   High DER Penetration Impacts on Distribution networks

With the addition of DERs in distribution networks, problems related to voltage variations will arise, and this can cause unintended operation of the voltage regulators in the system and the transformer LTC. ANSI C84.1-2011 suggests that customer service voltage must be maintained at 0.95-1.05 p.u. Therefore, there is a need to assess the transformer LTC and voltage regulator settings to increase DER penetration. The controller on the inverters interfacing the energy resources with the grid needs to work in tandem with these voltage regulating devices to avoid malfunctioning. To give a better perspective into the operating range and behavior of the regulating devices, the following conditions need to be studied:

- High or maximum distribution loading without DERs.

- High or maximum distribution loading with DERs.

- Low or minimum distribution loading without DERs.

- Low or minimum distribution loading with DERs.

Depending on the DER location and the active and reactive power management technique, the DER can shield the substation LTC controller from observing the feeder current. For line regulators, once it is observing reverse power flow, the regulator will attempt to regulate the front section of the feeder. This can cause the regulator to saturate to either its maximum or minimum tap, regulating the voltage to the desired level. High DER penetration at the end of the regulation zone or the feeder's backbone can cause issues during light loading conditions; Large DER power exports during this time can cause the voltage at the PCC and buses upstream to swell. These cases provide valuable insight into the necessity for coordination between the line regulator and DERs for voltage regulation for different loading scenarios and DER location impact.

Fig.6.1 shows the impact of DERs located at the far end of the feeder for different loading conditions. This test was performed on the IEEE 123-bus system in Simulink with 3 DERs rated at 1MVA. The x-axis of Fig.6.1 is the backbone buses (0-being the substation and 13 being the farthest bus on that backbone), and the y-axis is the voltage at that particular bus per unit. During light loading conditions, as shown in Fig.6.1, when there is high generation output from the PVs or DERs (if not curtailed or compensated for) can cause the voltage levels to exceed beyond the ANSI c84.1 allowable voltage upper limit of 1.05 p.u. on the downstream buses which are further down the line from the substation OLTC. Similarly for heavy loading and low DER output can trigger the lower limit; this can be avoided if reactive power compensation can be provided during this time when PV generation is low or zero.

similarly, Fig.6.2 shows the effect of DERs placed near the substation or the line regulator. This would affect the tapping of the regulator and the regulator, hidden by the DER generation of the loading downstream. The effect can be observed in Fig.6.2, as when the loading is heavy for a high DER output or low, the lower limit of the ANSI allowable range is violated. This is because even when the DER is pushing
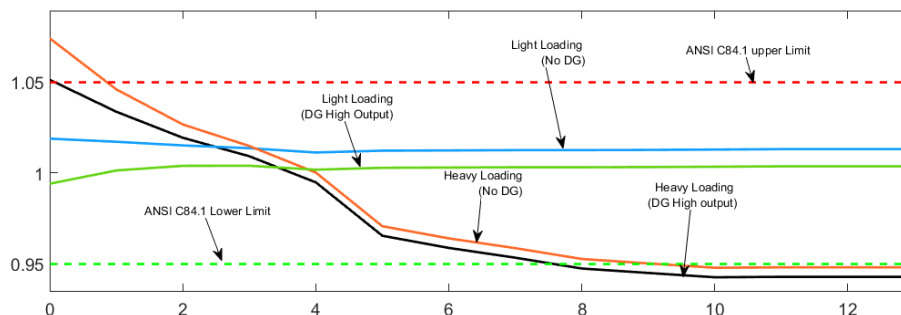
Figure 6.2: Effect of DER near the substation.

power into the network, the regulator taps down excessively, causing the voltage to collapse below 0.95 p.u.

6.4   Distribution Voltage Control/Support

This section discusses the methodologies utilized to support voltage regulation by the inverters. Also, how ADMM can be adapted to provide a sensitivity-based VAR compensation for the network and downstream buses to improve system voltage profile.

6.4.1   Conventional Control Architecture of Traditional Voltage Improvement Devices

This section will talk about OLTC, LTC, STATCOM, Switch Caps, SVR, and other voltage-improving methodologies that revolve around DER participation using local controllers. To improve nodal voltage profiles in medium-voltage distribution networks. The substation transformers are typically equipped with on-load tap changers (OLTC). Another way to utilize the Step voltage regulators (SVR), is that it can be installed in the middle of the feeder utilize a transformer with LTC and boost the voltage. Loads absorbing high amounts of reactive power are also one of the reasons for the presence of voltage sag or drop, i.e., lagging power factor. Traditionally, the compensation was provided by devices such as, fixed or adjustable capacitor banks, and various power electronics-based compensator, e.g. Substations are often equipped
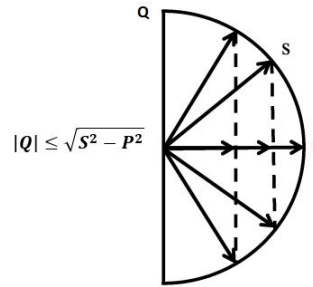
Figure 6.3: Inverter reactive power capability.

with static var compensators (SVC) and STATCOM along with feeders, at the end section of feeders or close to particular loads. Traditionally, direct compensating devices are seldom found in distribution networks.

Locally, the inverters modulate the voltage at the PCC, either by active power curtailment or by controlling the injection of reactive power consumption. An increase in active power is not the best economical solution for the end-user or the PV owners as the PVs' full potential is curbed. Therefore, one solution is to control the flow of reactive power by the local controllers looking at the PCC voltage. As Fig. 6.3 This capability of the inverter is dependent on the apparent power (S); if the instantaneous active power (P) is less than S, then the range of the allowable reactive power (Q) can be given by,

$$|Q| \leq \sqrt{S^2 - P^2} \tag{6.1}$$

Although, depending on the X/R ratio, the impact of reactive power on voltage reduces as the circuit's resistivity increases, which is typically observed in distribution networks. Consideration of utilizing a voltage control loop for rooftop PVs are present in this study to help maintain the local voltage within certain limits. This can be considered as a form of Volt-VAR control in principle, conventionally done by different legacy devices already present in the grid.
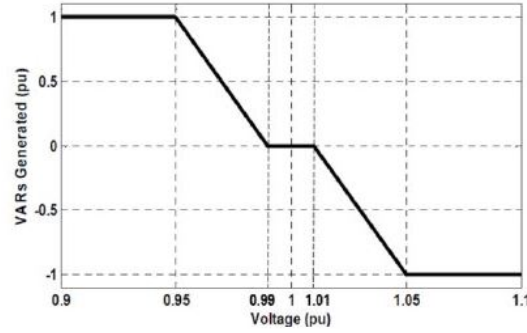
Figure 6.4: Volt-Var curve for the inverter.

6.4.2   Local and Centralized Volt/Var Optimization

Implementation of Volt/VAR-based controllers are formulated using the curve Fig.6.4, the operating mode of the inverter can be determined based on this curve that relates the reactive output power with the PCC voltage. The constant slopes below 0.99 p.u. and above 1.01 p.u. voltage is similar to the inverter's droop setting, which can be modified depending on the location of the DER, and the stagnant regions are either the maximum reactive power limit of consumption or injection or zero reactive power output. Communication improvement and increasing research dedicated to improve technology in this field has brought to light the importance of controlling voltage and voltampere reactive power levels in real time. the focus of minimizing energy consumption has shifted to controlling the voltage and voltampere reactive power levels, i.e., VAR, in near real-time. This is known to be referred to as Voltage/Var Optimization (VVO). There exist different VVO control structures, centralized and decentralized. Centralized VVO approaches use LTC transformers, voltage regulators, and fixed/switched capacitor banks to control voltage and reactive power flow. There are three different centralized VVO approaches, SCADA rule-based VVO, DMS model-driven VVO, and hybrid VVO. The rule-based the system uses a VVO processor in conjunction with a remote terminal unit (RTU) to control the automated devices. Local Volt/VAR control has issues with losses and line voltage drop not being incorporated in the evaluation of the inverter's reactive power setpoint gen-

eration. A similar disadvantage of the centralized control scheme is the dependence of information for each circuit segment for line drop for the centralized controller to evaluate the reactive power dispatch.

6.5   Proposed Controller Framework for Centralized Voltage Regulation

As discussed earlier, the reactive power reference generation for inverters based on local controller only has information regarding local power flows and not of the segment; hence an optimum setpoint cannot be evaluated. Hence, to get the sensitivity between the voltage and reactive power flow, the Alternate Direction of multipliers is utilized. As stated earlier, ADMM provides the relationship between two time-varying quantities. Then a Kalman LQR based controller combination provides the optimal control output to stabilize the transfer function identified by the ADMM. Hence, we will have to modify the generic ΔVoltage/ΔReactive power shown in (6.2), as this will work only when the voltage deviation provided is at the PCC of the MG or DER. Reactive power contribution or compensation for bus voltage deviations away for the MGs will need to be modified to

$$
\begin{bmatrix} \Delta V_{POIn} \end{bmatrix} = \begin{bmatrix} G_{VQ_1} & G_{VQ_2} & G_{VQ_3} \end{bmatrix} \cdot \begin{bmatrix} \Delta Q1 \\ \Delta Q2 \\ \Delta Q3 \end{bmatrix} \tag{6.2}
$$

$$
\begin{bmatrix} \Delta V_{POIn} \end{bmatrix} = \begin{bmatrix} G_{VQ_1} & G_{VQ_2} & G_{VQ_3} \end{bmatrix} \cdot \begin{bmatrix} \frac{\Delta Q1}{\Delta V1_{PCC}} \\ \frac{\Delta Q2}{\Delta V2_{PCC}} \\ \frac{\Delta Q3}{\Delta V3_{PCC}} \end{bmatrix} \tag{6.3}
$$

Where, $\Delta V1_{PCC}$,$\Delta V2_{PCC}$,$\Delta V3_{PCC}$ are the different PCC voltages deviations of the DERs or MGs, ΔV_{POIn} is the voltage deviation at the Point of Interest (POIn), $\Delta Q1$,$\Delta Q2$,$\Delta Q3$ are the deviation of the reactive power output from the nominal and $G_{VQ1}, G_{VQ2}, G_{VQ3}$ are the sensitivities between the quantities. Individual DER
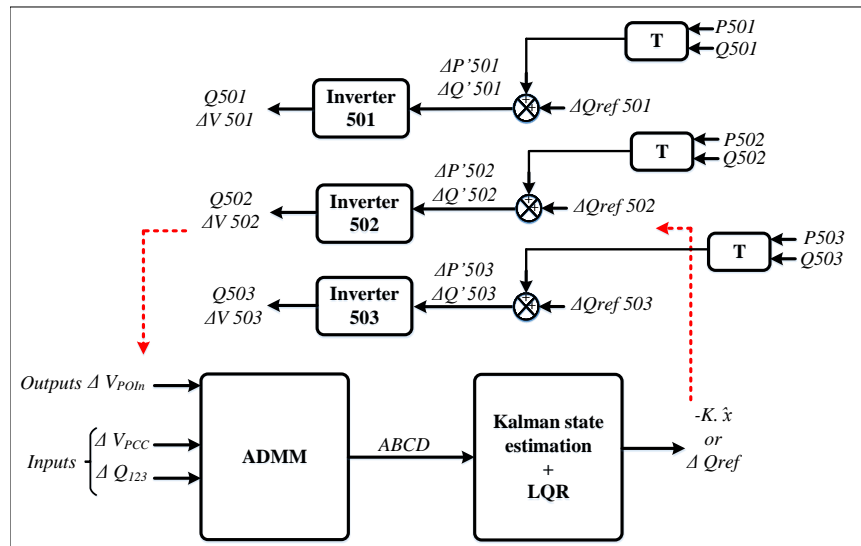
Figure 6.5: ADMM utilization for reactive power compensation from individual MGs or DERs.

Table 6.1: IEEE 123-bus System Power Specification

SUB P	4.2 MW
SUB Q	900 kVAR
SUB S	4.38 MVA
DER S	300kVA
DER penetration	40%

contribution to alleviating the voltage deviation at the POIn bus can be extracted utilizing this modification and implementing on the ADMM architecture.

6.6   DER compensation during different loading conditions

The setup for the different loading conditions is shown in Fig.6.6, where 6 DERs are placed randomly on the IEEE 123 bus system. Each DER is rated at 300kVA, and the inverter model utilized is detailed (switching-based model) provided in Simulink. For different loading conditions, every load is reduced to 20% its value for light loading conditions and 120% for heavy loading conditions. During these cases, the DERs are provided a reference of no power injection (P and Q), 30% active power (P) injection, 30% active power (P) injection with reactive power (Qsupp) support via ADMM for target voltage (VT) 1 p.u. and 0.95 p.u.
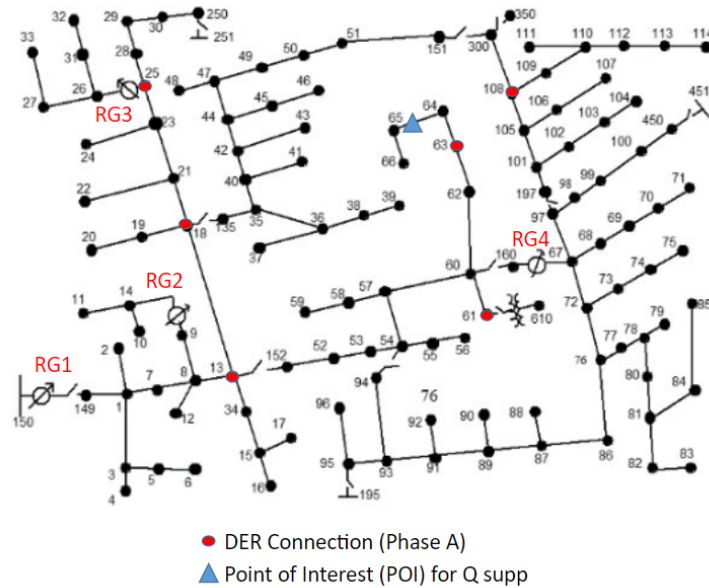
Figure 6.6: IEEE 123 bus system with connected DERs and POIn node.

Fig.6.7 shows the voltage profile of the entire 123-bus system when the POIn is bus 65 and different contributions for DERs are demanded. It can be seen from the figure that the overall voltage profile is close to a flat 1 p.u. when the DERs provide active power injection with reactive power compensation. Setting the target voltage to 0.95 p.u.lowers the overall curve towards 0.95 p.u., but it can be observed that not all buses are maintaining this voltage. It can be justified by mentioning that active power injection brings up the overall voltage profile, although a 0.95 p.u. profile is not possible as the negative reactive power set-point generation might be limited by the apparent power limitation.

Voltage Profiles improvements: This case involves 6 DERs randomly placed in the 123-bus system, providing reactive power compensation based on the ADMM and LQR control action. The six busses where the DERs are placed are 13, 18, 25, 61, 63, and 108. ADMM should adapt to different network configurations and load variations. In this case, different loading scenarios are created to test the inverter and ADMM's compensation capability to improve the voltage profile of the system.
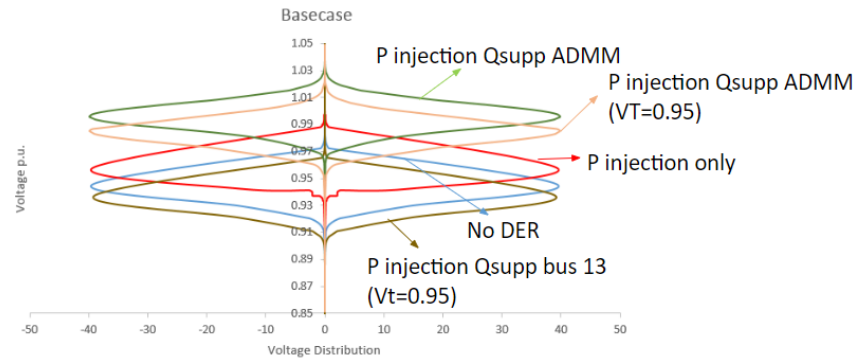
Figure 6.7: Voltage profile for different DER contributions during base loading conditions.
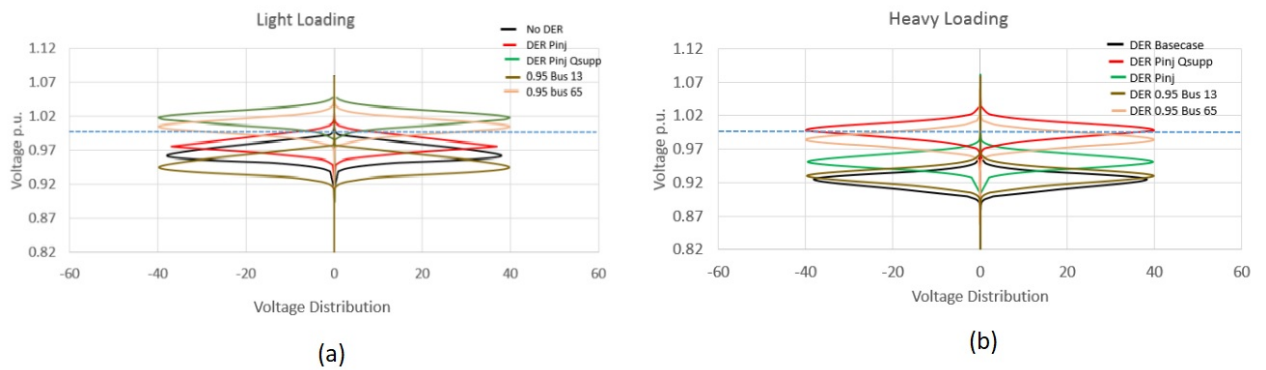
Figure 6.8: voltage profile for different DER contributions during (a) light and (b) heavy loading conditions.

Different loading scenarios simulated for the 123-bus system can be described as follows:

- Normal Loading: Loads in the system are unchanged or kept at the rated/nominal values.

- Light Loading: Every load in the system is reduced to 20% its (nominal) active power rating.

- Heavy Loading: Every load in the system is at 120% of its (nominal) active power rating.

To compare the effectiveness of the voltage improvement throughout the system, the DERs are scheduled to provide an active and reactive power in three different ways,
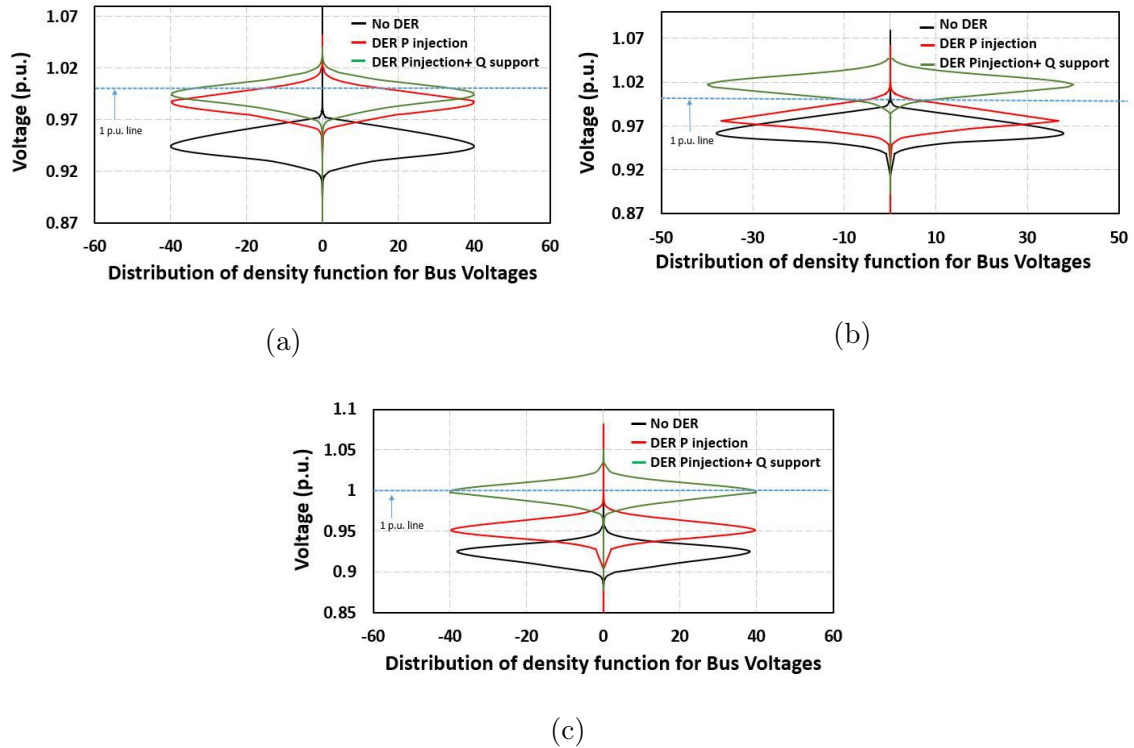
Figure 6.9: Voltage normal distribution based on probability density function for (a) normal (b) light and (c) heavy load conditions with different DER power for case 3. no power injection (No DER), active power (P) injection (DER P Injection), and active power (P) injection with reactive power (Qsupport) support via ADMM (DER P injection+ Q support). Referring to Fig. 6.9 this figure is generated by calculating the probability mass function of the entire system's bus voltages. It can be observed from Fig. 6.9a that the Highest Density Index (HDI) of measured voltage values for base-case loading and no DER intervention is around 0.94 p.u. Most of the buses in the system measure voltages <0.98 p.u and >0.92 p.u. Similarly, in the same figure, when DERs are programmed to inject 30% of their capacity as active power (90KW per DER), the voltage profile of the system swells, and the HDI value shifts to 0.98 p.u. with the band limits at 1.02 p.u. and 0.96 p.u. With reactive power compensation, this highest voltage density shifts to 0.99 p.u. with the upper and lower limit band of 1.024 p.u. and 0.965 p.u. Table 6.2 and Fig. 6.9 show the highest concentration of bus voltages and normal distribution of the voltage density of the
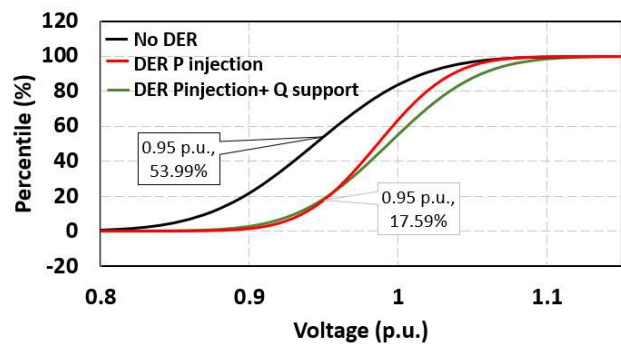
(a)
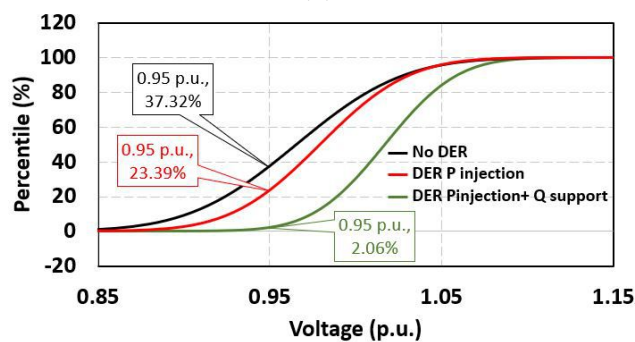
(b)
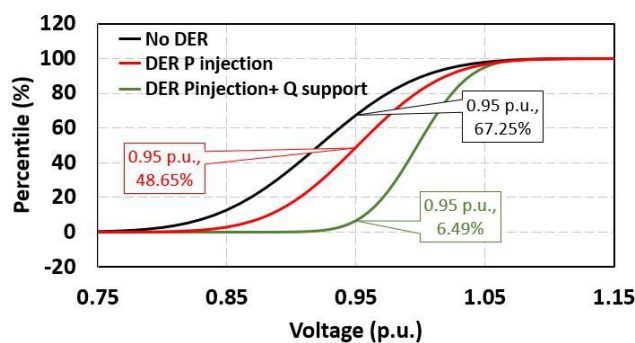
(c)

Figure 6.10: Voltage percentile curves for the entire 123-bus system for (a) normal (b) light and (c) heavy load conditions with different DER power actions for case 3.

entire system, respectively. HDI values obtained from Table 6.2 and Fig. 6.9 the following observations can be made:

- HDI values for normal loading conditions improve from 0.94 p.u. to 0.99 p.u. For light loading conditions, HDI values show an improvement from 0.96 p.u. to 1.01 p.u. Similarly, for heavy load conditions, the HDI voltage improvement is from 0.925 p.u. to 1 p.u.

- Voltage band encapsulates the entire system voltages between an upper and lower limit. ADMM based reactive power compensation significantly improves this voltage band for the different loading conditions.

From Table 6.2 and Fig. 6.10, it can be observed that in every loading scenario, the percentile of bus voltages below 0.95 p.u. significantly decreases when reactive power compensation is involved. For example, in the heavy loading scenario, no DER presence in the system causes 67.25% of the bus voltages to be below the 0.95 p.u. value; this is significantly higher than that of 6.5% when ADMM based reactive power compensation is involved. Similarly, for light loading conditions, the percentile of bus voltages below 0.95 p.u. falls from 37% to 2% when DER intervention is changed from a non-supportive function to an ADMM based compensation.

6.7 Summary

In this chapter, interactions of DERs and MGs with the regulating devices were elaborated. The MGs are equipped with ADMM based voltage regulation capability, which was tested on the IEEE 123-test feeder with OLTCs and line regulators. The discussion in the initial part of the chapter revealed that the placement of DERs has a significant impact on the voltage operational limits, which is also dependent on the overall loading conditions and DER generation. DER placed at the far end of the feeder drastically affected the downstream buses' profiles during light loading conditions. It was observed that for light loading conditions the upper voltage limits

Table 6.2: Case 3 Voltage metric for the entire 123-bus system for different DER contribution during varying loading conditions

DER type.	Voltage HDI p.u.	Voltage band p.u.	Voltage Percentile <0.95 p.u.
Normal Loading			
No DER	0.94	0.92-0.98	54%
Pinjection	0.98	0.96-1.02	17.6%
Pinject Qsupport	0.99	0.97-1.024	17.6%
Light Loading			
No DER	0.96	0.93-0.99	37%
Pinjection	0.976	0.95-1	23.4%
Pinject Qsupport	1.01	0.987-1.04	2%
Heavy Loading			
No DER	0.925	0.89-0.95	67.25%
Pinjection	0.95	0.92-0.99	48.65%
Pinject Qsupport	1	0.965-1.024	6.5%

of ANSI c84.1 was violated for these buses. Similarly, near-end placement caused the misoperation of the regulating device as the actual loading conditions are masked by the DER generation. Utilizing the ADMM assisted Volt-Var compensation, a significant improvement on HDI is observed for different loading conditions. For instance in a heavy loading scenario, the percentile of buses below 0.95 p.u. without any DER compensation was 67% which improves to 6.5% when ADMM based VAR compensation is implemented.

CHAPTER 7: Conclusions and Future Work

This dissertation explores Single-Phase Inverters (SPIs) in a solo-inverter, multi-inverter, and multi-inverter multi-microgrid (MG) framework. Investigating different aspects of the SPIs such as the synchronous reference frame modeling, primary-, secondary- and tertiary-level controllers, and the effect of different MG topologies in distribution networks with various legacy systems (OLTCs, SVRs, etc.). Conclusions drawn from each chapter can be categorically explained:

- Chapter 3 discusses the modeling and control aspects of a single-phase inverter in a synchronous reference frame. The chapter provides the dq-control topology with two cascaded control loops, the inner loop being current-based control and the outer loop provides for active-reactive power or Voltage-frequency. However, the traditional architecture is modified to a unified-control topology that does not switch between control modes for different MG operating modes. The inverter seamless transfer parameters abide by the IEEE 1547.2018 regulations for grid interconnection and synchronization. The second half of the chapter introduces the recursive least squares-based estimation process and design methodology of minimum variance control that defines or identifies the 3rd order transfer function model of the single-phase inverter system and closely regulates the active and reactive power. This topology replaces the PI-controller in the dq-control framework. This controller boasts an improvement of 70%-80% in achieving absolute zero steady-state error. Also, the proposed architecture is implemented where the SPIs provide active and reactive power compensation for alleviated power unbalance and voltage deviations in an unbalanced distribution network. Further, the quantitative results can be summarized as follows:

– Unified Control architecture provides no current spikes and seamless transition as compared to Dual Outer-Loop dq-controller that produces a 50% of nominal spike for Âœ cycle.

– Adaptive control framework for local controllers discussed for better dynamic control of SPIs, where PI on average has overshoot and settling time of 40% and 0.26 s the adaptive controller has an overshoot and settling of 12% and 0.23 s.

– The adaptive control shows better dynamic performance and noise rejection capability compared to the conventional PI-control.

– A method to help mitigate the unbalanced nature of the three-phase system through the contribution of these SPIs was also presented.

  Scalability studies showcased adaptive control superiority as it was able to perform 70

• Chapter 4 introduced the multi-DER-based MG architecture on a single phase. The chapter explores the droop framework and how the ADMM algorithm can identify the grid impedance matrix and make the DERs more adaptive for different network topologies. The unified control structure described in the previous chapter is utilized here for grid-forming, supporting, and following modes. Power-sharing between the DERs for SA and GC mode has been discussed in this chapter while maintaining system voltage and frequency at rated values. In the second half, a sequence-based control topology is introduced that can be utilized to quench and suppress negative sequence components coming out of the DERs. This topology splits the local controller into two different local controllers, one is used for positive sequence dq-components, and the other is utilized for negative sequence components. Quantitative results are as follows:

– ADMM based droop was able to provide coequal power references for the

inverter local controllers.

- – MG PCC voltage was within 10% of the nominal value for a full load variation in the SA mode.

- – MG operating frequency during SA mode was within 0.3% of the nominal value for a full load variation.

- – Sequence based multi-inverter MG control showed a 0% injection of negative sequence component during steady state conditions of SA and GC mode of operation.

- – Maximum of 0.018 p.u. negative sequence current component detected during the transition period that lasts for <0.1 seconds

- • Chapter 5 provides an improvement in the hierarchical control topology by including a Multiple Input Multiple Output (MIMO) Identification technique that generates reference set-points for the outer loop local controllers autonomously. An Alternating Direction Method of Multipliers (ADMM) based MIMO identification is presented in the chapter which is implemented on multi-MG systems. The architecture proves to be useful at power management of multi-MG systems as the power reference generation for the inverters is based on a global consensus problem formulation for power balancing (using inverter active power) and voltage regulation (using inverter reactive power) at the POI. The results can be elaborated as follows:

- – This chapter discusses the modification of universal droop topology on the ADMM identification and control, with the objective of power unbalance mitigation and voltage regulation at the PCC.

- – System under varying loading conditions, the control topology was able to mitigate severe active power unbalance (22-30 KW) while providing grid ancillary for voltage regulation.

– Three MG setups are utilized in the chapter with the IEEE 123-bus system which is inherently unbalanced; it is concluded that the power injection/consumption from the MGs alleviate the unbalance and bring it down from a maximum of 15% to 2%.

– On the same distribution network architecture, a different order of identification proposed in the second half of the chapter performs a 6th order identification of the SPI that leads to a 30% increase in voltage profile improvement by reactive power compensation provided by the MGs.

– For 2nd order ADMM assisted voltage regulation the voltage improvement on average was 38%.

– For 6th order ADMM assisted voltage regulation the voltage improvement on average was 49%.

- Once power management strategies are in place for MGs and SPIs, the effect of power injection and consumption by these systems on the feeder substation and other legacy systems (OLTCs and SVRs) is discussed in chapter 6. It is shown that placement and generation of DERs during different loading conditions affect the regulator tap switching and overall voltage profile of the system. Effect of DERs at the end of the regulation zones during light loading conditions was seen to cause voltages at the far end of the feeder to hit the upper limit of the ANSI C84.1 voltage profile. Similarly, DERs near the substation OLTC cause the misoperation of the taps during heavy loading conditions as the generation from the DERs mask the actual load requirement in the system.

  – Chapter revealed that placement of DERs have a significant impact on the voltage operational limits, which is also dependent on the overall loading conditions and DER generation.

  – Active contribution from local DERs can improve system voltage profile

by 6-8%

- It was observed that HDI values for normal loading conditions improve from 0.94 p.u. to 0.99 p.u.

- For light loading conditions, HDI values show an improvement from 0.96 p.u.to 1.01 p.u. Similarly, for heavy load conditions, the HDI voltage improvement is from 0.925 p.u. to 1 p.u.

7.1   Future Work

Overall power management scheme proposed in this dissertation is centralized and a more active control scheme compared to the passive or decentralized nature of droop-based power management schemes or hierarchical control structure. There are few things identified which can add value to this study in the future, these are categorized as research based future work and application based:

- Research: Work on sequence-based control can be extended to provide sequence-based ancillary to the grid. This architecture can utilize the flexibility of SPIs and their ability to modulate power in every phase separately can help distribution networks tackle unbalances and reduce unnecessary losses in the system.

- Application: Negative sequence suppression for unbalanced fault utilizing the sequence-based control architecture.

- Research: Coordinated voltage regulation between the MGs and regulators in distribution networks need to be accomplished by generating the appropriate active and re-active power references for the local inverter control. ADMM proves to be useful in mitigating voltage deviations locally, which could help decrease instances of excessive tapping of line regulators and provide better voltage regulation

REFERENCES

[1] X. Zhang, T. Zhao, W. Mao, D. Tan, and L. Chang, "Multilevel inverters for grid-connected photovoltaic applications: Examining emerging trends," *IEEE Power Electronics Magazine*, vol. 5, no. 4, pp. 32–41, 2018.

[2] S. Parhizi, H. Lotfi, A. Khodaei, and S. Bahramirad, "State of the art in research on microgrids: A review," *IEEE Access*, vol. 3, pp. 890–925, 2015.

[3] A. H. Etemadi, E. J. Davison, and R. Iravani, "A decentralized robust control strategy for multi-der microgridsâpart i: Fundamental concepts," *IEEE Transactions on Power Delivery*, vol. 27, no. 4, pp. 1843–1853, 2012.

[4] S. J. Hossain, T. G. Paul, R. Bisht, A. Suresh, and S. Kamalasadan, "An integrated battery optimal power dispatch architecture for end-user-driven microgrid in islanded and grid-connected mode of operation," *IEEE Transactions on Industry Applications*, vol. 54, pp. 3806–3819, July 2018.

[5] J. Liang, T. C. Green, G. Weiss, and Q. C. Zhong, "Hybrid control of multiple inverters in an island-mode distribution system," in *Power Electronics Specialist Conference, 2003. PESC '03. 2003 IEEE 34th Annual*, vol. 1, pp. 61–66 vol.1, June 2003.

[6] M. Ebrahimi, S. A. Khajehoddin, and M. Karimi-Ghartemani, "Fast and robust single-phase dq current controller for smart inverter applications," *IEEE Transactions on Power Electronics*, vol. 31, no. 5, pp. 3968–3976, 2016.

[7] J. Liu, Y. Sun, Y. Li, and C. Fu, "Theoretical harmonic analysis of cascaded h-bridge inverter under hybrid pulse width multilevel modulation," *IET Power Electronics*, vol. 9, no. 14, pp. 2714–2722, 2016.

[8] R. Zhang, M. Cardinal, P. Szczesny, and M. Dame, "A grid simulator with control of single-phase power converters in d-q rotating frame," in *2002 IEEE 33rd Annual IEEE Power Electronics Specialists Conference. Proceedings (Cat. No.02CH37289)*, vol. 3, pp. 1431–1436 vol.3, 2002.

[9] R. Bisht, S. Subramaniam, R. Bhattarai, and S. Kamalasadan, "Active and reactive power control of single phase inverter with seamless transfer between grid-connected and islanded mode," in *2018 IEEE Power and Energy Conference at Illinois (PECI)*, pp. 1–8, Feb 2018.

[10] Z. Jianguo, S. Qiuye, Z. Huaguang, and Z. Yan, "Load balancing and reactive power compensation based on capacitor banks shunt compensation in low voltage distribution networks," in *Proceedings of the 31st Chinese Control Conference*, pp. 6681–6686, July 2012.

[11] M. Y. Suliman and M. Emad Farrag, "Power balance and control of transmission lines using static series compensator," in *2018 53rd International Universities Power Engineering Conference (UPEC)*, pp. 1–5, Sep. 2018.

[12] S. Weckx and J. Driesen, "Load balancing with ev chargers and pv inverters in unbalanced distribution grids," *IEEE Transactions on Sustainable Energy*, vol. 6, pp. 635–643, April 2015.

[13] S. Hashemi, J. Ãstergaard, and G. Yang, "A scenario-based approach for energy storage capacity determination in lv grids with high pv penetration," *IEEE Transactions on Smart Grid*, vol. 5, pp. 1514–1522, May 2014.

[14] K. H. Chua, Y. S. Lim, P. Taylor, S. Morris, and J. Wong, "Energy storage system for mitigating voltage unbalance on low-voltage networks with photovoltaic systems," *IEEE Transactions on Power Delivery*, vol. 27, pp. 1783–1790, Oct 2012.

[15] T. L. Vandoorn, J. C. Vasquez, J. De Kooning, J. M. Guerrero, and L. Vandevelde, "Microgrids: Hierarchical control and an overview of the control and reserve management strategies," *IEEE Industrial Electronics Magazine*, vol. 7, pp. 42–55, Dec 2013.

[16] "Ieee standard conformance test procedures for equipment interconnecting distributed energy resources with electric power systems and associated interfaces," *IEEE Std 1547.1-2020*, pp. 1–282, 2020.

[17] F. E. Aamri, H. Maker, A. Mouhsen, and M. Harmouchi, "A new strategy to control the active and reactive power for single phase grid-connected pv inverter," pp. 1–6, Dec 2015.

[18] J.-W. Choi and S.-K. Sul, "Fast current controller in 3-phase ac/dc boost converter using d-q axis cross-coupling," in *PESC Record. 27th Annual IEEE Power Electronics Specialists Conference*, vol. 1, pp. 177–182 vol.1, Jun 1996.

[19] F. Briz, M. W. Degner, and R. D. Lorenz, "Analysis and design of current regulators using complex vectors," *IEEE Transactions on Industry Applications*, vol. 36, pp. 817–825, May 2000.

[20] "Comparison of current control techniques for pwm rectifiers," in *Industrial Electronics, 2002. ISIE 2002. Proceedings of the 2002 IEEE International Symposium on*, vol. 4, pp. 1259–1263 vol.4, 2002.

[21] K. Dai, P. Liu, J. Xiong, and J. Chen, "Comparative study on current control for three-phase svpwm voltage-source converter in synchronous rotating frame using complex vector method," in *Power Electronics Specialist Conference, 2003. PESC '03. 2003 IEEE 34th Annual*, vol. 2, pp. 695–700 vol.2, June 2003.

[22] B. Crowhurst, E. F. El-Saadany, L. E. Chaar, and L. A. Lamont, "Single-phase grid-tie inverter control using dq transform for active and reactive load power compensation," in *2010 IEEE International Conference on Power and Energy*, pp. 489–494, Nov 2010.

[23] G. Franceschini, E. Lorenzani, C. Tassoni, and A. Bellini, "Synchronous reference frame grid current control for single-phase photovoltaic converters," in *2008 IEEE Industry Applications Society Annual Meeting*, pp. 1–7, Oct 2008.

[24] N. A. Ninad, L. A. C. Lopes, and A. Rufer, "A vector controlled single-phase voltage source inverter with enhanced dynamic response," in *2010 IEEE International Symposium on Industrial Electronics*, pp. 2891–2896, July 2010.

[25] S. Samerchur, S. Premrudeepreechacharn, Y. Kumsuwun, and K. Higuchi, "Power control of single-phase voltage source inverter for grid-connected photovoltaic systems," in *2011 IEEE/PES Power Systems Conference and Exposition*, pp. 1–6, March 2011.

[26] R. Bisht, S. Subramaniam, R. Bhattarai, and S. Kamalasadan, "Active and reactive power control of single phase inverter with seamless transfer between grid-connected and islanded mode," in *2018 IEEE Power and Energy Conference at Illinois (PECI)*, pp. 1–8, Feb 2018.

[27] S. Yang, Q. Lei, F. Z. Peng, and Z. Qian, "A robust control scheme for grid-connected voltage-source inverters," *IEEE Transactions on Industrial Electronics*, vol. 58, pp. 202–212, Jan 2011.

[28] N. A. Ninad and L. A. C. Lopes, "Per-phase dq control of a three-phase battery inverter in a diesel hybrid mini-grid supplying single-phase loads," in *2011 IEEE International Conference on Industrial Technology*, pp. 204–209, March 2011.

[29] R. Teodorescu, F. Blaabjerg, M. Liserre, and P. C. Loh, "Proportional-resonant controllers and filters for grid-connected voltage-source converters," *IEE Proceedings - Electric Power Applications*, vol. 153, pp. 750–762, September 2006.

[30] A. M. Mnider, D. J. Atkinson, M. Dahidah, and M. Armstrong, "A simplified dq controller for single-phase grid-connected pv inverters," in *2016 7th International Renewable Energy Congress (IREC)*, pp. 1–6, March 2016.

[31] L. Cui, L. Zhenxing, C. Li, and W. Jiying, "A novel control method for single-phase power inverter systems based on hilbert transform and dq transform," in *2017 29th Chinese Control And Decision Conference (CCDC)*, pp. 7430–7435, May 2017.

[32] J. Alvidrez, S. Ranade, S. Brahma, S. Bukowski, C. Silva-Monroy, and A. Ellis, "An analytical model of a single phase dq-controlled inverter for power system short circuit calculations," in *2016 North American Power Symposium (NAPS)*, pp. 1–5, Sept 2016.

[33] B. Saritha and P. A. Jankiraman, "Observer based current control of single-phase inverter in dq rotating frame," in *2006 International Conference on Power Electronic, Drives and Energy Systems*, pp. 1–5, Dec 2006.

[34] M. J. Ryan and R. D. Lorenz, "A synchronous-frame controller for a single-phase sine wave inverter," in *Proceedings of APEC 97 - Applied Power Electronics Conference*, vol. 2, pp. 813–819 vol.2, Feb 1997.

[35] M. Ebrahimi, S. A. Khajehoddin, and M. Karimi-Ghartemani, "Fast and robust single-phase *dq* current controller for smart inverter applications," *IEEE Transactions on Power Electronics*, vol. 31, pp. 3968–3976, May 2016.

[36] D. Divan and H. Johal, "Distributed facts - a new concept for realizing grid power flow control," in *2005 IEEE 36th Power Electronics Specialists Conference*, pp. 8–14, June 2005.

[37] Z. Yuan, S. W. H. d. Haan, J. B. Ferreira, and D. Cvoric, "A facts device: Distributed power-flow controller (dpfc)," *IEEE Transactions on Power Electronics*, vol. 25, pp. 2564–2572, Oct 2010.

[38] D. Dong, T. Thacker, R. Burgos, D. Boroyevich, and F. Wang, "On zero steady-state error of single-phase pwm inverters voltage control and phase-locked loop system," in *2009 IEEE Energy Conversion Congress and Exposition*, pp. 892–899, Sept 2009.

[39] T. Thacker, R. Wang, D. Dong, R. Burgos, F. Wang, and D. Boroyevich, "Phase-locked loops using state variable feedback for single-phase converter systems," in *2009 Twenty-Fourth Annual IEEE Applied Power Electronics Conference and Exposition*, pp. 864–870, Feb 2009.

[40] J. R. C. Piqueira, A. Z. Caligares, and L. H. A. Monteiro, "Considering double frequency terms from phase detectors in synchronous master-slave networks," in *2006 Proceeding of the Thirty-Eighth Southeastern Symposium on System Theory*, pp. 453–456, March 2006.

[41] S. M. Silva, B. M. Lopes, B. J. C. Filho, R. P. Campana, and W. C. Bosventura, "Performance evaluation of pll algorithms for single-phase grid-connected systems," in *Conference Record of the 2004 IEEE Industry Applications Conference, 2004. 39th IAS Annual Meeting.*, vol. 4, pp. 2259–2263 vol.4, Oct 2004.

[42] F. Blaabjerg, Z. Chen, and S. B. Kjaer, "Power electronics as efficient interface in dispersed power generation systems," *IEEE Transactions on Power Electronics*, vol. 19, pp. 1184–1194, Sept 2004.

[43] Y. Xue, L. Chang, S. B. Kjaer, J. Bordonau, and T. Shimizu, "Topologies of single-phase inverters for small distributed power generators: an overview," *IEEE Transactions on Power Electronics*, vol. 19, pp. 1305–1314, Sept 2004.

[44] Q. Li and P. Wolfs, "A review of the single phase photovoltaic module integrated converter topologies with three different dc link configurations," *IEEE Transactions on Power Electronics*, vol. 23, pp. 1320–1333, May 2008.

[45] H. Kim, T. Yu, and S. Choi, "Indirect current control algorithm for utility interactive inverters in distributed generation systems," *IEEE Transactions on Power Electronics*, vol. 23, pp. 1342–1347, May 2008.

[46] J. M. Carrasco, L. G. Franquelo, J. T. Bialasiewicz, E. Galvan, R. C. PortilloGuisado, M. A. M. Prats, J. I. Leon, and N. Moreno-Alfonso, "Power-electronic systems for the grid integration of renewable energy sources: A survey," *IEEE Transactions on Industrial Electronics*, vol. 53, pp. 1002–1016, June 2006.

[47] A. C. Kyritsis, E. C. Tatakis, and N. P. Papanikolaou, "Optimum design of the current-source flyback inverter for decentralized grid-connected photovoltaic systems," *IEEE Transactions on Energy Conversion*, vol. 23, pp. 281–293, March 2008.

[48] D. Zhi, L. Xu, and B. W. Williams, "Improved direct power control of grid-connected dc/ac converters," *IEEE Transactions on Power Electronics*, vol. 24, pp. 1280–1292, May 2009.

[49] I. J. Gabe, V. F. Montagner, and H. Pinheiro, "Design and implementation of a robust current controller for vsi connected to the grid through an lcl filter," *IEEE Transactions on Power Electronics*, vol. 24, pp. 1444–1452, June 2009.

[50] R. Tirumala, N. Mohan, and C. Henze, "Seamless transfer of grid-connected pwm inverters between utility-interactive and stand-alone modes," in *APEC. Seventeenth Annual IEEE Applied Power Electronics Conference and Exposition (Cat. No.02CH37335)*, vol. 2, pp. 1081–1086 vol.2, 2002.

[51] Z. Yao, L. Xiao, and Y. Yan, "Seamless transfer of single-phase grid-interactive inverters between grid-connected and stand-alone modes," *IEEE Transactions on Power Electronics*, vol. 25, pp. 1597–1603, June 2010.

[52] B. J. Kim, J. H. Cho, J. M. Kim, J. H. Lee, and C. Y. Won, "An enhanced control strategy for seamless transfer of grid-connected single-phase inverter in synchronous rotating frame," in *2017 20th International Conference on Electrical Machines and Systems (ICEMS)*, pp. 1–6, Aug 2017.

[53] Y. Chen, Z. Wang, X. Zhou, L. Zhou, Z. Chen, A. Luo, and M. Wang, "Seamless transfer control strategy for three-phase inverter in microgrid," in *2016 IEEE 8th International Power Electronics and Motion Control Conference (IPEMC-ECCE Asia)*, pp. 1759–1763, May 2016.

[54] X. Li, H. Zhang, and R. Balog, "Control strategy for seamless transfer between island and grid-connected operation for a dual-mode photovoltaic inverter," in *2015 IEEE Energy Conversion Congress and Exposition (ECCE)*, pp. 5983–5990, Sept 2015.

[55] Z. Liu and J. Liu, "Seamless transfer strategy with outer current loop for three phase inverter in distributed generation," in *2010 IEEE Energy Conversion Congress and Exposition*, pp. 3556–3560, Sept 2010.

[56] D. Lei, T. Haolei, and X. Furong, "A universal droop-based control strategy for single-phase two-stage pv inverters," in *IECON 2017 - 43rd Annual Conference of the IEEE Industrial Electronics Society*, pp. 6369–6374, Oct 2017.

[57] K. Lim and J. Choi, "Pr based indirect current control for seamless transfer of grid-connected inverter," in *2016 IEEE 8th International Power Electronics and Motion Control Conference (IPEMC-ECCE Asia)*, pp. 3749–3755, May 2016.

[58] D. S. Ochs, B. Mirafzal, and P. Sotoodeh, "A method of seamless transitions between grid-tied and stand-alone modes of operation for utility-interactive three-phase inverters," *IEEE Transactions on Industry Applications*, vol. 50, pp. 1934–1941, May 2014.

[59] A. Mohd, E. Ortjohann, W. Sinsukthavorn, M. Lingemann, N. Hamsic, and D. Morton, "Supervisory control and energy management of an inverter-based modular smart grid," in *2009 IEEE/PES Power Systems Conference and Exposition*, pp. 1–6, March 2009.

[60] T. D. C. Buasarello and J. A. Pomilio, "Battery storage system with active filtering function based on the conservative power theory for wind generators," in *2018 IEEE International Conference on Industrial Electronics for Sustainable Energy Systems (IESES)*, pp. 21–26, Jan 2018.

[61] M. M. Haque, P. Wolfs, and S. Alahakoon, "Three-port converter with decoupled power control strategies for residential pv-battery system," in *2018 IEEE International Conference on Industrial Electronics for Sustainable Energy Systems (IESES)*, pp. 180–185, Jan 2018.

[62] J. Mishra, M. Pattnaik, and S. Samanta, "Speed sensorless mppt control of stand-alone seig based wind-battery hybrid system," in *2017 6th International Conference on Computer Applications In Electrical Engineering-Recent Advances (CERA)*, pp. 37–41, Oct 2017.

[63] J. Amini and M. Moallem, "A capacitor voltage balancing method for cascaded h-bridge multilevel inverters with application to facts," in *IECON 2016 - 42nd Annual Conference of the IEEE Industrial Electronics Society*, pp. 6447–6452, Oct 2016.

[64] A. shahariari, H. Mokhlies, A. H. B. A. Bakar, and M. Karimi, "The numerical estimation method of series facts compensator based on injection model of voltage source inverter," in *2011 IEEE Symposium on Industrial Electronics and Applications*, pp. 490–494, Sept 2011.

[65] M. P. Nandankar and D. S. More, "Performance analysis of transformer-less hybrid active power filter using different inverter topologies," in *2017 International Conference on Intelligent Computing, Instrumentation and Control Technologies (ICICICT)*, pp. 892–897, July 2017.

[66] H. Jaffar and N. A. Azli, "A nonconventional multilevel inverter for active power filtering using unified constant-frequency integration control," in *2016 IEEE Industrial Electronics and Applications Conference (IEACon)*, pp. 42–46, Nov 2016.

[67] J. M. Guerrero, L. G. de Vicuna, J. Matas, M. Castilla, and J. Miret, "A wireless controller to enhance dynamic performance of parallel inverters in distributed generation systems," *IEEE Transactions on Power Electronics*, vol. 19, pp. 1205–1213, Sept 2004.

[68] E. Barklund, N. Pogaku, M. Prodanovic, C. Hernandez-Aramburo, and T. C. Green, "Energy management in autonomous microgrid using stability-constrained droop control of inverters," *IEEE Transactions on Power Electronics*, vol. 23, pp. 2346–2352, Sept 2008.

[69] F. Katiraei and M. R. Iravani, "Power management strategies for a microgrid with multiple distributed generation units," *IEEE Transactions on Power Systems*, vol. 21, pp. 1821–1831, Nov 2006.

[70] A. Bendib, A. Kherbachi, K. Kara, and A. Chouder, "Droop controller based primary control scheme for parallel-connected single-phase inverters in islanded ac microgrid," in *2017 5th International Conference on Electrical Engineering - Boumerdes (ICEE-B)*, pp. 1–6, Oct 2017.

[71] T. Younis, M. Ismeil, M. Orabi, and E. K. Hussain, "A single-phase self-synchronized synchronverter with bounded droop characteristics," in *2018 IEEE Applied Power Electronics Conference and Exposition (APEC)*, pp. 1624–1629, March 2018.

[72] J. J. Seo, H. J. Lee, W. W. Jung, and D. J. Won, "Voltage control method using modified voltage droop control in lv distribution system," in *2009 Transmission Distribution Conference Exposition: Asia and Pacific*, pp. 1–4, Oct 2009.

[73] N. Karthikeyan, B. R. Pokhrel, J. R. Pillai, and B. Bak-Jensen, "Coordinated voltage control of distributed pv inverters for voltage regulation in low voltage distribution networks," in *2017 IEEE PES Innovative Smart Grid Technologies Conference Europe (ISGT-Europe)*, pp. 1–6, Sept 2017.

[74] H. S. V. S. K. Nunna and S. Doolla, "Energy management in microgrids using demand response and distributed storage x2014;a multiagent approach," *IEEE Transactions on Power Delivery*, vol. 28, pp. 939–947, April 2013.

[75] I. U. Nutkani, P. C. Loh, P. Wang, and F. Blaabjerg, "Decentralized economic dispatch scheme with online power reserve for microgrids," *IEEE Transactions on Smart Grid*, vol. 8, pp. 139–148, Jan 2017.

[76] I. U. Nutkani, P. C. Loh, and F. Blaabjerg, "Droop scheme with consideration of operating costs," *IEEE Transactions on Power Electronics*, vol. 29, pp. 1047–1052, March 2014.

[77] Y. Xu, Q. Guo, H. Sun, and Z. Fei, "Distributed discrete robust secondary cooperative control for islanded microgrids," *IEEE Transactions on Smart Grid*, pp. 1–1, 2018.

[78] S. Shinde, S. M. Tayebi, H. Haibing, N. Kutkut, and I. Batarseh, "Virtual resistance technique for power limit management of microgrid dg inverters," in *2017 IEEE Energy Conversion Congress and Exposition (ECCE)*, pp. 4453–4459, Oct 2017.

[79] G. Venkataramanan and M. Illindala, "Small signal dynamics of inverter interfaced distributed generation in a chain-microgrid," in *2007 IEEE Power Engineering Society General Meeting*, pp. 1–6, June 2007.

[80] J. Wang, L. M. Costa, and B. M. Cisse, "From distribution feeder to microgrid: An insight on opportunities and challenges," in *2016 IEEE International Conference on Power System Technology (POWERCON)*, pp. 1–6, Sept 2016.

[81] C. Marnay and O. C. Bailey, "The CERTS microgrid and the future of the macrogrid," in *ACEEE Summer Study on Energy Efficiency in Buildings*, (Berkeley), p. 14, LBNL, LBNL, 08/2004 2004.

[82] Z. Liu and J. Liu, "A novel control strategy of inverter in distributed generation with seamless transfer capability," in *2011 Twenty-Sixth Annual IEEE Applied Power Electronics Conference and Exposition (APEC)*, pp. 1594–1598, March 2011.

[83] X. Chen, Y. H. Wang, and Y. C. Wang, "A novel seamless transferring control method for microgrid based on master-slave configuration," in *2013 IEEE ECCE Asia Downunder*, pp. 351–357, June 2013.

[84] W. C. Shan, L. X. Lin, G. Li, and L. Y. Wei, "A seamless operation mode transition control strategy for a microgrid based on master-slave control," in *Proceedings of the 31st Chinese Control Conference*, pp. 6768–6775, July 2012.

[85] C. Yoon, H. Bai, R. N. Beres, X. Wang, C. L. Bak, and F. Blaabjerg, "Harmonic stability assessment for multiparalleled, grid-connected inverters," *IEEE Transactions on Sustainable Energy*, vol. 7, pp. 1388–1397, Oct 2016.

[86] V. Kaura and V. Blasko, "Operation of a phase locked loop system under distorted utility conditions," *IEEE Transactions on Industry Applications*, vol. 33, pp. 58–63, Jan 1997.

[87] B. Meersman, J. D. Kooning, T. Vandoorn, L. Degroote, B. Renders, and L. Vandevelde, "Overview of pll methods for distributed generation units," in *45th International Universities Power Engineering Conference UPEC2010*, pp. 1–6, Aug 2010.

[88] C. Subramanian and R. Kanagaraj, "Rapid tracking of grid variables using prefiltered synchronous reference frame pll," *IEEE Transactions on Instrumentation and Measurement*, vol. 64, pp. 1826–1836, July 2015.

[89] S. Golestan, M. Monfared, F. D. Freijedo, and J. M. Guerrero, "Performance improvement of a prefiltered synchronous-reference-frame pll by using a pid-type loop filter," *IEEE Transactions on Industrial Electronics*, vol. 61, pp. 3469–3479, July 2014.

[90] F. E. Aamri, H. Maker, A. Mouhsen, and M. Harmouchi, "A new strategy to control the active and reactive power for single phase grid-connected pv inverter," in *2015 3rd International Renewable and Sustainable Energy Conference (IRSEC)*, pp. 1–6, Dec 2015.

[91] K. Ogata, *Modern Control Engineering*. Upper Saddle River, NJ, USA: Prentice Hall PTR, 4th ed., 2001.

[92] W. H. Kersting, "Radial distribution test feeders," in *2001 IEEE Power Engineering Society Winter Meeting. Conference Proceedings (Cat. No.01CH37194)*, vol. 2, pp. 908–912, Jan 2001.

[93] R. Teodorescu, F. Blaabjerg, M. Liserre, and P. C. Loh, "Proportional-resonant controllers and filters for grid-connected voltage-source converters," *IEE Proceedings - Electric Power Applications*, vol. 153, pp. 750–762, Sep. 2006.

[94] J. Schiffer, T. Seel, J. Raisch, and T. Sezi, "Voltage stability and reactive power sharing in inverter-based microgrids with consensus-based distributed voltage control," *IEEE Transactions on Control Systems Technology*, vol. 24, pp. 96–109, Jan 2016.

[95] J. C. Vasquez, R. A. Mastromauro, J. M. Guerrero, and M. Liserre, "Voltage support provided by a droop-controlled multifunctional inverter," *IEEE Transactions on Industrial Electronics*, vol. 56, pp. 4510–4519, Nov 2009.

[96] J. Liu, Y. Miura, and T. Ise, "Comparison of dynamic characteristics between virtual synchronous generator and droop control in inverter-based distributed generators," *IEEE Transactions on Power Electronics*, vol. 31, pp. 3600–3611, May 2016.

[97] Q. Zhong and Y. Zeng, "Universal droop control of inverters with different types of output impedance," *IEEE Access*, vol. 4, pp. 702–712, 2016.

[98] X. Sun, Y. Tian, and Z. Chen, "Adaptive decoupled power control method for inverter connected dg," *IET Renewable Power Generation*, vol. 8, pp. 171–182, March 2014.

[99] Q. Zhong and Y. Zeng, "Universal droop control of inverters with different types of output impedance," *IEEE Access*, vol. 4, pp. 702–712, 2016.

[100] Q. Zhong, W. Ming, and Y. Zeng, "Self-synchronized universal droop controller," *IEEE Access*, vol. 4, pp. 7145–7153, 2016.

[101] R. Bisht, S. Subramaniam, R. Bhattarai, and S. Kamalasadan, "Active and reactive power control of single phase inverter with seamless transfer between grid-connected and islanded mode," in *2018 IEEE Power and Energy Conference at Illinois (PECI)*, pp. 1–8, Feb 2018.

[102] S.-B. Han, N.-S. Choi, C.-T. Rim, and G.-H. Cho, "Modeling and analysis of static and dynamic characteristics for buck-type three-phase pwm rectifier by circuit dq transformation," *IEEE Transactions on Power Electronics*, vol. 13, pp. 323–336, Mar 1998.

[103] M. A. Masrur, "Studies on the effect of filtering, digitization, and computation algorithm on the abc-dq current transformation in pwm inverter drive system," *IEEE Transactions on Vehicular Technology*, vol. 44, pp. 356–365, May 1995.

[104] S. Boyd, N. Parikh, E. Chu, B. Peleato, and J. Eckstein, "Distributed optimization and statistical learning via the alternating direction method of multipliers," *Foundations and Trends in Machine Learning*, vol. 3, no. 1, pp. 1–122, 2010.

[105] P. Å ulc, S. Backhaus, and M. Chertkov, "Optimal distributed control of reactive power via the alternating direction method of multipliers," *IEEE Transactions on Energy Conversion*, vol. 29, pp. 968–977, Dec 2014.

[106] Y. Khayat, M. Naderi, Q. Shafiee, Y. Batmani, M. Fathi, J. M. Guerrero, and H. Bevrani, "Decentralized optimal frequency control in autonomous microgrids," *IEEE Transactions on Power Systems*, vol. 34, no. 3, pp. 2345–2353, 2019.

[107] A. Khodaei, "Resiliency-oriented microgrid optimal scheduling," *IEEE Transactions on Smart Grid*, vol. 5, no. 4, pp. 1584–1591, 2014.

[108] K. P. Schneider, S. Laval, J. Hansen, R. B. Melton, L. Ponder, L. Fox, J. Hart, J. Hambrick, M. Buckner, M. Baggu, K. Prabakar, M. Manjrekar, S. Essakiappan, L. M. Tolbert, Y. Liu, J. Dong, L. Zhu, A. Smallwood, A. Jayantilal, C. Irwin, and G. Yuan, "A distributed power system control architecture for improved distribution system resiliency," *IEEE Access*, vol. 7, pp. 9957–9970, 2019.

[109] Y. Wang, C. Chen, J. Wang, and R. Baldick, "Research on resilience of power systems under natural disastersâa review," *IEEE Transactions on Power Systems*, vol. 31, no. 2, pp. 1604–1613, 2016.

[110] Y. Yang, H. Li, A. Aichhorn, J. Zheng, and M. Greenleaf, "Sizing strategy of distributed battery storage system with high penetration of photovoltaic for voltage regulation and peak load shaving," *IEEE Transactions on Smart Grid*, vol. 5, no. 2, pp. 982–991, 2014.

[111] I. J. Balaguer, Q. Lei, S. Yang, U. Supatti, and F. Z. Peng, "Control for grid-connected and intentional islanding operations of distributed power generation," *IEEE Transactions on Industrial Electronics*, vol. 58, no. 1, pp. 147–157, 2011.

[112] A. Micallef, M. Apap, C. Spiteri-Staines, and J. M. Guerrero, "Single-phase microgrid with seamless transition capabilities between modes of operation," *IEEE Transactions on Smart Grid*, vol. 6, no. 6, pp. 2736–2745, 2015.

[113] Z. Yao, L. Xiao, and Y. Yan, "Seamless transfer of single-phase grid-interactive inverters between grid-connected and stand-alone modes," *IEEE Transactions on Power Electronics*, vol. 25, no. 6, pp. 1597–1603, 2010.

[114] S. Dasgupta, S. K. Sahoo, and S. K. Panda, "Single-phase inverter control techniques for interfacing renewable energy sources with microgridâpart i: Parallel-connected inverter topology with active and reactive power flow control along with grid current shaping," *IEEE Transactions on Power Electronics*, vol. 26, no. 3, pp. 717–731, 2011.

[115] M. Ebrahimi, S. A. Khajehoddin, and M. Karimi-Ghartemani, "Fast and robust single-phase dq current controller for smart inverter applications," *IEEE Transactions on Power Electronics*, vol. 31, no. 5, pp. 3968–3976, 2016.

[116] D. I. Brandao, L. S. de Araújo, T. Caldognetto, and J. A. Pomilio, "Coordinated control of three- and single-phase inverters coexisting in low-voltage microgrids," *Applied Energy*, vol. 228, pp. 2050 – 2060, 2018.

[117] M. M. Rezaei and J. Soltani, "A robust control strategy for a grid-connected multi-bus microgrid under unbalanced load conditions," *International Journal of Electrical Power Energy Systems*, vol. 71, pp. 68 – 76, 2015.

[118] J. H. R. Enslin and P. J. M. Heskes, "Harmonic interaction between a large number of distributed power inverters and the distribution network," in *IEEE 34th Annual Conference on Power Electronics Specialist, 2003. PESC '03.*, vol. 4, pp. 1742–1747 vol.4, 2003.

[119] R. Bisht, S. Subramaniam, R. Bhattarai, and S. Kamalasadan, "Active and reactive power control of single phase inverter with seamless transfer between grid-connected and islanded mode," in *2018 IEEE Power and Energy Conference at Illinois (PECI)*, pp. 1–8, 2018.

[120] M. Karimi-Ghartemani, M. Mojiri, A. Safaee, J. A. Walseth, S. A. Khajehoddin, P. Jain, and A. Bakhshai, "A new phase-locked loop system for three-phase applications," *IEEE Transactions on Power Electronics*, vol. 28, no. 3, pp. 1208–1218, 2013.

[121] P. Roncero-Sanchez, X. del Toro Garcia, A. P. Torres, and V. Feliu, "Fundamental positive- and negative-sequence estimator for grid synchronization under highly disturbed operating conditions," *IEEE Transactions on Power Electronics*, vol. 28, no. 8, pp. 3733–3746, 2013.

[122] A. Thakallapelli and S. Kamalasadan, "Alternating direction method of multipliers (admms) based distributed approach for wide-area control," *IEEE Transactions on Industry Applications*, vol. 55, no. 3, pp. 3215–3227, 2019.

[123] A. Singhal, V. Ajjarapu, J. Fuller, and J. Hansen, "Real-time local volt/var control under external disturbances with high pv penetration," *IEEE Transactions on Smart Grid*, vol. 10, pp. 3849–3859, July 2019.

[124] M. G. Kashani, M. Mobarrez, and S. Bhattacharya, "Smart inverter volt-watt control design in high pv-penetrated distribution systems," *IEEE Transactions on Industry Applications*, vol. 55, pp. 1147–1156, March 2019.

[125] E. DallâAnese, S. V. Dhople, B. B. Johnson, and G. B. Giannakis, "Decentralized optimal dispatch of photovoltaic inverters in residential distribution systems," *IEEE Transactions on Energy Conversion*, vol. 29, pp. 957–967, Dec 2014.

[126] K. Turitsyn, P. Sulc, S. Backhaus, and M. Chertkov, "Options for control of reactive power by distributed photovoltaic generators," *Proceedings of the IEEE*, vol. 99, pp. 1063–1073, June 2011.

[127] Z. Jianguo, S. Qiuye, Z. Huaguang, and Z. Yan, "Load balancing and reactive power compensation based on capacitor banks shunt compensation in low voltage distribution networks," in *Proceedings of the 31st Chinese Control Conference*, pp. 6681–6686, July 2012.

[128] M. Y. Suliman and M. Emad Farrag, "Power balance and control of transmission lines using static series compensator," in *2018 53rd International Universities Power Engineering Conference (UPEC)*, pp. 1–5, Sep. 2018.

[129] S. Weckx and J. Driesen, "Load balancing with ev chargers and pv inverters in unbalanced distribution grids," *IEEE Transactions on Sustainable Energy*, vol. 6, pp. 635–643, April 2015.

[130] S. Weckx and J. Driesen, "Load balancing with ev chargers and pv inverters in unbalanced distribution grids," *IEEE Transactions on Sustainable Energy*, vol. 6, pp. 635–643, April 2015.

[131] M. Karimi-Ghartemani, "Universal integrated synchronization and control for single-phase dc/ac converters," *IEEE Transactions on Power Electronics*, vol. 30, pp. 1544–1557, March 2015.

[132] F. Tursun, M. Smiai, C. Åahin, and D. Gezer, "Impacts of pv installation on the low voltage residental distribution networks: A case study of yildiz," in *4th International Conference on Power Engineering, Energy and Electrical Drives*, pp. 1415–1420, May 2013.

[133] R. A. Jabr, "Robust volt/var control with photovoltaics," *IEEE Transactions on Power Systems*, vol. 34, pp. 2401–2408, May 2019.

[134] A. Thakallapelli and S. Kamalasadan, "Alternating direction method of multipliers (admms) based distributed approach for wide-area control," *IEEE Transactions on Industry Applications*, vol. 55, pp. 3215–3227, May 2019.

[135] A. Thakallapelli and S. Kamalasadan, "Alternating direction method of multipliers (admm) based distributed approach for wide-area control," in *2017 IEEE Industry Applications Society Annual Meeting*, pp. 1–7, Oct 2017.

[136] D. Montenegro and M. Bello, "Coordinating control devices and smart inverter functionalities in the presence of variable weather conditions," in *2018 IEEE/PES Transmission and Distribution Conference and Exposition (T D)*, pp. 1–9, 2018.

[137] Y. P. Agalgaonkar, B. C. Pal, and R. A. Jabr, "Stochastic distribution system operation considering voltage regulation risks in the presence of pv generation," *IEEE Transactions on Sustainable Energy*, vol. 6, no. 4, pp. 1315–1324, 2015.

APPENDIX A: CHECK BLOCKS FOR SYNCHRONIZATION

This section discusses the Matlab codes created for analyzing the grid side voltages and currents for disconnection and re-synchronization with the grid or local EPS. As discussed in section 3.4, the signals need to be within the bands prescribed by the IEEE 1547 2018 regulation, hence to check this the following check blocks were created and the codes are presented in this appendix.

1. Grid Health Check

   - Grid Voltage check

   - Grid frequency check

2. Synchronization Check

   - Inverter-Grid Voltage check

   - Inverter-Grid frequency check

   - Inverter-Grid phase angle check

A.1   Grid Health Checks

Firstly, we will be looking at the codes related to grid health checks.

I. Grid Voltage Check Code

```
    function [y,x] = fcn(u)
persistent countb countc countd b counta flaga flagb flagc flagd
if isempty(flaga)
    flaga=0;
end
if isempty(flagb)
    flagb=0;
end
```

```
if isempty(flagc)

    flagc=0;

end

if isempty(flagd)

    flagd=0;

end


if isempty(b)

    b=0;

end

if isempty(counta)

    counta=0;

end

if isempty(countb)

    countb=0;

end

if isempty(countc)

    countc=0;

end

if isempty(countd)

    countd=0;

end

x=b;

if (u<=0.3) && (u>=-0.1)

    counta=counta+1;

    if counta>3200

    b=1;
```

```
        counta=0;

        flaga=1;

        flagb=0;

        flagc=0;

        flagd=0;

    elseif(counta<3200 && flaga==1)

        b=x;countb=0;countc=0;countd=0;

    elseif(counta<3200 && flaga==0)

        b=x;countb=0;countc=0;countd=0;

    end

end

x=b;

if (u>0.55 || u<-0.2)

        countb=countb+1;

        if countb>3200

            b=0;

            countb=0;

            flaga=0;

            flagb=1;

            flagc=0;

            flagd=0;

        elseif (countb<3200 && flagb==1)

                b=x;counta=0;countc=0;countd=0;

        elseif (countb<3200 && flagb==0 && flaga==1)

                b=1;countc=0;countd=0;flaga=0;

        elseif (countb<3200 && flagb==0 && flagc==1)

                b=1;counta=0;countd=0;flagc=0;
```

```
        end

end

x=b;

if ((0.3<u && u<0.55) || (-0.2<u && u<-0.1))

        countc=countc+1;

        if countc>40000

            b=0;

            countc=0;

            flaga=0;

            flagb=0;

            flagc=1;

            flagd=0;

        elseif (countc<40000 && flagc==1)

                b=x;counta=0;countb=0;countd=0;

        elseif (countc<40000 && flagc==0 && flagb==1)

                b=x;counta=0;countd=0;

        elseif (countc<40000 && flagc==0 && flaga==0)

                b=1;countb=0;countd=0;

        end

end

x=countb;

y=b;

end
```

II. Grid Frequency check code

```
function [y,x] = fcn(u)
```

```
persistent countb countc countd b counta flaga flagb flagc flagd

if isempty(flaga)

    flaga=0;

end

if isempty(flagb)

    flagb=0;

end

if isempty(flagc)

    flagc=0;

end

if isempty(flagd)

    flagd=0;

end


if isempty(b)

    b=0;

end

if isempty(counta)

    counta=0;

end

if isempty(countb)

    countb=0;

end

if isempty(countc)

    countc=0;

end

if isempty(countd)
```

```
    countd=0;
end
x=b;
if (u>-0.016) && (u<0.03)
     counta=counta+1;
   if counta>3200
   b=1;
   counta=0;
   flaga=1;
   flagb=0;
   flagc=0;
   flagd=0;
   elseif(counta<3200 && flaga==1)
       b=x;countb=0;countc=0;countd=0;
   elseif(counta<3200 && flaga==0)
       b=x;countb=0;countc=0;countd=0;
   end
end
x=b;

if (u<=-0.03) || (u>=0.05)
   countb=countb+1;
       if countb>3200
           b=0;
           countb=0;
           flaga=0;
           flagb=1;
```

```
            flagc=0;

            flagd=0;

        elseif (countb<3200 && flagb==1)

                b=x;counta=0;countc=0;countd=0;

        elseif (countb<3200 && flagb==0 && flaga==1)

                b=1;countc=0;countd=0;flaga=0;

        elseif (countb<3200 && flagb==0 && flagc==1)

                b=1;counta=0;countd=0;flagc=0;

    end


end


x=b;


if ((u>0.03&& u<0.05) || (u>-0.03 && u<-0.016))

         countc=countc+1;

        if countc>5980000

            b=0;

            countc=0;

            flaga=0;

            flagb=0;

            flagc=1;

            flagd=0;

        elseif (countc<5980000 && flagc==1)

                b=x;counta=0;countb=0;countd=0;

        elseif (countc<5980000&& flagc==0 && flagb==1) %if fault is adminstered by

                b=x;counta=0;countd=0;
```

```
    elseif (countc<5980000 && flagc==0 && flaga==0)

            b=1;countb=0;countd=0;

    end

    end

x=b;

y=b;


end
```

A.2   Synchronization Checks

Synchronization compares the parameters derived from the grid and inverter side voltages. Hence the inputs to these codes are Vgrid and Vinverter.

I. Inverter-Grid Voltage Check

```
    function [y,x] = fcn(u)
persistent count b counta flaga flagb
if isempty(flaga)
    flaga=0;
end
if isempty(flagb)
    flagb=0;
end


if isempty(b)
    b=0;
end
```

```
if isempty(count)

    count=0;

end

if isempty(counta)

    counta=0;

end

x=b;

if (u<=0.05) && (u>=-0.05)

    counta=counta+1;

    if counta>1000

    b=1;

    counta=0;

    flaga=1;

    flagb=0;

    elseif(counta<1000 && flaga==1)

        b=x;

    elseif(counta<1000 && flaga==0)

        b=0;

    end

end

%the count was 500

x=b;

if (u>0.05 || u<-0.05)

        count=count+1;

        if count>100

            b=0;

            count=0;
```

```
                flaga=0;

                flagb=1;

            elseif (count<100 && flagb==1)

                    b=x;

            elseif (count<100 && flagb==0)

                    b=1;

            end

    end

x=count;

y=b;


end
```

II. Inverter-Grid frequency Check

```
function [y,x] = fcn(u)

persistent count b counta flaga flagb

if isempty(flaga)

    flaga=0;

end

if isempty(flagb)

    flagb=0;

end

if isempty(b)

    b=0;
```

```
end

if isempty(count)

    count=0;

end

if isempty(counta)

    counta=0;

end

x=b;

if (u<=0.005) && (u>=-0.005)

    counta=counta+1;

    if counta>1000

    b=1;

    counta=0;

    flaga=1;

    flagb=0;

    elseif(counta<1000 && flaga==1)

        b=x;

    elseif(counta<1000 && flaga==0)

        b=0;

    end

end

x=b;

if (u>0.005 || u<-0.005)

        count=count+1;

        if count>300

            b=0;

            count=0;
```

```
            flaga=0;

            flagb=1;

        elseif (count<300 && flagb==1)

                b=x;

        elseif (count<300 && flagb==0)

                b=1;

        end

end


x=count;

y=b;


end
```

III. Inverter-Grid Phase Angle Check

```
    function [y,x] = fcn(u)



persistent count b counta flaga flagb
if isempty(flaga)

    flaga=0;
end
if isempty(flagb)

    flagb=0;
end


if isempty(b)

    b=0;
```

```
end

if isempty(count)

    count=0;

end

if isempty(counta)

    counta=0;

end


x=b;

if (u<=10) && (u>=-10)

    counta=counta+1;

    if counta>1000

    b=0;

    counta=0;

    flaga=1;

    flagb=0;

    elseif(counta<1000 && flaga==1)

        b=x;

    elseif(counta<1000 && flaga==0)

        b=1;

    end


end


x=b;

if (u>10 || u<-10)

        count=count+1;
```

```
        if count>1000

            b=1;

            count=0;

            flaga=0;

            flagb=1;

        elseif (count<1000 && flagb==1)

                b=x;

        elseif (count<1000 && flagb==0)

                b=0;

        end


end

x=count;

y=b;

end
```